Geochemical and mineralogical evaluation of mineral-water reactions and leaching potential in a black shale depot

Weathering and transport of Ni, Zn, Cd, Sr and Co from Alum- and Black shale

Håkon Skumsrud Børresen

Master Thesis in Geosciences
Environmental Geology
60 credits
Department of Geosciences
Faculty of Mathematics and Natural Sciences

UNIVERSITY OF OSLO

June 2017

Geochemical and mineralogical evaluation of mineral-water reactions and leaching potential in a black shale depot

Weathering and transport of Ni, Zn, Cd, Sr and Co from Alum- and Black shale

Håkon Skumsrud Børresen

Master thesis

Environmental Geology

Department of Geosciences

University of Oslo

June 2017

2017

Geochemical and mineralogical evaluation of mineral-water reactions and leaching potential in a black shale depot – Weathering and transport of Ni, Zn, Cd, Sr and Co from Alum- and Black shale

Håkon Skumsrud Børresen

http://www.duo.uio.no/

Trykk: Reprosentralen, Universitetet i Oslo

Abstract

Alum- and black shales are lithologies rich in sulphides and trace elements including uranium, and may pose harm to the environment during weathering. Acidification of surface- and groundwater and swelling may occur. During construction of a road tunnel through Gran, Norway, an alum shale deposit was established. Reducing conditions in the deposit groundwater are supposed to prevent weathering of alum shale, but it is uncertain if release of elements of environmental concern is primarily controlled by redox conditions.

This study investigated the distribution of elements in alum shale from Gran and Jevnaker to understand the potential risk of release of these elements. This was done by examinations of the materials utilizing X-Ray Diffraction, Scanning Electron Microscopy, and by performing leaching experiments in both laboratory and natural environments together with inverse modelling in PHREEQC.

Zinc, cadmium, cobalt, arsenic, copper and lead were identified in sulphides, while uranium was identified in phosphates. Weathering is suggested to release large amounts of sulphate, zinc, nickel and uranium to percolating water, though acidity is buffered through dissolution of calcite. The PHREEQC inverse model was applied to a depot water sample, and gave a similar output as an average of leaching water samples. This implies that alum shale releases elements of environmental concern under conditions with near-neutral pH, and that depot conditions may not be reducing yet.

Acknowledgements

This master thesis (60 credits) is part of a 2-year master program in Environmental Geology at the Department of Geosciences at the University of Oslo. All laboratory work was done at the Department of Geosciences, while field data have been obtained from material sampled by Statens Vegvesen.

I would like to thank my supervisors Helge Hellevang and Per Aagaard have come up with ideas for analysis methods, input on results and general feedback and confirmation on the work done for this thesis. Thanks to fellow MSc student Lars A. Erstad for collaboration in field and lab work, and several healthy discussions regarding methods and results.

I also want to thank Halldis Fjermestad (Statens Vegvesen) for an introduction to the project, and for supplying data and information regarding the field experiments and rock samples taken.

In relation to laboratory work I would thank PhD Candidate Beyene Girma Haile for helping with sample preparation and analysis during X-Ray Diffraction of rock samples. Thanks to Head Engineer Mufak Said Naoroz and Senior Engineer Siri Simonsen for help with preparation and analysis of water samples through IC and ICP-MS respectively. I also want to thank Senior Engineer Salahalldin Akhavan for preparing thick sections of rock samples, and Senior Engineer Berit Løken Berg for helping during the Scanning Electron Microscope analysis.

In the end, I would like to thank fellow MSc students at the Department of Geosciences for contributing to a nice and social study environment.

Håkon S. Børresen

Table of Contents

List of Figures

List of Tables

1 Introduction

"Alum shale" is a term used in Scandinavia for Cambrian to Ordovician black shales typically containing high organic carbon and metal concentrations. In Eastern Norway this alum shale is common in densely populated areas in and around Oslo, and often represents a challenge for both infrastructure and the environment when exposed to weathering. Radioactivity, swelling, and acid drainage as well as an extreme weathering effect on concrete are common consequences of the weathering reactions in alum shale (Bastiansen et al., 1957).

Problems with the lithology have been known for a while, with "The Alum Shale Committee" and the Norwegian Geotechnical Institute (NGI) working on characterizing the shale since the middle of the 20th century (Bastiansen et al., 1957). New focus was put on the alum shale with NGI and their "Black Shale Project" resulting in a guide for identification of acid producing rocks (NGI, 2015). The Norwegian Public Roads Administration (Statens Vegvesen) has studied alum- and black shales through their Nordic Road Water (NORWAT) program (Statens Vegvesen, 2016b), where Fjermestad (2013), Helmers (2013) and Santos (2014) among others have studied alum shale and other lithologies related to a new tunnel at Riksvei 4 (Rv. 4) at Hadeland, Norway. The complete study of sulphide rich lithologies and challenges related to building roads through these is summarised by Skipperud et al. (2016).

This study is conducted at the University of Oslo in collaboration with Statens Vegvesen, with alum shale material gathered by Statens Vegvesen related to current road projects at Hadeland. Hadeland is situated between Oslo and Mjøsa, where alum shale is commonly found. The work has direct relevance towards Rv. 4 Lunner grense - Jaren (Statens Vegvesen, 2016c) and the planned new E16 Eggemoen - Olum past Jevnaker towards Hønefoss (Statens Vegvesen, 2016a). Due to high content and potential release of elements of environmental concern alum shale is classified as hazardous waste in Norway (Hagelia and Fjermestad, 2016), and regularly has to be transported to a suitable depot away from the construction site. About 67 000 m^3 of alum- and black shale have been extracted during the roadworks at Hadeland (Fjermestad, 2017), where Statens Vegvesen opted for a local depot for the shale in a nearby bog that will also serve as the road fundament (Skipperud et al., 2016, Fjermestad, 2017). The depot is supposed to hinder weathering of the shale on a long term scale, but it is not done previously to this extent in Norway.

In order to estimate the natural weathering of alum shale in natural oxidizing conditions at Hadeland, several pallet experiments with alum- and black shale in open plastic containers were set up with runoff water being sampled and analysed chemically. Mineralogical and chemical analysis utilizing X-Ray Diffraction (XRD) and Scanning Electron Microscope (SEM) were conducted. Simple laboratory runoff experiments were carried out with crushed alum shale. Results have been analysed both using simple correlation tools in Microsoft Excel as well as PHREEQC groundwater chemistry modelling.

1.1 Objectives of the research

The main objectives of the research were to:

- Improve our understanding of the mineral reactions in the weathering process of alum shale.
- Identify the possible effects of alum shale weathering, and investigate how to limit the environmental impact of alum shale waste.

The study gives an insight to the weathering products of the shale, both in terms of development and transport. This includes:

- A detailed description of the behaviour of the trace elements Ni, Zn, Cd, Sr, Co, U and Mo relative to the behaviour of light elements and mineral weathering through water sample and rock analyses.
- Discussion of the possible effects of contact metamorphosis on alum shale weathering, including differences in mineral content and related elements.

The decision to focus on Ni, Zn, Sr, Cd and Co in this thesis is based on the results of a correlation analysis performed on water sample data, described in section 5.3.1. Another master thesis written by Lars A. Erstad utilises the same experiments and datasets as this study, but with different objectives. Field work at Hadeland and laboratory work including XRD and SEM analyses at the Department of Geosciences, University of Oslo were done in collaboration with Erstad. The available raw data for each thesis is thus identical. The main differences between the theses are application and analysis of the data, and each thesis is written without cooperation.

2 Study Area

2.1 Regional Geology

The Hadeland region has geologically much in common with what is found around Oslo and Mjøsa. The regional geology of the Oslo region features Precambrian granites and gneisses, folded Cambro-Silurian sedimentary to low-grade contact- and regional metamorphic rocks (Nyland and Teigland, 1984) and Permian volcanic rocks (Figure 1). The Cambro-Silurian sedimentary rocks of the Oslo region are divided into formations, units and members, with formations numbered from 1-10 starting with the oldest formations (Bjørlykke and Englund, 1979), units labelled alphabetically within formations and members labelled with Greek letters (see Figure 2).

In the Oslo region the sedimentary rocks were folded during the Caledonian orogenesis from late Ordovician to early Devonian, and rock units moved relative to each other (Larsen and Gabrielsen, 2013). Between Oslo and Gjøvik this thrust deformation lies within the alum shales, while north of Gjøvik the alum shale has been overthrusted by older lithologies (Foslie, 1919) while the shale formed a gliding plane (Morley, 1986). This adds to the geological complexity of this area, and identification of the extent of alum shale horizons is difficult.

The preservation of the Cambro-Silurian rocks in the area is partly due to a Permian rifting event extending from Langesund to Mjøsa, often called the Oslo rift (Nakrem and Worsley, 2013). Cambro-Silurian rocks situated in the Oslo graben were protected from erosion, lying lower in the terrain and possibly shielded by other rocks. This rift event introduced extensive volcanism, and intrusive rocks are commonly found in the same area, bordering to the Cambro-Silurian sedimentary rocks and locally inducing contact metamorphism.

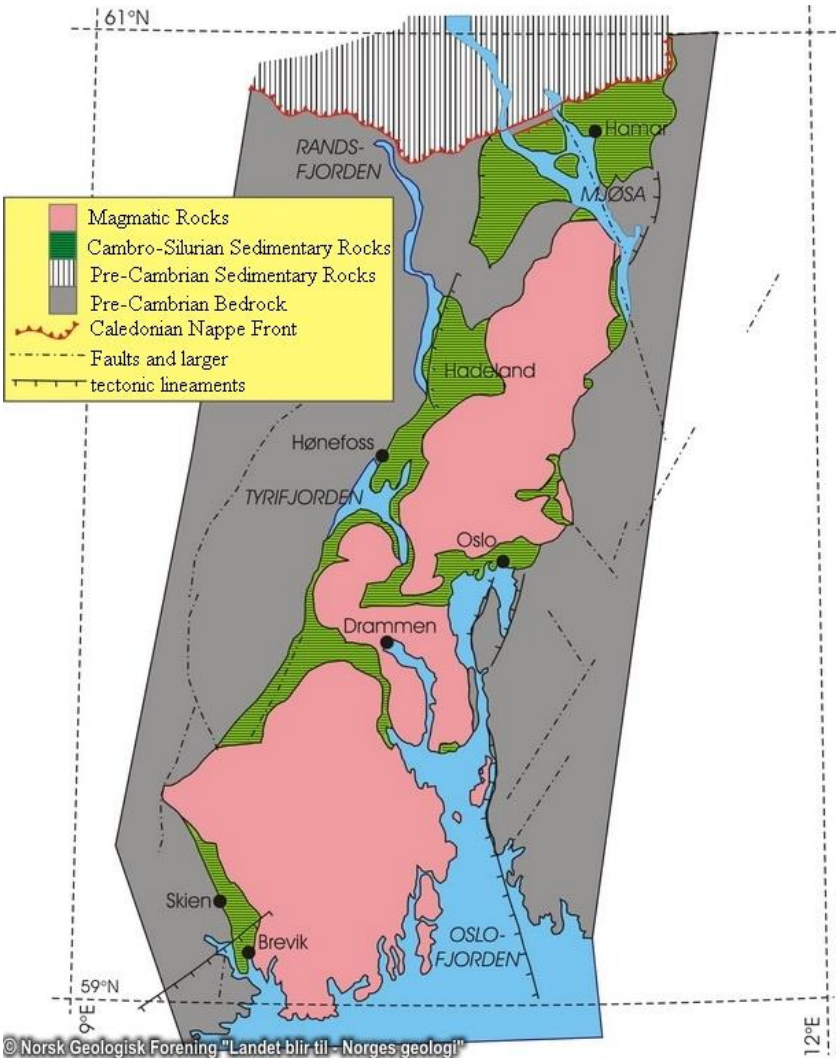

Figure 1: Simplified regional geology of the Oslo area, with Pre-Cambrian bedrock/basement, allochtonous Pre-Cambrian sedimentary rocks, Cambro-Silurian sedimentary rocks and Permian magmatic rocks. Modified from Nakrem and Worsley (2013).

The new road at Hadeland passes through an area with the alum shale formation (2e-3a), Tøyen formation (3b) including Hagastrand (Hagaberg) dark limestone (3bα) and Galgeberg black shale (3bβ) (Owen et al., 1990), Huk formation (3c) with limestone and Elnes formation (3cd-4aα) with limestone and black shale, all part of the Røyken group (Skipperud et al., 2016). This is the bottom part of Cambro-Silurian sedimentary rocks in the Oslo area (Figure 2), from Cambrium and Ordovicium (Nakrem and Worsley, 2013). The sedimentary rocks are in places intruded by mænaite or camptonite. These intrusions have a primary mineralogy and chemistry that can be classified within the alkali basalt suite of rocks, with ultrabasic to basic composition (Scott and Middleton, 1983). Both at Gran (Figure 3) and Jevnaker (Figure 4) the Cambro-Silurian sedimentary rocks may be subject to contact metamorphism due to larger intrusive bodies (Fjermestad et al., 2017).

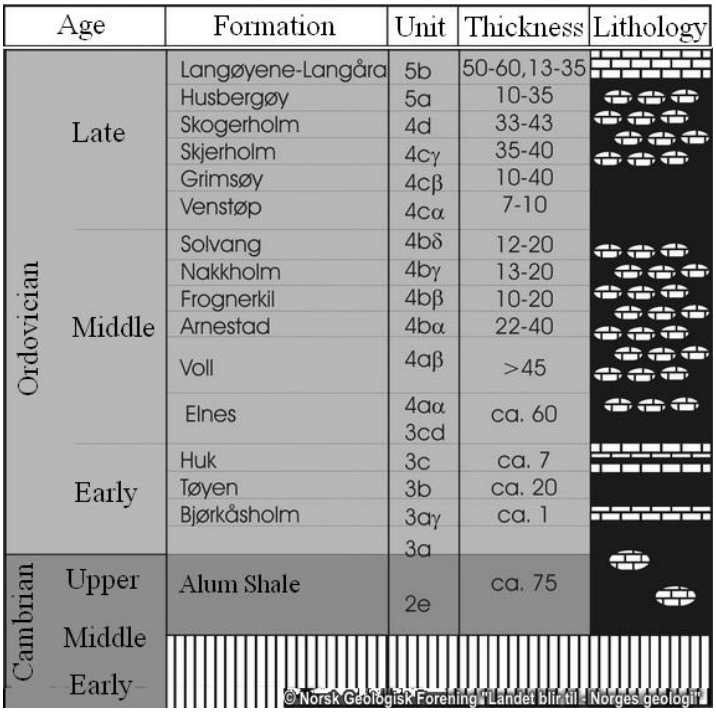

Figure 2: Stratigraphical column of the Cambrian and Ordovician sedimentary rocks in the Oslo-Mjøsa area. Modified from Nakrem and Worsley (2013)

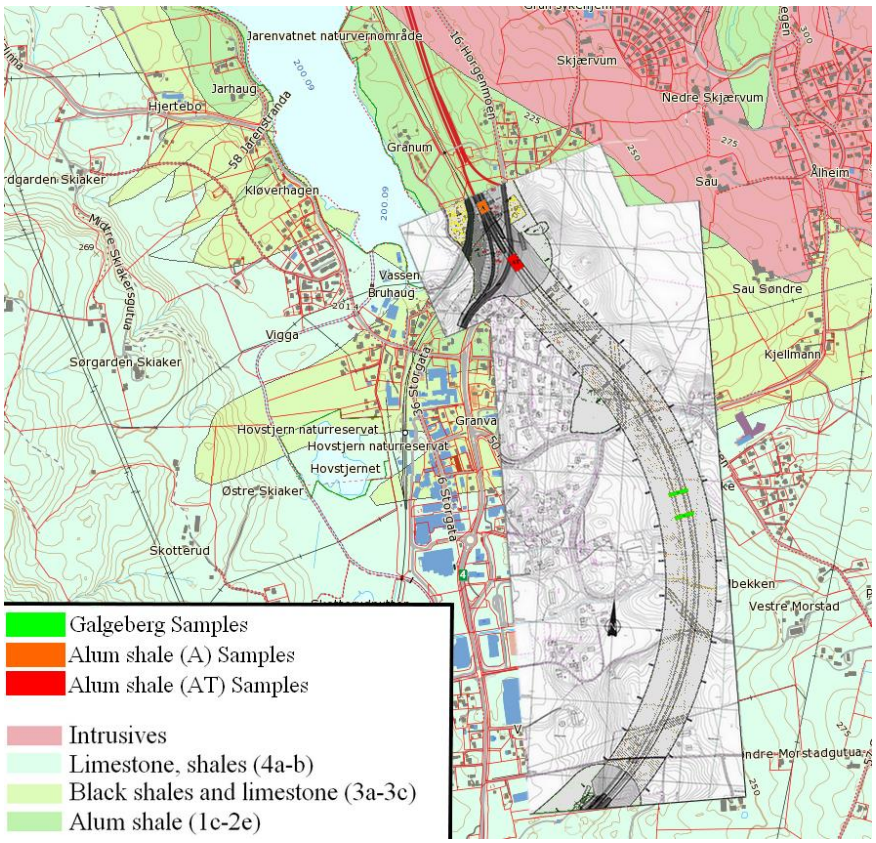

Figure 3: Geological map of Gran, Hadeland with a map of the tunnel and alum shale road-cut added. Sampling locations marked according to Fjermestad et al. (2017).
Modified from NGU (2017), Rambøll (2006a) and Rambøll (2006b).

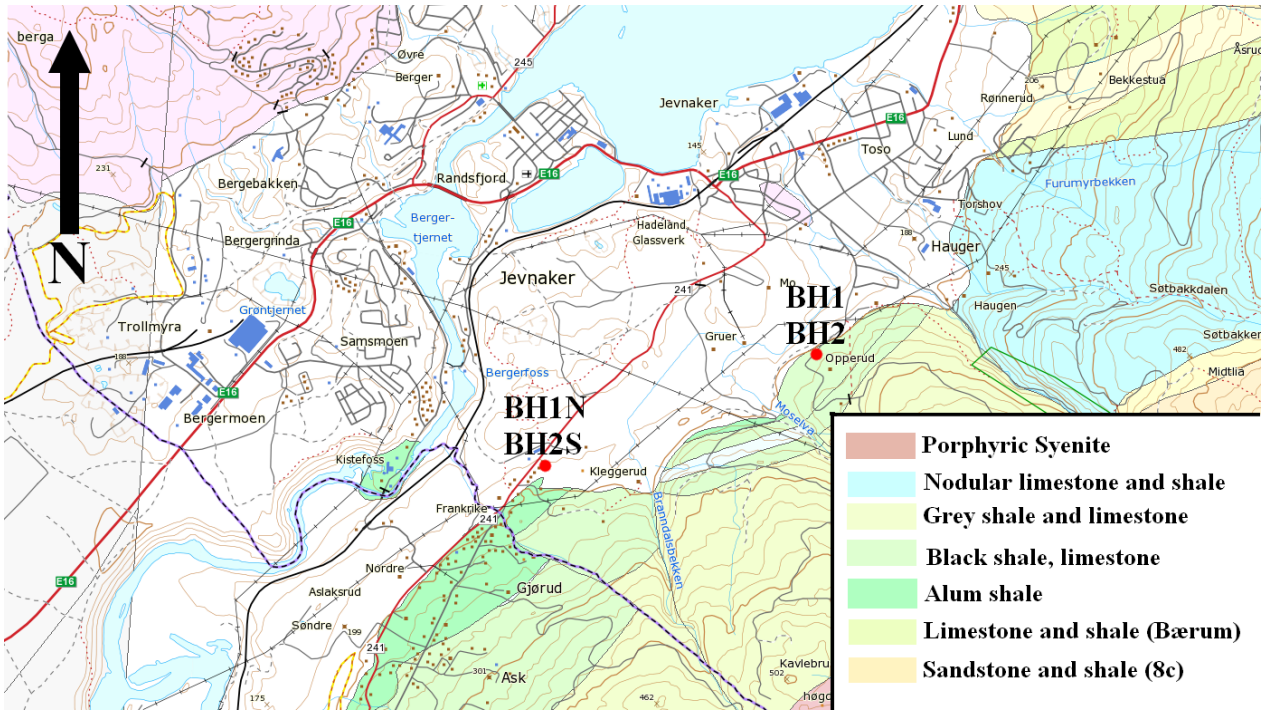

Figure 4: Geological map of the Jevnaker area. Modified from NGU (2017), with sampling (core) locations marked according to information from Multiconsult (2014)

2.2 Hydrogeological setting

The alum shale depot is situated in an old bog where the original material was replaced by alum shale material (Figure 5) and later used as a fundament for the new road (Fjermestad, 2017). The shale is supposed to be stored below the groundwater table, where the deeper groundwater is expected to have low oxygen content (Skipperud et al., 2016) and not contribute to oxidative weathering. The groundwater is supposed to have a long residence time in the depot, due to relatively impermeable rock on each side of the depot acting as a natural barrier and low recharge to the depot area (Fjermestad, 2014, Skipperud et al., 2016). A synthetic membrane was not installed, but the depot was covered with crushed shale that was classified as environmentally safe, other rock masses and soil (Fjermestad, 2017). The permeability of this covering layer is uncertain, but assumed to be low.

Figure 5: Aerial photo (Eidstuen, 2014) of the area around the Southern tunnel opening at Rv. 4 Gran, underneath Morstad farm in front. The alum shale depot is located to the upper right of the photo.

Water samples from the (then uncapped) depot runoff exhibit concentrations of 77-140 µg/l U, with relatively high concentrations from other elements as well (Skipperud et al., 2016). The U, Mo, As, Ca, V and S concentrations did not go down after a simple treatment process involving sedimentation of particles, indicating that these elements are dissolved in water (not present as colloidal material or particles) and not sensitive to sorption and precipitation processes (Skipperud et al., 2016). The elements Al, Fe, Mn, Co, Ni, Cu, Zn, Cd, Pb and ^{210}Po had reduced concentrations after sedimentation, and thus show different behaviour (Skipperud et al., 2016). Especially Al and Fe are assumed to be in particle form. Release of all these elements from the depot during construction confirms the relevance of investigating alum shale to prevent further mineral reactions during storage and spreading of elements of environmental concern.

3 Literature Review

3.1 Alum Shale Characteristics

Shales are in general composed of fine grained clay minerals, quartz and feldspars, but may also contain carbonates, sulphides and iron oxides as well as organic matter (Boggs, 2014). The composition depends on the depositional environment, which is often affected by the tectonic setting and the source of material. The middle to upper Cambrian alum shales were formed from sedimentation in a stagnant epicontinental sea with a sedimentation rate of 1 mm/ky (Bjørlykke, 1974a, Bjørlykke, 1974b) with relatively high supply of organic material which through degradation lead to hypoxic to anoxic oxygen conditions (Nakrem and Worsley, 2013). Organic carbon present in the depositional environment was not completely consumed through bio-degradation, but preserved in the sediments. Reduction of sulphate during carbon degradation in reducing sediments led to precipitation of sulphides and heavy metals fixated in organic matter by ion exchange and adsorption processes (Armands, 1972).

The rock exhibits a characteristic appearance and smell, with a black shiny presence and foliation with very fine grains together with the characteristic sulphide scent. Alum shale is traditionally distinguished from other shales in the Cambro-Silurian stratigraphy on the basis of its black streak (Nakrem and Worsley, 2013). Newer recommended classification methods under development include comparing the acidification and neutralization potential, the Fe/S content and element content to reference rocks (NGI, 2015, Pabst et al., 2016).

The term “alum shale” comes from the manufacturing of alum during the 17th to 20th century (Sjöblom, 2014). Alum is a group of aluminium sulphates (typically $KAl(SO_4)_2 \cdot 12H_2O$) with several industrial applications for instance as a pigment or in paper production (Falk et al., 2006). Alum shale has in addition been used as a fertiliser, fuel for lime production, brick production and in sulphur extraction (Armands, 1972, Sjöblom, 2014). In Oslo there was an alum plant active between 1737 and 1815 (Bastiansen et al., 1957). The shale has an average Total Organic Carbon (TOC) content of 7-8 %, but there are localities with 30-50 % TOC (Bastiansen et al., 1957) which has previously been considered as fuel (Foslie, 1919), and it has been investigated for possible oil and gas resources (Andersson et al., 1982, Erlström, 2014, Gautier et al., 2014).

Alum shale has become interesting in Sweden because of U and V extraction (Armands, 1972), with 1.5 million tonnes of shale containing 215 tonnes of U being extracted (Sjöblom, 2014). The radioactivity of alum shale is closely related to its U content. The daughter inert radioactive gas Radon is mobile in both water and air (Banks et al., 2000), and of environmental interest with a half-life of 3.8 days (vanLoon and Duffy, 2011). Its daughters ^{210}Po and ^{210}Pb may precipitate to radioactive dust, which leads to negative effects on the environment (Skipperud et al., 2016). Houses in the Gran area at Hadeland show high radioactivity, with 33 % of studied houses having a radioactivity above the threshold value of 200 Bq/m^3 (Jerstad et al., 2005). The threshold value for radioactive waste has been set to 1 Bq/g, which represents 90 mg U/kg in black shales (NGI, 2015). Alum shale of similar age and chemistry is found in Sweden and Estonia, where it due to environmental concerns has been the subject of several studies (Allard et al., 1991, Puura et al., 1999, Falk et al., 2006).

3.1.1 Mineralogy

The mineralogy of the alum shale has been looked in several studies with different objectives. Quartz, mica, feldspar, calcite and pyrite have been found to be the most common minerals in samples from both Oslo and the Mjøsa region, with quartz and mica representing up to 50 % of the total content (Sopp, 1966, Antun, 1967, Bjørlykke, 1974a, Jeng, 1991a). Bjørlykke (1974a) mentions quartz, illite, chlorite, feldspar, calcite and dolomite as the quantitatively most important minerals in the Lower Palaeozoic sediments of the Oslo region, while sulphides are mentioned to be important in some black shales. Similar mineralogy and appearance in surrounding lithologies adds to the difficulty of correctly identifying alum shale. Bjørlykke and Englund (1979) found that the alum shale contained illite and no chlorite, and represented a mineralogically very mature sediment. It is derived from a mature continental source, and transported in suspension through water or air before deposition (Bjørlykke and Englund, 1979).

Bastiansen et al. (1957) identified pyrite as the main sulphide mineral in alum shale from the Oslo region, with the content of pyrrhotite varying and depending on metamorphism. Antun (1967) even mentions the reaction from pyrite to pyrrhotite as a defining character of the extent of contact metamorphism in the Oslo region. The more recent MSc thesis of Abreham (2007) analysed alum shale from a central part of Oslo (Konows gate) and Slemmestad southwest of Oslo, in addition to black shale from Slemmestad. Pyrite was determined to be

the most abundant sulphide mineral in the alum shale, with pyrrhotite, chalcopyrite and sphalerite present as well. Barite was found in minor amounts. Sphalerite, barite, rutile, chalcopyrite, pentlandite, monazite and xenotime are mentioned by Terefe (2016) as accessory minerals.

The alum shale at Billingen, Sweden has a matrix made up of quartz (20-25 %), muscovite-illite (25-30 %), K-feldspar (15-20 %), calcite as well as chlorite and micas, and with about 10-15 % pyrite and 12-17 % organic carbon (Armands, 1972). This can to some extent be considered similar to the Norwegian shale. The feldspars and muscovite-illite show several different compositions and trace elements could substitute in the mineral structure. Mica could be identified optically in the form of minute flakes, while calcite occurs as veins (Assarsson and Grundulis, 1961).

In Maardu, Estonia alum shale has low Ca, Mg and Mn concentrations, a high K/Na ratio, high organic carbon and pyrite contents and high concentrations of U, Mo and V (Pukkonen 1989, via Puura et al. 1999). Pyrite concentrations are estimated to be 4-6 %, with most of the matrix being clay-sized mica-illite minerals as well as K-feldspar (Puura et al., 1999), similarly to the Norwegian shale. During the mining process the alum shale was mixed with the overlying limestone, and gypsum growth was observed where limestone was disposed directly next to alum shale (Puura et al., 1999).

Fjermestad (2013) did a MSc Thesis on the mobility of U and other trace elements in the tunnel rocks at Gran, Hadeland. One sample from the alum shale unit was analysed, with nine samples analysed from other units including other black shales and limestones. Quartz was found to be the dominating mineral, with calcite and dolomite present. Marcasite and pyrite are the main sulphide minerals found in alum- and black shale at Hadeland, while pentlandite and chalcopyrite are found in minor amounts (Fjermestad, 2013, Skipperud et al., 2016)

In terms of mineralogy the studies of the Norwegian alum shales seem to be marginally more relevant to the alum shale roadworks and waste deposit at Hadeland, Norway. This is particularly due to the possible presence of pyrrhotite prone to weathering in the Norwegian samples (Oftedahl, 1955, Bastiansen et al., 1957, Antun, 1967, Abreham, 2007), which is not mentioned by any of the foreign studies. Studies from other regions may still be relevant in order to obtain a sufficient understanding of the connection between mineralogy and trace elements in the alum shale. Despite being a region with extended contact metamorphism, pyrrhotite has not yet been identified in alum shales from Gran (Skipperud et al., 2016).

3.1.2 Trace elements

"Trace elements" is a term commonly used for elements that occur in low concentrations. Increased concentrations of trace elements such as zinc, nickel, copper and uranium in alum shale compared to other lithologies are thought to have its origin in precipitation from seawater under reducing conditions with a low sedimentation rate reducing the dilution by siliciclastic material. Another factor proposed by Snäll (1988) and Leventhal (1991) among others involve the redistribution and precipitation of metals from hydrothermal activity at a later stage such as during the Caledonian orogeny, though this is only relevant where the shale is influenced by other geological processes. The trace elements in alum shale can be situated in several different minerals with different strength, stability and reactivity, affecting the mobility of these elements. Studies of shale have been conducted mainly on unweathered shale in Norway, while Sweden has several studies on unweathered, weathered and industrially processed shale. The degree of weathering before full exposure to weathering can influence the release of weathering products to the environment (Lavergren et al., 2009b), which might explain varying results found by different studies. Due to the varying occurrence in minerals and leaching behaviour of each element, different trace elements will be discussed grouped related to occurrence and behaviour.

One of the key features of the alum shale is the sulphide content, and it is expressed in the 1-7 % values found for S throughout previous studies (Table 1). In studies where several samples have been measured at one location, the average concentrations have been calculated. From the results from previous studies in Table 1 it is clear that concentrations of trace elements in general are elevated in the Scandinavian alum shale, compared to the average values of the Earth's continental crust. From these values there is no clear spatial pattern concerning where the highest trace element values occur. The alum shale sample from Hadeland (Fjermestad, 2013) is similar to the samples from around Mjøsa described by Bjørlykke and Englund (1979). In general the samples from Mjøsa and Hadeland have lower trace elements and sulphur concentrations than most of the other studied alum shales. While the Oslo-Asker alum shale in Bjørlykke and Englund (1979) has slightly higher values than the Mjøsa alum shale, the values are lower than what is found by Abreham (2007) in the same region (apart from S and U).

Table 1: Overview of selected data from previous alum shale studies in Norway and Sweden. The highest measured value of each element is written in bold.

Study	Description	S (%)	TOC (%)	Ni (ppm)	Zn (ppm)	Cd (ppm)	Sr (ppm)	Co (ppm)	U (ppm)	Mo (ppm)
Abreham (2007)	Konows gate, Oslo	5.3		151	132			64	120	
Abreham (2007)	Slemmestad	2.3		252	141			**103**	108	
Abreham (2007)	Black Shale, Slemmestad	0.5		114	99			45	5	
(Nyland and Teigland, 1984)	Upper Cambrian, Norway		8.9	154	85				40	210
Fjermestad (2013)	Gran, Hadeland	1.4		85	202	2-5		80	33	21
Bjørlykke and Englund (1979)	Alum Shale, Mjøsa	1.9	7.9	125						
Bjørlykke (1974a)	Alum Shale, Oslo-Asker	5.9		125	141				150	
Armands (1972)	Upper Cambrian, Sweden	6.7	13.7	160	149		40	<50	206	270
Leventhal (1991)	Avg. Jämtland Autochthonous, Sweden	6.2	5.0	155	73			31	60	99
Leventhal (1991)	Avg Jämtland Allochthonous, Sweden	4.7	12.9	**470**	**440**			23	201	312
Falk et al. (2006)	Alum shale, Öland			107	277	**5.5**				
Lavergren et al. (2009b)	Alum shale, Öland	5.91		99.5	241	3.02	**74.8**	20.4	72.6	96.0
(Allard et al., 1991)	Alum shale, Billingen	**7.0**	**15.1**	200	130	2.5			**300**	**340**
Average	Scandinavian Alum Shale	4.7	10.6	174	183	3.5	57	52	129	193
Taylor (1964), Nesse (2012)	Earth's continental crust	0.026		75	70	0-2	375	25	1.8	1-5

Nickel and Zinc

Nickel is assumed to be present in the sulphide phase as well as in chlorites, and may be related to S content in alum shale (Bjørlykke, 1974a). Zinc is not enriched to a large degree in the alum shale compared to the rest of the Cambro-Silurian rocks in the Oslo area, and thus shows a different behaviour than for instance Cu (Bjørlykke, 1974a). Antun (1967) found traces of sphalerite in alum shale, and zinc is regarded to be found in relation to sulphides including pyrite (Armands, 1972). Zinc would need to exist in sulphides or silicates separate from pyrite because of the large concentrations (Bjørlykke, 1974a). According to Leventhal (1991) Ni and Zn do not correlate with Fe or Al, and values from allochthonous shale are not correlated with S even if the elements are greatly enriched in these rocks.

Zinc-sulphides is regarded to be as reactive as pyrite (Lavergren et al., 2009a), and can be considered a potential pollutant as Zn is easily released in an oxidising environment (Jeng, 1991b). Contrary to Zn, Ni needs more aggressive leachates to be released into solution (Armands, 1972, Jeng, 1991b). Nickel could be related to sulphides in samples from Hadeland, as it is extracted using hydrogen peroxide, while Zn was extracted from Hadeland samples both using a low pH solution and hydrogen peroxide (Skipperud et al., 2016). This relates Zn to both easily mobilised elements and sulphide minerals (Skipperud et al., 2016). Presence of Fe-(oxyhydr)oxide and Mn-oxides may retard the movement of Ni to a larger degree than Zn in groundwater (Appelo and Postma, 2013). Their leaching pattern is similar according to Lavergren et al. (2009a), but with slightly higher release for Zn.

Cadmium, Cobalt and Strontium

Cadmium is enriched in alum shale compared to the average of the Earths continental crust (Table 1), with values between 2-5 ppm (Fjermestad, 2013). Leaching tests of alum shale material have shown that it has a high mobility, as a large percentage is mobilised by both ion-exchange as well as in both reducing and oxidising conditions (Fjermestad, 2013). The occurrence of Cd in alum shale is uncertain, as Fjermestad (2013) implies a relation to sulphides but Skipperud et al. (2016) mentions an association to carbonates where Cd would replace Ca (Appelo and Postma, 2013). Similarly Sr is mentioned by Bjørlykke (1974a) to commonly substitute for Ca, and to have an average concentration of 57 ppm in Cambrian shales. This is lower than in the average continental crust. The concentration increases in mid-Ordovician (Bjørlykke, 1974a).

Cobalt is enriched in the alum shale, though some reported values are similar to the average continental crust. Cobalt content is sometimes mentioned to follow the S concentration, but this is not universally supported by the values in Table 1 and Table 12. Cobalt has a similar leaching pattern as Ni, and can be related to sulphides in alum shale (Fjermestad, 2013, Skipperud et al., 2016). It is usually found as a divalent ion in neutral pH solutions (Collins and Kinsela, 2010), and can similarly to Cd and Sr replace Ca in calcite (Appelo and Postma, 2013). Transport of Co may be as a dissolved ion, but also complexed with both organic and inorganic ligands as well as bound to colloidal material (Collins and Kinsela, 2010).

Uranium and Molybdenum

Uranium occurs in relatively high concentrations in alum shale (up to 300 ppm), but its occurrence is not yet explained in detail. U^{4+} is the most important form of U in primary minerals, and is only stable in a reducing environment. U^{6+} and the oxy-ion Uranyl (UO_2^{2+}) is formed from oxidation (Armands, 1972). The valence has a large impact on mobility, as hexavalent U is more soluble in water than tetravalent U. A possibility could be that U is transported as a hexavalent ion or uranyl, and reduced to tetravalent before deposition (Altschuler et al., 1958). Uranium is thought to be related to organic phases during deposition, and correlates well with organic carbon in Swedish studies (Leventhal, 1991, Schovsbo, 2002). U resources in alum shale has regularly been driven from the uraniferous kerogen called “kolm”, which is described as lenses up to 10 cm thick and 2 m long (McKelvey, 1955). If U is associated with organic phases, it is thought to occur as uranyl humates (Armands, 1972), but reduction of U^{6+} may relate U^{4+} to organic matter (Altschuler et al., 1958). The relationship between Th/U is low in the alum shale due to a high U content (144-154 ppm) and a stable low (12-14 ppm) Th content (Armands, 1972). A low Th/U ratio is an indication of precipitation from seawater (Dypvik, 1984).

The leachability of U is directly related to the total U content and a large part of available U can be leached by solutions with a pH between 2-8 (Armands, 1972, Skipperud et al., 2016). Lavergren et al. (2009b) found highest concentrations of U in acidic groundwater, though it also has high concentrations in near-neutral waters. In groundwater with a negative redox potential the U content was observed to be lower, relating this observation to insoluble U^{4+} and related minerals (Lavergren et al., 2009b). The highest U concentrations have been found

by Allard et al. (1991) in alum shale briefly used as a source of U. In samples from Hadeland U was extracted using a low pH solution (Skipperud et al., 2016)

Higher than average concentrations of Mo are measured in alum shales, where it is mainly correlated to organic carbon or K-feldspar and not enriched in pyrite (Armands, 1972). Uranium and molybdenum are the only metals to correlate well with organic carbon (Leventhal, 1991). Preliminary concentrations are lower at Hadeland than in Sweden and other samples taken in Norway (Fjermestad, 2013). Leaching tests show that some Mo are released with ion-exchange and changed redox conditions, but most are situated in more stable phases (Fjermestad, 2013).

3.1.3 Mobilization and transport of trace elements

The stability of minerals containing trace elements and the transport properties of trace elements in water depend on pH and redox conditions together with the solubility of related mineral phases, as well as the cation exchange capacity (CEC) of the surrounding material. The CEC is in turn dependent on the amount of organic matter, Fe-oxides and clay minerals present in the environment (Davis and Kent, 1990, Appelo and Postma, 2013). CEC of alum shale has been measured to be between 21.1-22.4 meq/100g (Sopp, 1966), and is mentioned to be mostly dependent on the TOC. The capacity to sorb trace elements also depend on the pH, as the mineral surfaces become protonated or deprotonated as a function of pH (Parks, 1990). The surface has a point of zero charge (PZC) at a certain pH, and a lower pH value indicates conditions where there are less available sorption sites due to protonation leading to higher mobility of trace elements (Davis and Kent, 1990).

Dissolved Organic Matter (DOM) may contribute to trace element transport through complexation with humic acids, leading to increased total concentrations of ions such as Ni^{2+}, Zn^{2+} and Cd^{2+} (Christensen and Christensen, 2000). Binding to colloidal material as well as complexation to organic matter (vanLoon and Duffy, 2011) may explain increased transport of certain trace elements. Since the trace elements are susceptible to sorption, the sulphate concentration may be a better indicator of the amount of sulphide weathering in the shale.

3.1.4 Environmental impact of trace elements

The environmental impact of trace elements and their direct toxicity to humans or animals vary between each element, and different maximal admissible water concentrations are usually given for different elements by the local authorities, European Union (EU), United States Environmental Protection Agency (EPA) or World Health Organization (WHO). Some elements may not pose any environmental risk, and in the case of Zn, Co and Mo possibly be an essential element for human health (Prasad, 2013). Of the trace elements studied here, Ni, Zn and Cd is mentioned by Appelo and Postma (2013) to be important in terms of concentrations in drinking water and health effects.

Local authorities often use a classification scheme where Class I is considered background level conditions while Class V is considered especially hazardous (severe toxic effects). In between class II is defined to be below the Predicted No Effect Concentrations (PNEC), class III giving chronic toxicity and class IV giving acute toxicity (Miljødirektoratet, 2016).

Different threshold values for each class given by various sources are given in Table 2 where some sources only list the guideline value for no observed effects. EPA (2009) gives a threshold value for no health effects for U, equivalent to the upper limit in Class II. WHO (1996) gives a guideline value based on the No Observed Adverse Effect (NOAEL) of Mo, which is in line with the toxicological studies in animals and that Mo is an essential element for humans. Co is not considered toxic for humans in drinking water, but Kim et al. (2006) mentions a guidance value derived from effects on freshwater organisms. Sr is not described as toxic, and EPA (2007) gives relatively high water concentrations before any health effects take place.

Table 2: Environmental guideline values for Ni, Zn, Cd, Sr, Co, U and Mo, based on health and environmental consequences. Class I represents background levels, II is Predicted No Effect Concentration, III chronic toxicity, IV acute toxicity and V severe toxic effects.

Element (source)	Class I	Class II	Class III	Class IV	Class V
Ni (Miljødirektoratet, 2016)	<0,5 µg/l	0,5-4 µg/l	4-34 µg/l	34-67 µg/l	>67 µg/l
Zn (Miljødirektoratet, 2016)	<1,5 µg/l	1,5-11 µg/l	11 µg/l	11-60 µg/l	>60 µg/l
Cd (Miljødirektoratet, 2016)	<0,003 µg/l	0,003-0,08 µg/l	0,08-0,45 µg/l	0,45-4,5 µg/l	>4,5 µg/l
Sr (EPA, 2007)	-	<17 mg/l	17-25 mg/l	>25 mg/l	-
Co (Kim et al., 2006)	-	< 8 µg/l	-	-	-
U (EPA, 2009)	0	<30 µg/l	-	-	-
Mo (WHO, 1996)	-	<0,07 mg/l	-	-	-

3.2 Sulphides and other Accessory Minerals

3.2.1 Sulphides

Sulphides comprise nearly 600 minerals, where only a few are abundant rock forming minerals. Elements necessary for the modern industrial society are often extracted from sulphide minerals, including Cu, Zn, Pb, Sb, Mo, Co, Ni and Ag (Nesse, 2012). Many sulphide minerals have a substantial metallic character, but a widely accepted classification for sulphide minerals is not used (Nesse, 2012).

Pyrite (FeS_2) is an isometric mineral which often appears as cubes and dodecahedrons, but also as spherical framboids made up of several pyrite grains (Nesse, 2012). It is the most common sulphide mineral, and is often found as fine grains in shale precipitated via transition minerals from seawater under sulphate reducing conditions (Berner, 1984). Pyrite formation appears to start with microbial catalysed reduction of sulphate to hydrogen sulphide, continuing with oxidation of hydrogen sulphide by iron-hydroxide before precipitation of an amorphous FeS phase. Subsequent nucleation and crystallization of this amorphous iron-sulphide together with loss of iron or addition of sulphur leads to pyrite formation (Bektursunova and L'Heureux, 2011, Nesse, 2012). It is often associated to other sulphide minerals such as chalcopyrite, galena and sphalerite (Nesse, 2012). Due to release of sulphuric acid after pyrite oxidation, pyrite is often considered responsible for acidification and thus environmental issues.

Pyrite in Norwegian alum shale mainly appears as dispersed euhedral cubes or fine framboidal particles that occurs both dispersed and in concretions (Bastiansen et al., 1957, Nyland and Teigland, 1984). Jeng (1990) expands on this, explaining that massive pyrite appears as porous bodies around framboids. Pyrite aggregates are commonly less than 5 µm in diameter with the microcrystals rarely larger than 0.6 µm. Concretions occur as nodules or flakes (Jeng, 1990). Most of these forms have a high surface area that could lead to high reactivity, and Jeng (1990) mentions framboidal pyrite as particularly important due to the large surface area. The different reactivity of alum shales is often related to pyrite, and Jeng (1991b) relates the framboidal pyrite to high Fe release from a shale sample taken in central Oslo. In Swedish alum shale pyrite is similarly present as thick lenses as well as microscopic to sub-microscopic crystals (Assarsson and Grundulis, 1961).

Pyrrhotite ($Fe_{1-x}S$) is a non-stoichiometric mineral with either monoclinic, hexagonal or orthorhombic symmetry, depending on the Fe content and related to a system of ordered vacancies within the Fe lattice (Belzile et al., 2004). The chemical formula $Fe_{1-x}S$ where x is between 0-0,13 (Nesse, 2012) reflects this variation. Pyrrhotite has been found in contact metamorphic deposits (Jamtveit et al., 1997), which is abundant in the Oslo region.

Bastiansen et al. (1957) and NGI managed to make a concentrate of alum shale where monocline pyrrhotite ($FeS_{1,14}$) was identified using XRD, and Antun (1967) identified the alum shale pyrrhotite as monoclinic and ferromagnetic. Metamorphism is likely to be the cause of the pyrrhotite content in alum shale, as the mineral does not occur in unmetamorphosed shale (Bastiansen et al., 1957, Antun, 1967). The most important factor in this metamorphism appears to be temperature, and reactive sulphides were found in unusually high amounts in alum shales in contact with Permian intrusives (Bastiansen et al., 1957). The transformation of pyrite to more reactive sulphides similar to pyrrhotite seems to occur at lower temperature in conditions with carbon (unknown form, most likely graphite) and H_2O present, similar to the conditions in alum shale (Bastiansen et al., 1957). The occurrence of other sulphide minerals such as chalcopyrite and sphalerite can be related to pyrrhotite formation, as Zn and Cu were either released from the reacting pyrite or taken from surrounding minerals (Antun, 1967). With all the later studies of alum shale, it is clear that there are large spatial lithological differences both related to mineral content and trace element content. It is uncertain how far from Permian intrusives pyrrhotite can be found. Bastiansen et al. (1957) assume that unclear XRD reflections provided by the pyrrhotite in alum shale are due to more structural errors in the monocline pyrrhotite structure. In addition the pyrrhotite content may be both low and reactive during sample preparation (Bastiansen et al., 1957), making identifying the mineral with XRD difficult.

In addition to the main sulphide minerals mentioned above, sphalerite (ZnS), galena (PbS), chalcopyrite ($CuFeS_2$) and arsenopyrite ($FeAsS$) can all be found in sedimentary rocks related to reducing conditions (Nesse, 2012). Pentlandite $(Ni, Fe)_9S_8$ is previously mentioned in relation to alum shale (Terefe, 2016), generally occurs intergrown with pyrrhotite (Francis et al., 1976), and can be associated to chalcopyrite and pyrite (Nesse, 2012). Otherwise the occurrences of these minerals in alum shale are rarely described in detail, other than identifying their presence in the rock.

3.2.2 Phosphates

Apatite $\left(Ca_5(PO_4)_3(OH,F,Cl)\right)$ is a common accessory phosphate mineral, and frequently found as detrital grains in clastic sedimentary rocks as it is relatively stable in most geological environments (Nesse, 2012). The main composition varies with the OH, F and Cl content, but substitution of Ca can occur together with substitution of the phosphate group. Trace elements such as U, V, Mn and Fe can occur in apatite (Nesse, 2012). The ionic radii of U^{4+} (0.97Å) and Ca^{2+} (0,99Å) are virtually identical, and substitution may occur together with an anion such as F^- (Altschuler et al., 1958). This may explain enrichment or leaching of U in apatite, either through groundwater or diagenetic processes. Altschuler et al. (1958) explains that more than 50 % of the U in apatite is tetravalent, while the hexavalent U may be sorbed as uranyl ions. The apatite uptake of U^{4+} from solution may allow for reduction of more U^{6+} or uranyl in the depositional environment, described by Altschuler et al. (1958) as regenerative uptake.

Monazite $\left((Ce,La,Th)PO_4\right)$ is stable in weathering environments, and may be found in sedimentary rocks as a heavier mineral (Nesse, 2012). It can contain most of the lighter Rare Earth Elements (REE), but Ce, La and Th are the most common. Armands (1972) found that REE's in alum shale could account for 0.02 % of the total rock, with La, Ce and Nd commonly found.

3.3 Chemical Reactions in Alum Shale

Weathering of alum shale by oxygen and water is believed to cause problems for constructions and buildings in addition to the release of toxic elements. The Geological Museum (W. C. Brøgger's house) at Tøyen in Oslo, built between 1911-1917 (NHM, 2007), is built on top of alum shale and has been deformed because of expansion of the alum shale (Bastiansen et al., 1957, Nakrem and Worsley, 2013). Forty years after construction active deformation still occurred, suggesting possible long term effects of alum shale weathering. During construction of the railway between Jaren and Røykenvik, Hadeland alum shale was used as filling material. Weathering of this shale caused development of high temperatures and the railway had to be lowered in places (Bastiansen et al., 1957). Quicker weathering reactions with alum shale are also reported by Bastiansen et al. (1957), where expansion of several centimetres occurs within the first year after exposure. Exposed alum shale that does

not exhibit such expansion or unusual weathering patterns are also reported, suggesting that not all alum shales are equally reactive. Despite the similar age and chemical content, the Swedish shales have not proved to be as problematic as the Norwegian shales (Bastiansen et al., 1957). Oxidation of pyrite and following trace metal release is the dominating weathering process in alum shale (Allard et al., 1991). It is observed that larger pyrite particles can seem unaffected even if the rest of the shale sample is fully weathered, and Bastiansen et al. (1957) assumes that this part of the sulphide content cannot be related to the high reactivity of alum shale. A pyrrhotite content of 0.01 % has been given as a threshold value concerning increased reactivity and effect on constructions.

Weathering products of alum shale can be either ions dissolved in runoff water or secondary minerals. Acid produced during sulphide oxidation may increase the weathering of micas and feldspars, and mobilise both light and heavy elements situated in these minerals (Jeng, 1991a, Jeng, 1991b). Studies have shown release of elements with high pH solutions (Skipperud et al., 2016). High K^+ concentrations in water can be attributed to the mica and feldspar content of the shales, while Fe release is mostly related to pyrite oxidation (Jeng, 1991a). High concentrations of Ca^{2+} and Mg^{2+} in water samples are related to the presence of calcite (Jeng, 1991a) and possibly mica. Water samples taken by Lavergren et al. (2009b) showed higher Ca^{2+} concentrations than Mg^{2+}, suggesting that the calcite in alum shale contains only minor amounts of Mg. Jeng (1991a) found that Ca^{2+} and Mg^{2+} were released in larger amounts than K^+, and relates this to a smaller ionic radius.

Secondary minerals formed during alum shale weathering are generally believed to be different kinds of hydrated sulphates such as gypsum ($CaSO_4 \cdot 2H_2O$) and jarosite ($KFe_3(SO_4)_2(OH)_6$), which can be related to the oxidation of sulphide bearing minerals as well as free sulphur in the rock. One may experience precipitation of other hydrated sulphates such as pickeringite ($MgAl_2(SO_4)_4 \cdot 22H_2O$), slavikite ($(H_3O^+)_3Mg_6Fe_{15}(SO_4)_{21}(OH)_{18} \cdot 98H_2O$) and ettringite ($Ca_6Al_2(SO_4)_3(OH)_{12} \cdot 26H_2O$) in relation to swelling of concrete, Fe(III)(oxyhydr)-oxides and organic C precipitating as possible secondary phases (Chi Fru et al., 2016, Nakrem and Worsley, 2013). Bastiansen et al. (1957) found that the amount of sulphate released is larger than the amount of sulphur in pyrrhotite in alum shales, implying that pyrite weathers at the same time. They found that the sulphate content in alum shale solutions is dependent on oxygen availability, and that ferrous iron is found in elevated conditions until the water is exposed to oxygen.

Weathered and burnt (in industry-related deposits) alum shale samples generally feature a lower pH than non-weathered samples, a characteristic that can be attributed to the production of sulphuric acid during weathering/burning (Falk et al., 2006). Alum shale deposits related to lime production have been found to feature a higher pH than weathered and processed shale used for alum production (Falk et al., 2006). Metal concentrations have been found to be high in non-weathered rock samples (Table 1), and lower in weathered and burnt samples (Falk et al., 2006). This can be related to higher mobility of metals at low-pH conditions found in weathered and processed shale. Release of trace elements have been connected to changes in pH, especially after 8-12 weeks during a leaching test (Falk et al., 2006). Field studies have shown that the concentrations of trace elements in acidic groundwater is poorly correlated with the relative enrichment in the shale (Lavergren et al., 2009b), which could be related to trace element occurrence in minerals with different weathering properties and the aqueous transport properties of the elements.

PHREEQC groundwater modelling has shown that the presence of calcite inhibit the pyrite oxidation rate, while pyrrhotite catalyses pyrite oxidation (Abreham, 2007). Catalytic effects with both pyrite and pyrrhotite present were also suggested by Oftedahl (1955) and Bastiansen et al. (1957). Modelling of gypsum growth investigate the assumption that formation of this mineral is responsible for the apparent swelling of the alum shale. The amount of gypsum precipitated as a secondary mineral was found to be dependent on the amount of calcite, pyrrhotite and oxygenated water available in the alum shale (Abreham, 2007).

3.3.1 Aqueous oxidation

Oxidation of pyrite and other sulphide minerals is thought to be the main acidifying process in the alum- and black shales of the Oslo region. The steps of pyrite oxidation are described by Appelo and Postma (2013), starting with the oxidation of disulphide to sulphate using oxygen:

$$FeS_2 + \frac{7}{2}O_2 + H_2O \rightarrow Fe^{2+} + 2SO_4^{2-} + 2H^+ \quad (1)$$

Incomplete oxidation of disulphide from this reaction generates a solution where divalent iron and sulphate is enriched (Appelo and Postma, 2013).

The reaction continues with the oxidation of Fe^{2+} to Fe^{3+} using oxygen:

$$Fe^{2+} + \frac{1}{4}O_2 + H^+ \rightarrow Fe^{3+} + \frac{1}{2}\,H_2O \tag{2}$$

Depending on pH, iron may hydrolyse and precipitate.

$$Fe^{3+} + H_2O \Leftrightarrow Fe(OH)_3 + 3H^+ \tag{3}$$

Reactions (1) and (2) is thought to only oxidise, while the hydrolysis reaction may go both ways releasing Fe^{3+} into solution during changes in redox conditions (Figure 6).

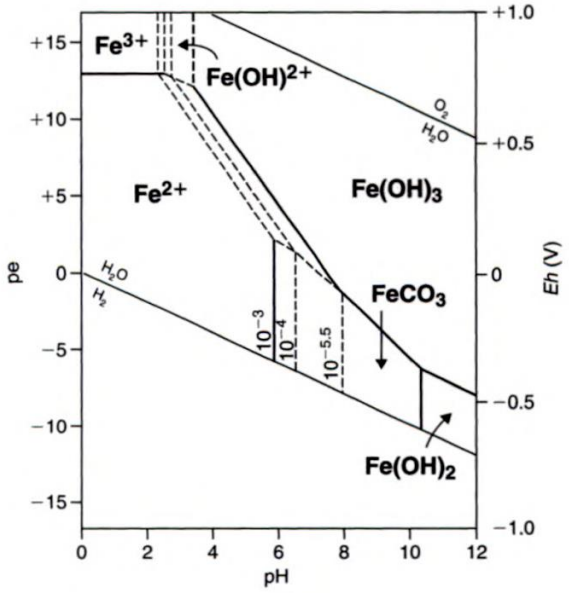

Figure 6: Redox stability diagram for iron at 25°C, with solid solution boundaries specified for different Fe^{2+} concentrations. Figure from Appelo and Postma (2013).

The described pathway is considered the normal route of pyrite oxidation in oxic conditions, and oxidation of one mole of pyrite leads to release of four moles of acid-equivalents (H^+). The reactions show pyrite oxidation as an oxygen dependent process, and reducing the oxygen availability would be an obvious solution to the acidification. Laboratory experiments describe this as a slow process, but field examples both with regular mine waste and alum shale show a more vigorous behaviour. Pyrite may also be oxidised by trivalent iron (Appelo and Postma, 2013), a process which is quicker:

$$FeS_2 + 14Fe^{3+} + 8H_2O \rightarrow 15Fe^{2+} + 2SO_4^{2-} \tag{4}$$

Since the trivalent iron solubility is low with higher pH (Figure 6), this reaction is dependent on the oxidation of divalent iron and dissolution of previously precipitated iron. The oxidation may be accelerated by bacterial catalysis of *Thiobacillus ferrooxidans*, enabling a rapid oxidation of pyrite at low pH (Kirby and Brady, 1998). This may mean that low oxygen conditions are not enough to remove the potential for acid generation. Such a reaction will though lead to rising concentrations of divalent iron in solution, and the process may still depend on oxygen availability (Jeng, 1991a).

Oxidation of monosulphides may not directly contribute to acidity, as the example with sphalerite shows (Younger et al., 2002):

$$ZnS + 2O_2 \rightarrow Zn^{2+} + SO_4^{2-} \quad (5)$$

Oxidation of pyrrhotite would however contribute to the concentration of divalent iron either rapidly under acidic conditions or more slowly via oxidation and dissolution (Belzile et al., 2004). This reaction is initially acid-consuming (Reaction 6), before producing acid through oxidation of sulphur and iron (Bhatti et al., 1993).

Acidic conditions:

$$Fe_{1-x}S + 2H^+ \rightarrow (1-x)Fe^{2+} + H_2S \text{ (x = 0)} \quad (6)$$

Oxidative conditions:

$$Fe_{1-x}S + 2O_2 \rightarrow Fe_{1-x}^{2+} + SO_4^{2-} \quad (7)$$

Mobilization and oxidation of iron (Reaction 3) may again contribute to more pyrite oxidation through Reaction 4.

Oxidation of pyrite may take several other paths depending on the redox environment, but the end products are in general sulphate and iron oxides (Jeng, 1991a). Twenty to hundred times faster oxidation rate for pyrrhotite compared to pyrite can be attributed to the lower crystal symmetry (Belzile et al., 2004), and similar to pyrite pyrrhotite could be oxidised more rapidly by trivalent iron. Oxidation rate also increases with increasing temperature (Belzile et al., 2004).

3.3.2 Electrochemical oxidation

As mentioned earlier, the presence of pyrrhotite is thought to increase the weathering rate for pyrite. Bastiansen et al. (1957) says that it is more likely that the pyrrhotite crystals affect the pyrite than the weathering products from pyrrhotite doing so. This could imply that a direct contact between pyrrhotite and pyrite is necessary, something that would be commonly found if the pyrrhotite is formed from pyrite by metamorphism (Bastiansen et al., 1957).

Both minerals are considered semi-conductive, and can be mutually catalysing in oxidation processes (Bastiansen et al., 1957). Pyrite may act as both a positive and a negative pole towards pyrrhotite depending on the weathering conditions (Bastiansen et al., 1957). Pyrrhotite is mentioned to behave anodically in mixed-sulphide leaching systems (Bhatti et al., 1993),

If there is a large amount of oxygen present the weathering process seems to affect only pyrrhotite. If there is limited oxygen availability, pyrrhotite seems to first catalyse the oxidation of pyrite crystals directly in contact before being oxidised itself (Bastiansen et al., 1957). This is a possible explanation of the different amounts of sulphate in the weathering products.

Impurities of minor elements in pyrite such as As, Co and Ni may affect the oxidation kinetics. Lehner et al. (2007) found that pyrite containing As, Ni or Co is more reactive than pyrite containing little or no impurities. Pyrite containing the least impurities are the least reactive (Lehner et al., 2007).

3.3.3 Kinetics

The rate of which a chemical reaction and transport may proceed is controlled by several factors. Both the mineral reaction and the transport of water and dissolved elements past the minerals control the rate of weathering. In addition elements may adsorb or desorb to mineral surfaces dependent on the environment, which could affect the weathering rate (Appelo and Postma, 2013). The overall rate in a sequential reaction will depend on the slowest step/process, and it is thus important to identify and describe each process. Rates may be different for each element, as these could have their origin in minerals with different weathering properties, have different sorption properties and different solubilities together with the other ions in solution. Normally rates are either surface controlled or transport

controlled, and in general silicate minerals have a surface controlled rate while salt and some carbonate minerals are wholly or partly transport controlled (Appelo and Postma, 2013).

In general the dissolution rate *R* for a mineral can be described with a specific rate constant *k* for the mineral, surface area *A* related to volume *V* and solution characteristics *g(C)* such as pH, pe and distance from thermodynamic equilibrium (Appelo and Postma, 2013).

A general reaction rate formula using these variables is given by Appelo and Postma (2013):

$$R = k \cdot \frac{A_0}{V} \cdot \left(\frac{m}{m_0}\right)^n \cdot g(C) \tag{8}$$

Where $\left(\frac{m}{m_0}\right)^n$ accounts for changes in surface area and thus reactive surface sites during weathering, as m_0 is the initial moles of solid, m the moles of solid at any given time and n a function of the grain size distribution.

3.3.4 Possible remedial action

The consequences of acid production in alum shale are related to lime content and neutralizing capacity of the rest of the weathering minerals (Jeng, 1991a). Industrial alum shale deposits have proven to be challenging in terms of acid production, and a number of remedies have been tried. Sjöblom (2014) mentions mixing with limestone powder in order to introduce a higher pH, stopping the weathering reaction and transport of trace elements. This is regarded as a very expensive method (Sjöblom, 2014), and requires a large deposit area. Another method is disposal of tailings underneath the water table, where little to no groundwater flow is desired with respect to oxygen input (Appelo and Postma, 2013). A method used for Swedish tailings related to U mining has been a cover of clay moraine and crushed limestone with little to no water percolation (Sjöblom, 2014).

4 Methodology

4.1 Pallet Experiments

4.1.1 Previous work by Statens Vegvesen

The methods used in this study related to the experiments at Gran, Hadeland were developed and used by Statens Vegvesen especially for this road project. A description of the experiment setup including rock- and water sampling done by Statens Vegvesen represented by Halldis Fjermestad follows below, together with modifications applied when monitoring of the experiment was continued by the University of Oslo. More details about the experiment can be found in Fjermestad et al. (2017).

Research sites

Rock sampling and initial site experiment setup have been done by Statens Vegvesen during the roadworks at Rv. 4 Lunner grense - Jaren and during prospecting for E16 Eggemoen - Olum. Rock samples taken from both traditional road-cuts and from the 1.7 km tunnel through Gran were put in pallet containers used for the leaching experiment, while only core samples have been taken from E16. Material for containers A1, A2K and A3 (A) was taken from a road-cut north of the tunnel 23.09.2014 around pole number 9500 (Figure 3, 6670000, 255980; EU89, UTM Zone 33), G1, G2 and G3K (G) were sampled from the tunnel 18.09.2014 between pole number 8514-8520 in the southwards tunnel and 19.09.2014 between pole number 8586-8589 in the northwards tunnel (Figure 3, 6699500, 256400; EU89, UTM Zone 33), and AT1, AT2, AT3K and AT4K (AT) from the tunnel 19.05.2015 just south of the A samples around pole number 9354 (Fjermestad et al., 2017). In addition to the experiments used in this study, Fjermestad et al. (2017) had pallet containers with a mix of black shale and limestone. The rocks from Hadeland have been identified as either alum- or black shale using handheld XRF (Hagelia and Fjermestad, 2016), while the cores from E16 have been classified as either alum shale, limestone, calcareous shale or dikes (Multiconsult, 2014). Coordinates for the core samples are 6685100, 244400; EU89, UTM Zone 33.

Experiment setup

Alum- and black shale were stored outside in plastic containers with an open top, exposed to rainwater and air (Figure 11). Approximately 200 litres of shale were stored in each container. It is unknown what the large plastic containers initially contained, but they were cleaned prior to the experiment. Regular plastic buckets were used to fill up the containers with alum shale (pers. comm. H. Fjermestad, 07.09.2016). Three containers with alum shale from the roadcut (A), four with alum shale from the tunnel (AT) and three using Galgeberg shale from the tunnel (G) were used in this study. The material used in the pallet containers has a grainsize varying from silt to boulders, though only boulders were used in container A1. Rainwater passed through the shale and out of the container to a 20 litre sampling bottle. During the sampling done by Statens Vegvesen the water that had percolated through the large plastic containers passed through air to a funnel placed in the sampling bottle, and was shielded from precipitation by a plastic cover (Fjermestad et al., 2017). This was modified in this study using a continuous flexible plastic pipe attached to both the containers and sampling bottles making it a closed path. Between the sampling conducted by Statens Vegvesen and the sampling done by UiO the sampling bottles were stored at the work rig at Roa, Hadeland.

The setups using alum shale from roadcuts and Galgeberg shale were initialised by Statens Vegvesen in October 2014, while the setups using alum shale from the tunnel were initialised in May 2015. Some of the containers had minor amounts of lime produced by Franzefoss Miljøkalk AS added to them (Figure 7) in order to see if this had any effect on weathering (Fjermestad et al., 2017). It is possible that traces of concrete used during tunnel construction have been included in the containers as well (Fjermestad et al., 2017). Details can be found in Table 3, while the sample locations can be viewed in Figure 3.

Table 3: Overview and description of rock samples used in the pallet experiments

Sample	Lithology	Comments
G1	Galgeberg	From tunnel
G2	Galgeberg	From tunnel
G3K	Galgeberg	From tunnel, added 10 litre of granulated dolomite
A1	Alum Shale	From roadcut
A3	Alum Shale	From roadcut
AT1	Alum Shale	From tunnel
AT2	Alum Shale	From tunnel
AT3K	Alum Shale	From tunnel, added 10 litre crushed limestone
AT4K	Alum Shale	From tunnel, added 20 litre crushed limestone

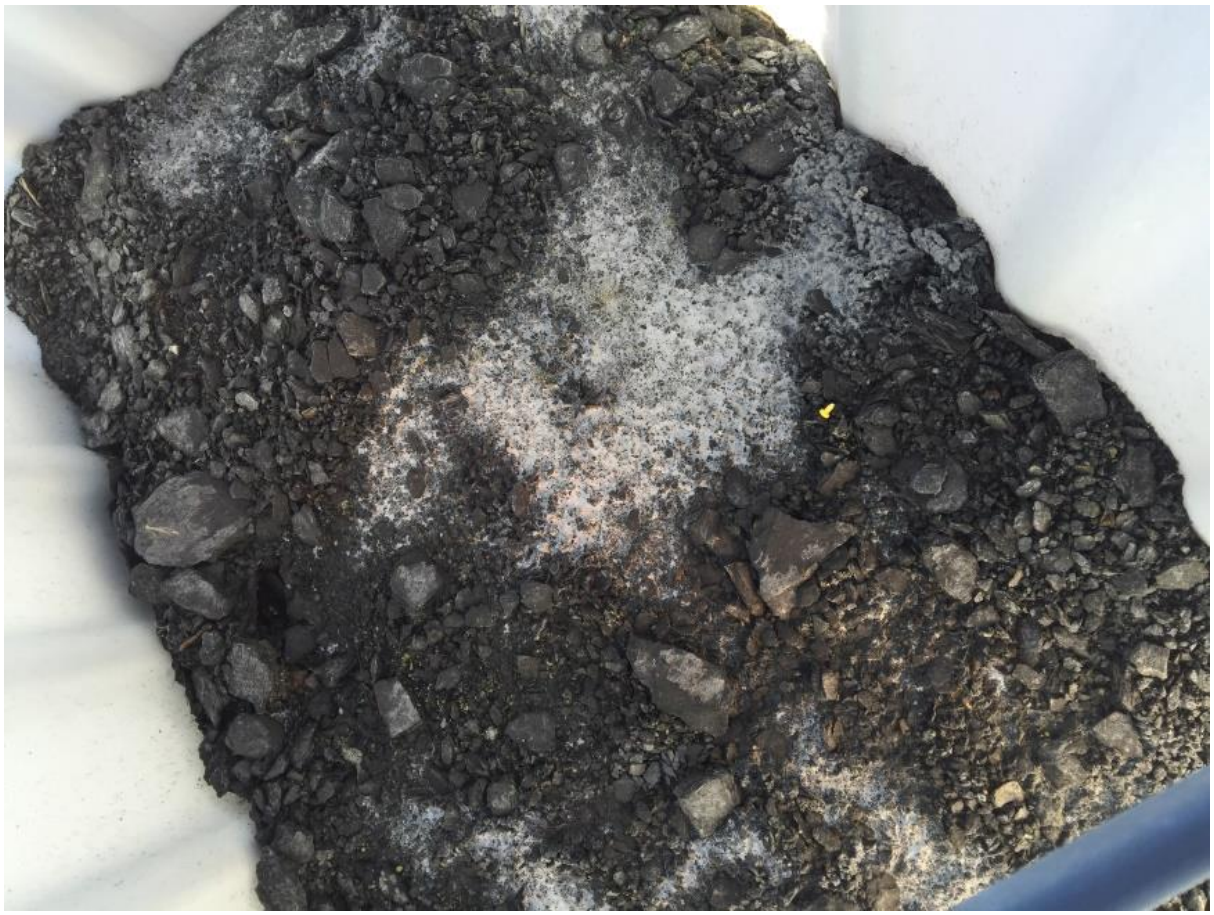

Figure 7: Alum shale surface inside a pallet experiment, most likely AT3K or AT4K due to the lime residues. The material is visibly heterogeneous in terms of grainsize.

Water Sampling by Statens Vegvesen

Water was sampled by Statens Vegvesen from the 20 litre sampling containers with an initial weekly sampling interval. Longer, irregular intervals were introduced after four weeks. In dry periods tap water was added to the containers in order to obtain enough sample volume, in wet periods rainwater was used. The pallet experiments were initiated in late 2014, and until December 2015 the sampling and analyses were conducted by Statens Vegvesen. Results from analyses before 2016 are also commented by Fjermestad et al. (2017).

4.1.2 Rock Sampling

Rocks from the pallets were sampled 07.09.2016 at the Statens Vegvesen rig at Gran. Nine samples were taken, one rock from each experiment with alum- or black shale only (Table 3). The rocks were selected based on size and the amount of weathering, where less weathering was considered desirable due to the objective of studying unweathered rock as well as

practical reasons like sample durability. These rock samples are supposed to form the basis of analysing the mineralogy and chemistry of the shales at Hadeland. After the initial rock sampling, the pallet experiments were moved to a new location by the old football field at Roa.

At 05.10.16 eight more samples of alum shale were obtained from the two cores taken at the new E16 – Jevnakerveien (Figure 8). Samples were chosen based on the information provided by Multiconsult (2014), and picked from different core depths with the goal to reflect the local variation in the lithology. A stratigraphical description or bulk chemistry analysis of the cores are unavailable. Samples were only taken from the cores BH1N (Figure 9) and BH2S (Figure 10) as these were the only one containing a significant amount of alum shale (Multiconsult, 2014). The rock samples were named according to which core and depth they were taken from, and are marked in Figure 9 and Figure 10.

Figure 8: Sampling from the E16 cores.
Left: Overview of BH1N 0-7m. Right: Example of a sample from the E16 cores.

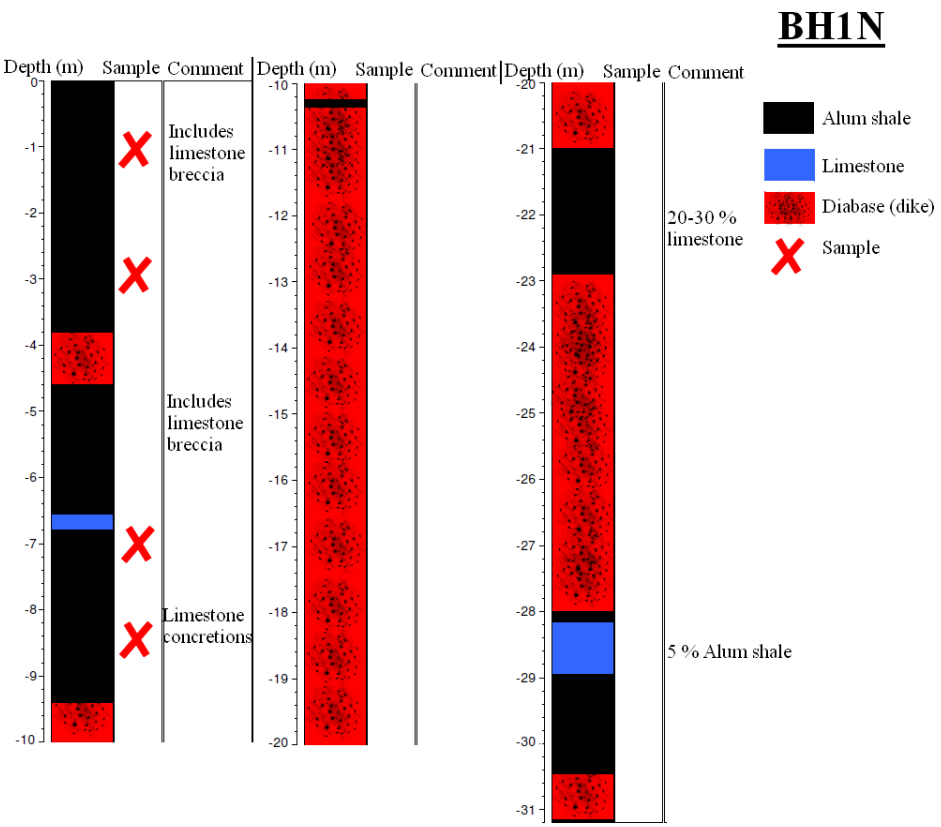

Figure 9: Core log of BH1N, modified from Multiconsult (2014).

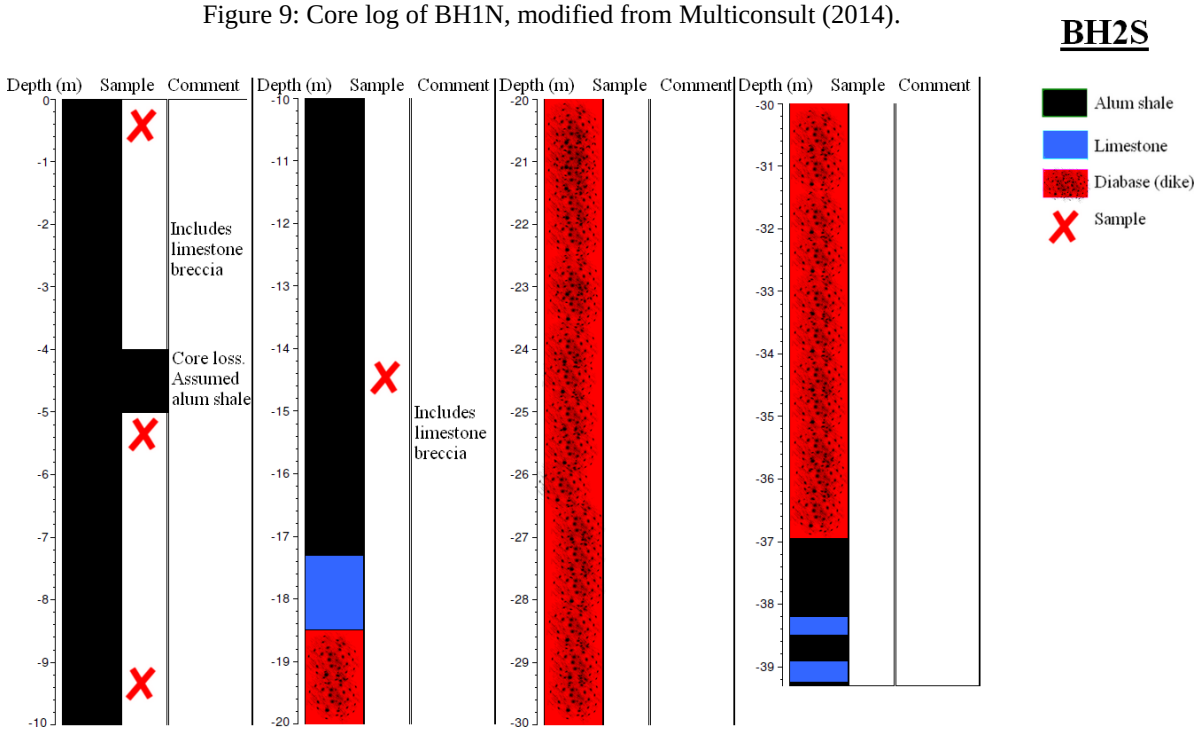

Figure 10: Core log of BH2S, modified from Multiconsult (2014)

4.1.3 Water Sampling

Collection of water by the University of Oslo started at 21.09.16, and samples were taken 05.10, 19.10, 01.11 and 16.11. More water sampling was initially planned, but temperatures below 0°C made this impractical due to frozen water in the sampling bottles. Sampling containers were cleaned with tap water before reconnecting them with the experiment.

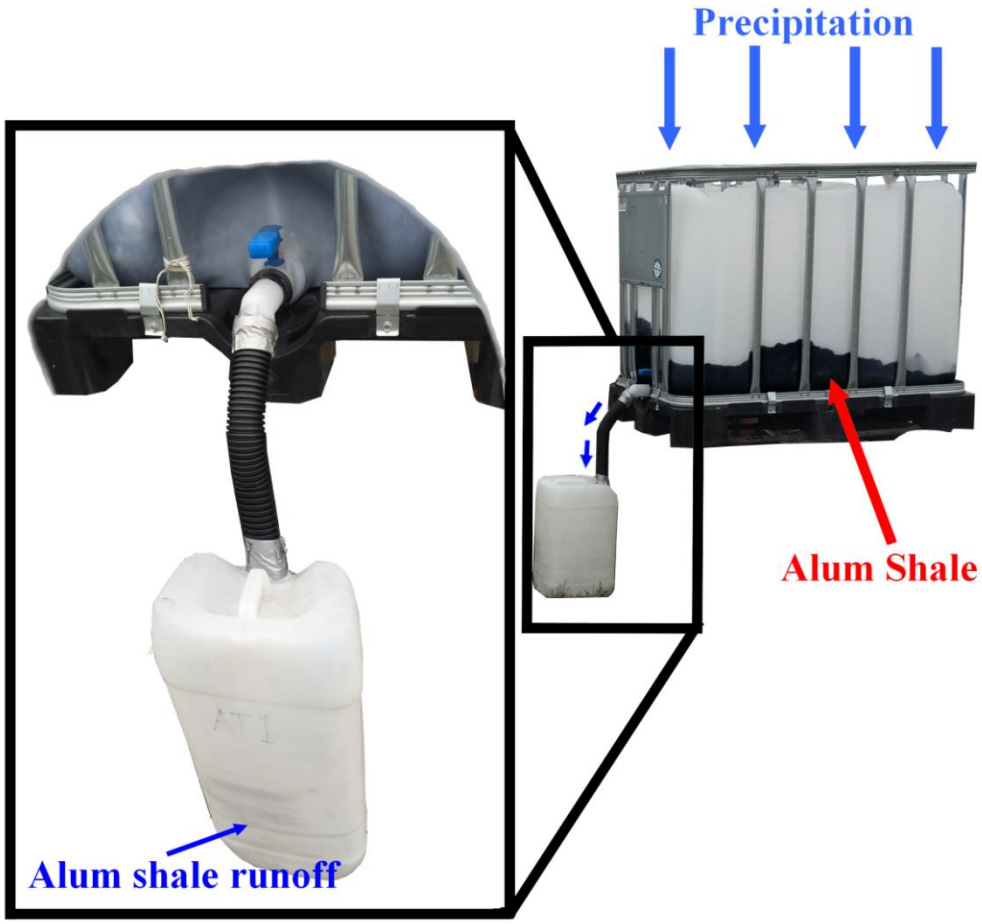

Figure 11: Pallet experiment setup used for this study.

Water from the sampling containers were put into a 1 litre measuring jug where on site measurements of pH, Electrical Conductivity (EC) and Eh were conducted (described in section 4.2.4) and water samples were taken up using a syringe. Water was filtered through 0.45 µm filters to avoid any pollution from particles and sampled in two sampling bottles. One sampling bottle had two to three drops of HNO_3 added in order to avoid precipitation of elements. The HNO_3 was provided by the laboratory at the Department of Geosciences.

After the water samples were taken, the water volume in the 20 l sampling bottles was measured while water was poured out using the 1 litre jug. No significant amount of water remained in the large sampling containers after sampling.

4.2 Mineralogical and Chemical Analysis

4.2.1 X-Ray Diffraction

The interaction of X-rays with minerals allows these mineral structures to be identified, and together with knowledge about the lithology the mineral content of a rock can be determined. All rock samples given in Table 3 and marked in Figure 9 and Figure 10 were analysed, with 16 samples analysed in total.

Diffraction of X-rays from parallel planes of atoms are used to identify the distance between the atom planes (d-spacing) (Nesse, 2012). The X-rays hit the mineral surface at different angles, and reflections of the X-rays in phase are produced at certain angles for different minerals. The relationship is defined by the Bragg equation:

$$n\lambda = 2dsin\theta \quad (9)$$

Here n is an integer, λ is the wavelength of the X-rays, d is the interplanar spacing and θ is the diffraction angle (Nesse, 2012).

Because each mineral has many different atomic planes that potentially scatter and diffract X-rays, a powdered sample is used for the analysis to provide as many orientations as possible (Nesse, 2012). This is commonly referred to as the *Powder Method*. In this case samples were crushed, milled and placed on sample holders. Crushing was conducted using a small swing mill. The samples were then milled down to approximately 10 µm using a McCrone Micronising Mill, with 3.2-3.5 g of sample taken into the mill together with 8-9 ml of ethanol and run for 12 minutes. Afterwards the samples were dried (heated to 50°C). For both crushing and milling the equipment was cleaned thoroughly with tap water and ethanol between samples. After milling the samples were dried and placed on sample holders parallel to the sample holder surface without orientating the minerals too much. The samples were run through a Bruker D8 Advance with DaVinci design, a Lynxeye detector and Cu tube radiation of 1.54Å generated by a voltage of 40 kV (Department of Geosciences, 2011b). Orientation of

minerals may give unlikely high intensities, especially for clay minerals which have a prominent preferred orientation. Intensities can be affected if the samples are not grounded small enough (Nesse, 2012). The samples here have similar characteristics overall, and an eventual error in a sample will be evident because the result may not be found in any other sample.

The results are given as diffractograms which is interpreted through DIFFRAC.EVA provided by Bruker using the *Powder Diffraction File* (PDF) database published by The International Centre for Diffraction Data (Department of Geosciences, 2011b). Each mineral gives several peaks, where one usually has significantly larger intensity than the others (Nesse, 2012). This major peak and at least two other peaks were considered necessary to identify minerals. Each peak represents a certain d-spacing in the mineral unit cell, and the intensity is due to the x-ray reflectivity of the atomic planes (Nesse, 2012). The diffractograms produced will in this case include peaks for all the minerals present in the sample. When one mineral is identified, all the peaks belonging to that mineral are removed. This process is then repeated until most peaks in the diffractogram are assigned to a mineral. DIFFRAC.EVA is mainly used for identification of minerals, but is also semi-quantitative based on the intensity of the peaks.

Due to inaccurate instrument zero calibration, the x-axis was shifted towards the right in most samples. Because quartz is assumed to be present in all the samples, the 3.346Å peak was used for calibration of the diffractogram. The diffractogram was modified using the strip kα function in DIFFRAC.EVA, minimizing the effect of the kα2 peaks. When several minerals showed a possible fit, previous studies were consulted and the most probable mineral was chosen. Since the detection limit of XRD is 1-2 %, accessory minerals cannot be definitely identified. Only one feldspar phase was selected for each sample to avoid overestimation of feldspars, and avoid using the same peaks for different minerals. The major peaks used for each mineral are given in Table 4.

Table 4: Major peaks used for identifying minerals in the XRD diffractogram.

Mineral	Peaks
Quartz	3.346Å, 4.26Å, 2.46Å, 2.28Å, 2.24Å, 2.13Å, 1.98Å
Muscovite-Illite	10Å, 2.56Å
Calcite	3.035Å, 2.495Å, 2.285Å, 2.095Å
Pyrite	2.71Å, 2.42Å, 2.21Å
Pyrrhotite	3.00Å, 2.65Å, 2.08Å
Microcline	3.245Å, 3.83Å, Minor peaks
Albite	4.02Å, ~3.2Å

A quantitative analysis using Siroquant provided by Sietronics was done in February 2017, where the mineral selection was based on the previous analysis in DIFFRAC.EVA. The method used in Siroquant is described by Hillier (2000). If any peaks were not taken into account these were further investigated and revisited in DIFFRAC.EVA before running Siroquant an additional time. A Last Global Chi Squared factor of less than 3.5 and an R factor of less than 0.2 were considered to be sufficient for a good analysis.

It is important to keep in mind that the quantity of minerals compared to total rock content may be overestimated as amorphous substances such as Fe-oxides and organic carbon are not taken into account. The mineral quantification is affected by the lack of ability to identify accessory minerals, and can only represent the relative composition of the major mineral components of the alum shale.

4.2.2 Thick Sections and Scanning Electron Microscope

Rock pieces for thick sections were prepared using a diamond saw. Initially thin sections were supposed to be made, but due to high risk of losing sample material during grinding it was decided to make the thin sections thicker than usual. This is the reason for using the term “thick section”. This is not optimal for a normal petrographic analysis underneath a polarizing microscope as it will not be transparent, but it is sufficient for an analysis with a Scanning Electron Microscope (SEM). The thick sections correspond to the samples previously taken at

Hadeland and analysed using XRD. Several pieces of rocks were prepared from each sample, at different angles and directions with respect to the structure in the shale. This was done to get a best thick section possible, and to minimise any effects due to spatial differences. Only one thick section was made for each sample. Sample G1 proved to be too weathered for a proper rock piece, while the AT2 thick section failed during preparation with all the rock flaking off the glass. Several other samples lost some of the thick section material due to flaking under preparation.

The thick sections with the least flaking or calcite inclusions (AT1, A3, BH2S-9-10m) were chosen to be analysed with SEM first. These are assumed to be representative for the bulk of the shale, and relevant to investigate when it comes to accessory minerals and trace element distribution in the shale. The thick sections from each sampling location with the least flaking were analysed first. The thick sections were coated with carbon by Berit Løken Berg using a Cressington 208C (Department of Geosciences, 2011a) before the SEM analysis. This is in order to inhibit charging, reduce thermal damage and improve the image (Höflinger, 2013).

The equipment used for SEM was a Hitachi SU500 FE-SEM (Schottky FEG) and in-lens SE-detector, with a Dual Bruker XFlash30 EDS system and HR EBSD system with Argus running on Quantax 800 (Department of Geosciences, 2011a), using the Bruker Esprit 1.9.4 graphical user interface. A SEM strikes the sample with an electron beam, and afterwards records electrons that has interacted and emitted from the sample (Nesse, 2012). The electron beam systematically sweeps the thick section surface, and the sweeping velocity was chosen according to the preferred amount of detail. During SEM heavier elements appear brighter due to a higher backscatter of electrons, and because of this pyrite and other heavy minerals are visually brighter sections compared to the shale matrix. Sections with heavy minerals were selected and both point measurements of element content and element mapping of a section were conducted. Adjusting the brightness and contrast of the scan helped distinguish between different types of heavy minerals.

The elemental composition of points was visualised as elemental spectrums (Figure 19), where relative elemental composition creates known spectrum patterns used to identify the mineral. The distribution of elements in the mappings was visualised with different colours representing different elements.

4.2.3 Column experiments

Due to the small amount of rock samples available from E16 – Jevnakerveien, it was decided to conduct a simple lab column experiment to estimate the reactivity of this alum shale. From the eight samples taken four shale mixes were made by crushing with a small swing mill in a similar manner as the XRD preparation. The shale samples were mixed in order to have enough material for repetitions. The mixing effect is considered to be minimal since both mixes were obtained using samples from the same core and at similar depths. The crushed shale was then mixed with beach sand to provide sufficient permeability, and filled into syringes acting as columns.

Four columns were prepared with shale/sand mix, while a fifth column was filled with the sand in order to estimate any contribution of trace elements from the sand. The mixes consisted of approximately 70 wt. % of sand and 30 wt. % alum shale, as approximately 70 g sand and 30 g shale was mixed. The sand contribution could be estimated using equation 10:

$$K(\%) = \frac{C_K \cdot \left(\frac{m_s}{m_s + m_a}\right)}{C_C} \cdot 100 \qquad (10)$$

Here *K(%)* is the sand contribution percentage, C_K is the concentration measured in the control column, m_s is the mass of sand, m_a is the mass of alum shale. C_C is the concentration measured in column 1, 2, 3 or 4 at the same date. The data for the different columns are available in Table 5.

Table 5: Experiment setup, with the mass of shale and sand mix and the mass used in the columns.

Samples	BH1N-3m	BH1N 7 and 8m	BH2S 5 and 9-10 m	BH2S 15m	Sand
Column	1	2	3	4	K
Mass column (g):	29.4	27.3	28.9	28.8	27.8
Mixing box mass/w lid (g):	34.5/44.5	34.5/44.3	34.5/44.2	34.5/44.3	n/a
Sand (g):	69.7	69.9	69.7	70.0	100.0
Shale (g)	30.3	30.1	27.4	30.0	0.00
Filled column (g):	59.3	97.6	88.6	87.1	90.8
Filled column - column weight (g):	29.9	70.3	59.7	58.3	63
Mass sand in column (g):	20.84	49.14	42.85	40.81	63.00
Mass shale in column(g):	9.06	21.16	16.85	17.49	0.00

Milli-Q de-ionised water was then run through the experiment continuously with low velocity using a Gilson Minipuls 3 peristaltic pump. The pump velocity was 7.5 rounds per minute between 07.12.2016 to 15.12.2016, corresponding to a water velocity of approximately 0.175 ml/s. After that the pump velocity was turned down to 1.0 round per minute, corresponding to a water velocity of approximately 1 ml/hour depending on the column. Factors that may affect the water velocity could be column length, porosity of the column material and permeability through the column. These factors are expected to differ between the different columns. Flexible containers were used as water reservoirs, and refilled when necessary. Samples were taken during the weekdays, and the time taken to fill the sampling bottles was measured to be able to calculate the residence time using the formula below.

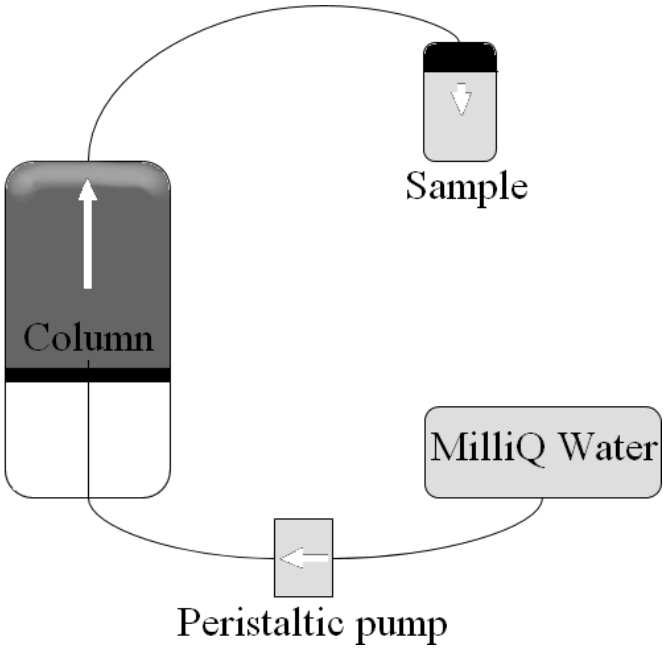

Figure 12: Simplified sketch of experimental setup used in the column experiments.

$$\tau = \frac{V_p}{f} \qquad (11)$$

Here τ is the residence time, Vp is the pore volume in the column and f the measured water discharge. A porosity of 40 % and a column volume of 70 ml were assumed.

The pump was stopped after sampling 21.12.2016, and the water situated in the columns was sampled 16.01.2017 giving a residence time of 26 days.

4.2.4 Water Chemistry Analysis

Water chemistry analysis of the runoff from the Hadeland pallet experiments were done in three parts. While sampling at Hadeland pH, Eh and EC was measured, light cations and anions were analysed at the University of Oslo soon after sampling using Ion Chroma-

tography (IC), and in January 2017 using Inductively Coupled Plasma Mass Spectrometry (ICP-MS). The samples were stored at approximately 4°C until analysis

The on-site measurements of pH, Eh and EC were conducted using Sensorex SAM-1 pH, ORP and conductivity electrodes. These measurements were done in the same container as the one used for taking samples for further analysis. The electrodes were washed with deionised water between each sample, but not calibrated for these measurements specifically. It is assumed that the calibration of the instrument done for earlier studies is sufficient.

Using IC, Na^+, K^+, Mg^{2+}, Ca^{2+}, F^-, Cl^-, SO_4^{2-}, Br^- and NO_3^- were analysed at the chemistry lab at the Department of Geosciences, University of Oslo. Dionex ICS-1000 was used for cations, Dionex ICS-2000 for anions with all reagents and standards made with deionised Milli-Q water. The sample is injected into a stream of eluent and passed through an ion exchange column where ions are separated based on their affinity (Naoroz, 2013), and thus gives different retention times. For cations a methanesulphonic acid eluent was used (Naoroz, 2013), while for anions a KOH eluent was used (Naoroz, 2016). The standards used to make the calibration solutions can be found in Appendix 1.

Due to expectations of high concentrations of certain ions based on the field conductivity measurements, the pallet experiment samples were diluted 10, 100 and 1000 times using Milli-Q deionised water. To ensure sufficient accuracy and to establish a calibration curve, each measurement ran several blank samples and three standard solutions with known concentrations. The system was rinsed with a blank solution, and ran a new standard solution between two blanks before running the samples. After the samples a new blank was run before more standard solutions separated by blanks, in order to confirm the accuracy of the measurements. Data was collected with chromatography software that produces a chromatogram and converts the peaks to sample concentrations. Identification and quantification of ions were calculated based on a comparison with the peak retention times in the chromatogram obtained using the standard solutions (Naoroz, 2016). Different dilution factors were used for different elements in order to be within the calibration values. Anions were not analysed for the lab leaching experiment due to miscommunication.

Trace elements were analysed at the chemistry lab at the Department of Geosciences, University of Oslo, using ICP-MS (Bruker Aurora Elite) in order to have a lowest possible detection limit. The elements analysed were Al, V, Cr, Fe, Co, Ni, Cu, Zn, Sr, Mo, Cd, Th, U

and Pb. The sample is nebulised and ionised, and any chemical bonds are destroyed so that the total concentration of an element is measured. Internal standard solutions with known concentrations were used to make a calibration curve relating counts to concentrations. A drinking water standard (TMDW-B) with known concentrations was used to control the measured concentration of the lighter elements, while a different standard (68A) was used for the heavier elements (Appendix 1). Both standards were produced by High-Purity Standards. In order to estimate the accuracy of the measurements, samples were measured five times during each run.

Before running ICP-MS the samples from Hadeland were diluted ten times using 1 % HNO_3, as high concentrations of some elements were expected based on the IC analysis and the conductivity measurements. A diluted sample was run three times before the measurements, to see if concentrations were too high for the machine detection limits. Some elements exhibited too many counts, and the machine sensitivity was thus turned down during the main measurements. The samples from the column experiments were not diluted, but 5 drops of concentrated HNO_3 were added giving roughly a 1 % HNO_3 concentration.

The ICP-MS measurements were run in two portions. One portion with He used as a collision gas for the lighter elements, one portion for the heavier elements using no collision gas. Helium was used as a collision gas in order to limit the interference from other molecules (PerkinElmer, 2011). A rinse was run between every fifth samples. The rinse consisted of a blank sample, and a similar blank sample was run from a different sampling bottle. The rinse may become contaminated from repeated measurements, and this provides a possible error within the measurements.

For the pallet experiments the detection limits of the analysed trace elements in µg/l were: Al: 0.303, V: 0.005, Cr: 0.066, Fe: 1.990, Co: 0.012, Ni: 2.860, Cu: 0.015, Zn: 0.230, Sr: 0.31/0.13, Mo: 0.06/0.0550, Cd: 0.002, Pb: 0.002, U: 0.02.

For the column experiments the detection limits of the analysed trace elements (µg/l) were: Al: 0.180, V: 0.009, Cr: 0.024, Fe: 0.502, Co: 0.007, Ni: 4.630, Cu: 0.010, Zn: 0.045, Sr: 0.137/0.022, Mo: 0.123/0.145, Cd: 0.001, Pb: 0.001, U: 0.014.

4.3 Statistical analysis and Modelling

4.3.1 Correlation analysis

A correlation analysis on the water samples were conducted in order to see which elements behave similarly in an alum shale weathering environment. Water samples was grouped into alum shale from the roadcut (A), alum shale from the tunnel (AT), Galgeberg shale (G) and alum shale from E16 (BH). This is in order to have a sufficient dataset for the data to be representative, and it is assumed that the weathering rock sample within each group has a composition representing the general composition of alum- or Galgeberg shale at Gran. The correlation analysis utilised 10 samples for A and G, while 15 samples was used for AT and 42 samples for BH.

The correlation tool in the advanced data analysis module in Microsoft Office Excel was used to make a correlation matrix. This correlation tool is based on the Pearson correlation coefficient, where the covariance of the two variables is divided by the product of their standard deviation (Equation 12) (Upton and Cook, 2016):

$$r = \frac{S_{xy}}{\sqrt{S_{xx}S_{yy}}} \tag{12}$$

Where:

$$S_{xy} = \sum_{j=1}^{n} x_j y_j - \frac{1}{n}\left(\sum_{j=1}^{n} x_j\right)\left(\sum_{j=1}^{n} y_j\right) \tag{13}$$

$$S_{xx} = \sum_{j=1}^{n} x_j^2 - \frac{1}{n}\left(\sum_{j=1}^{n} x_j\right)^2 \tag{14}$$

and S_{yy} is defined similarly to S_{xx} (Equation 14) (Upton and Cook, 2016).

The correlation matrix consists of numbers between -1 and 1, where values above 0.70 are considered a strong positive correlation and values below -0.70 a strong negative correlation, while values between 0.50-0.70 are considered to represent a weak correlation. The same threshold values were used by Nyland and Teigland (1984). Values closer to zero is considered to represent little to no positive or negative correlation.

4.3.2 PHREEQC Groundwater Modelling

PHREEQC is a computer program based on equilibrium chemistry of aqueous solutions interacting with minerals, gases, solid solutions, exchangers and sorption surfaces, in batch (0D) or including 1D transport (Parkhurst and Appelo, 2013).

All water samples were checked for accuracy using PHREEQC, which incorporates the relationship between cations and anions in water samples as the Electrical Balance (E.B.).

Appelo and Postma (2013) give an equation for the quality of water sampled based on the requirement of zero net charge of aqueous solutions:

$$E.B.(\%) = \frac{\sum Cat + \sum An}{\sum Cat - \sum An} \cdot 100 \qquad (15)$$

The average water sample composition from each experiment (A, AT, G) was added into PHREEQC using the SOLUTION_SPREAD function. For the inverse modelling, the solutions were charge balanced with SO_4^{2-} since sulphate is the main anion in every solution, and because the high measured concentrations (Section 5.2.1) implies that this value has a larger possible error.

The LLNL database was used, prepared at the Lawrence Livermore National Laboratory by Jim Johnson and converted to PHREEQC format by Greg Anderson with help from David Parkhurst (Anderson and Parkhurst, 2015).

In order to run an inverse model, the elements and ions assumed to be unimportant in the main mineral composition of the alum shale was removed. Sr, Mo, Cl, Cr, Cd, U, F^- and NO_3^- is assumed either reside as impurities in the included phases, or occur in the system as a conservative element. Nickel is assumed to reside in sulphides, but the most likely phase

(pentlandite) is not included in the database. The model uses the INVERSE_MODELING function in PHREEQC, which attempts to determine sets of mole transfers of phases that account for changes of water chemistry between two water samples (Parkhurst and Appelo, 2013). The uncertainty of the model was set to 0.05, with the multiple-precision version of the optimization solver Cl1 activated with a tolerance set at 1e-7. The default tolerance in PHREEQC is 1e-12 (Parkhurst and Appelo, 2013). In addition mineral water was not taken into account in this model.

The phases used in this model were forced to either dissolve or precipitate. Pyrite, illite, muscovite, maximum_microcline, albite, chalcopyrite, sphalerite, calcite, O_2(g) and CO_2(g) were assumed to only dissolve, while gypsum, jarosite, $Fe(OH)_3$, goethite, gibbsite, kaolinite, montmor-Ca (smectite) and C were forced to precipitate. In addition to CO_2(g) and O_2(g) the dissolving phases were minerals that have either been found in the XRD or SEM-analysis, while the precipitating phases are common secondary weathering minerals either found in relation to alum shale in previous studies or in weathering in general.

Assuming a constant weathering rate is obtained, the time it would take to dissolve a certain mineral completely was calculated by the formula:

$$t[y] = \frac{m[g]}{f_m\left[\frac{g}{d}\right]} \cdot \frac{1[y]}{365[d]} \tag{16}$$

Here m is the mass of the mineral, and f_m is the calculated weathering rate. The mass of the mineral is calculated using the mass of the shale situated in the container m_s and a chosen percentage value min based on the results of the mineralogical analysis.

$$m[g] = m_s[g] \cdot \min[\%] \tag{17}$$

The weathering rate is calculated using the results from PHREEQC f_M, the molar mass of the mineral Mm, and the average volume of the samples V multiplied with 1/14d as the model represents the amount of weathering in 14 days.

$$f_m\left[\frac{g}{d}\right] = f_M\left[\frac{mol}{l}\right] \cdot Mm\left[\frac{g}{mol}\right] \cdot V[l] \cdot \frac{1}{14d} \tag{18}$$

5 Results

5.1 Mineralogical analysis

5.1.1 X-Ray Diffraction

Mineral content from 16 samples representing Alum Shale and Galgeberg shale from Rv. 4 and E16 were measured qualitatively and quantitatively. Silicate-, sulphide- and carbonate minerals were the main constituents of these samples, but the specific mineral composition and relative amounts vary between the samples. Diffractograms of all samples from DIFFRAC.EVA and Siroquant can be found in Appendix 2.

The mineral content is similar in all alum shale samples from Rv. 4 Gran (Figure 13a). The minerals identified are quartz (23.6-36.4 %), microcline (6.9-21.4 %), muscovite-illite (11.7-18.6 %), pyrite (21.7-33.1 %) and calcite (0-33.1 %). There are some variations in the calcite content which affects the relative amounts of the other minerals, and samples with little to no calcite will have higher relative amounts of sulphides and silicate minerals. The Galgeberg shale only consists of quartz (33.3-40.1 %), mica (59.9-63.2%) and pyrite (0-3.5 %), though here only two samples were analysed (Figure 13b).

In terms of the core samples from E16 there are mainly two different mineral compositions. The three uppermost samples (1-7 m) from BH1N (Figure 13c) consist of quartz (23.6-40.8 %), albite (9.6-21.0 %), muscovite-illite (16.7-29.4), calcite (0-17.4 %) and either pyrite or pyrrhotite (12.8-20.2 %), while the 8 m sample is almost pure calcite (94.5 %) with some quartz. Pyrrhotite is identified at 3 and 7 m in BH1N, while the 1 m sample includes pyrite.

BH2S shows a similar mineralogy in the samples taken from 5-15 m down the core. Here 5.3-18.1 % quartz, 8.7-11.9 % pyrite/pyrrhotite, 9.9-15.5 % albite and 59.0-73.4 % calcite have been identified (Figure 13d). The only sample without a considerable amount of calcite is the 1 m sample, where only quartz (45.3 %), muscovite (38.5 %) and pyrite (16.2 %) are detected. Pyrite is found in the 9 m sample, while pyrrhotite is detected at 5 and 15 m.

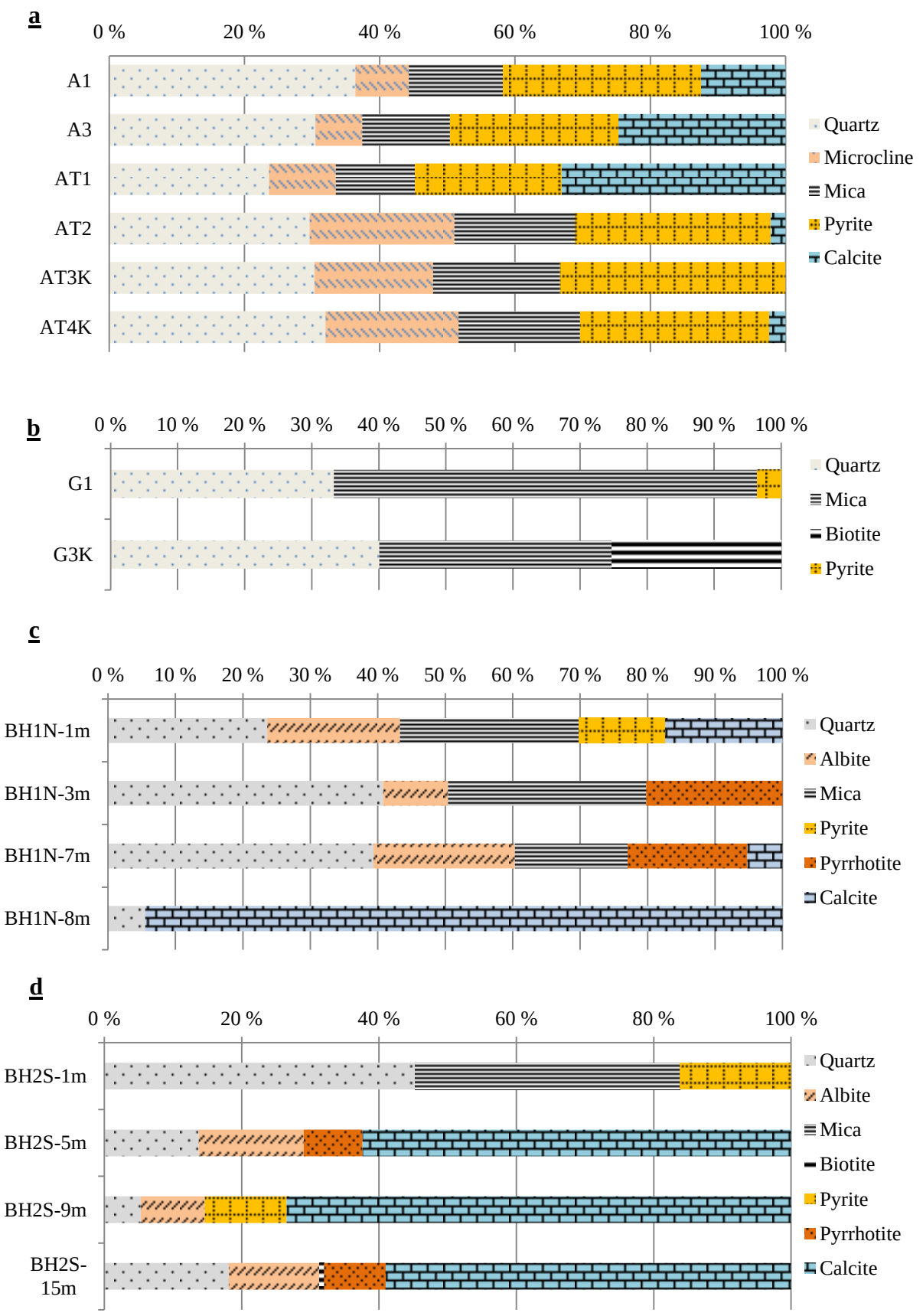

Figure 13: XRD results including quantitative distribution obtained via Siroquant. a: Alum shale at Gran (Rv. 4), both from road-cut and tunnel. b: Galgeberg shale at Gran (Rv. 4). c, d: Core samples from Jevnaker (E16).

5.1.2 Thick Section and Scanning Electron Microscope

From examining the thick sections underneath a regular polarizing microscope, it is evident that they display a large difference in composition from sample to sample. All samples exhibit alum- or black shale characteristics except BH1N-1m, BH1N-8m, BH2S-5m and BH2S-15m where calcite is dominant. In the sections with alum- or black shale a black matrix with sulphide mineral veins and grains are observed, with abundant calcite concretions and veins. The sulphides are usually well distributed and rarely occur as larger continuous grains.

Mineral phases identified in SEM are iron-sulphide phases with more S than Fe, sulphides with more equal amounts of Fe and S, and sulphides containing As, Co, Zn, Ni and Cu (Table 6). There are phosphate phases containing U, as well as a Ba-containing sulphate. Spectrums of the different phases along with more SEM scans can be found in Appendix 3.

Gran Alum Shale (Rv. 4)

In A1 and A3 the main characteristic of the sample is disperse framboidal pyrite in fine-grained matrix consisting of lighter minerals, with some larger pyrite grains along with larger mica, feldspar and quartz grains (Figure 14a, Figure 15a). Minor amounts of phosphate minerals such as apatite and monazite were identified in addition to the more common minerals. Phosphate minerals were observed to be more common in A1 compared to A3, though this was not measured quantitatively. The rock seems very homogeneous, with no larger features.

Some heavier minerals were observed after closer investigation with higher contrast (Figure 14b, Figure 15b). Monazite was the main phosphate mineral together with smaller amounts of a U-bearing phosphate mineral. These heavier phosphate minerals follow the same trend as the pyrite, as it distributed throughout the thick section and in grains with similar 1-5 µm size as the framboidal pyrite grains.

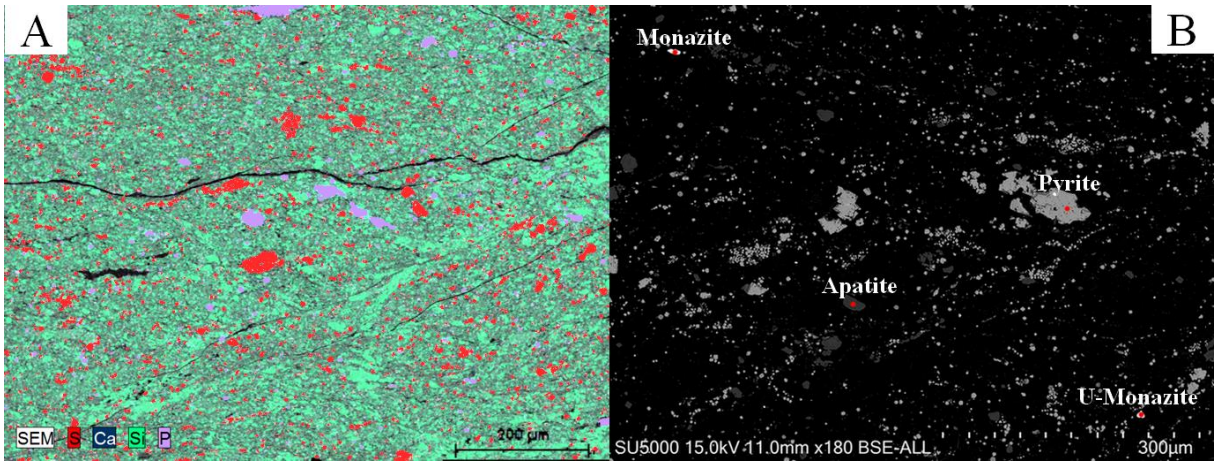

Figure 14: SEM scans of sample A1 showing general alum shale characteristics.
A: Element mapping with S (red), Ca (blue), Si (green) and P (purple).
B: Identification of monazite, apatite and U-bearing monazite in relation to pyrite.

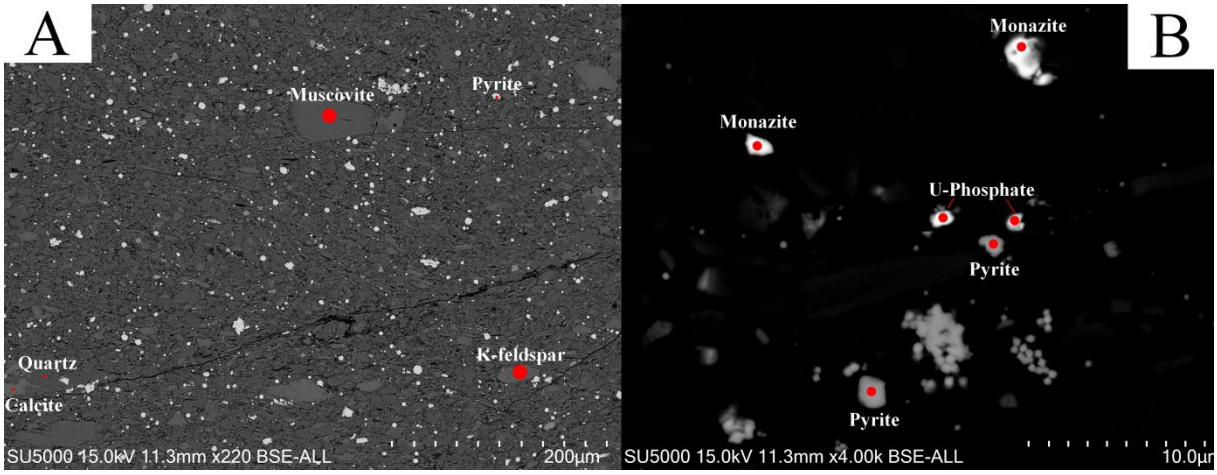

Figure 15: SEM scans of sample A3 showing general alum shale characteristics.
A: Overview of sample with identification of common minerals quartz, calcite, K-feldspar, muscovite and pyrite.
B: Identification of monazite and pyrite grains, including one U-bearing phosphate mineral grain.

AT1 shows relatively homogeneous shale with disperse framboidal pyrite in a lighter mineral matrix, but with larger pyrite and calcite grains clearly visible. The shale seems foliated, and has some cracks where barite has formed in areas containing framboidal pyrite and monazite. An element mapping (Figure 16a) clearly shows the distribution of S in both larger grains and smaller inclusions in the matrix. The phosphate phases are present in the matrix, but even more interestingly phosphate seems concentrated around the rim of the large calcite grain in Figure 16a. An example of pyrite, monazite and barite in coexistence is visible in Figure 16b.

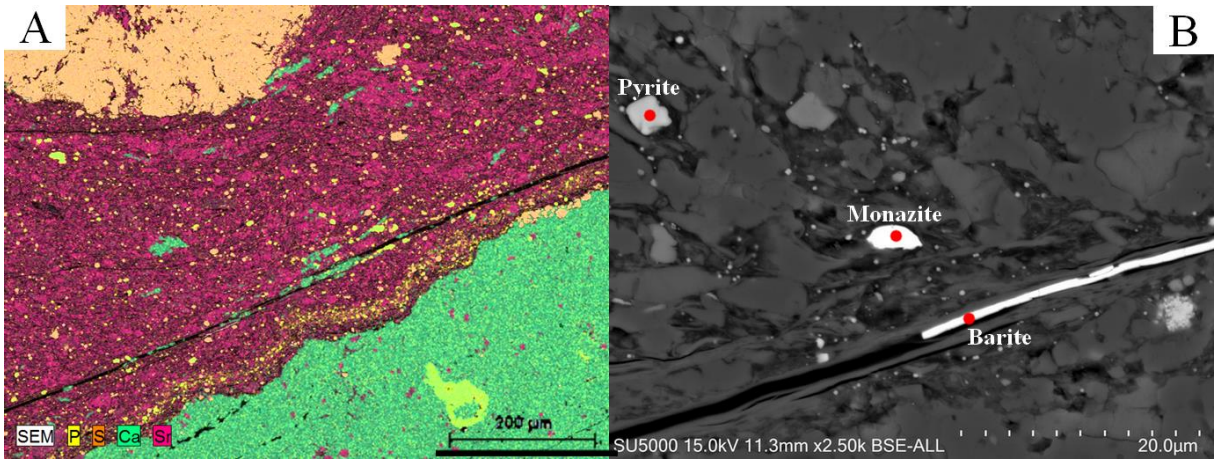

Figure 16: SEM scans of sample AT1 in an area with larger calcite and pyrite crystals.
A: Element mapping with P (yellow), S (orange), Ca (green) and Sr (purple, peak overlapping with K).
B: Pyrite, monazite and barite in coexistence.

Pyrite containing Zn as well as phosphates containing U were observed in this sample. AT3K and AT4K is similar to AT1, with especially AT3K being very homogenous. Here Cd-bearing sphalerite was observed together with pyrite, and the Zn-bearing phases were easily distinguished from the regular pyrite (Figure 17a). In AT4K larger areas with calcite were observed in addition to the regular shale matrix, with pyrite veins and grains included in the calcite (Figure 17b). Monazite was observed in AT3K and AT4K.

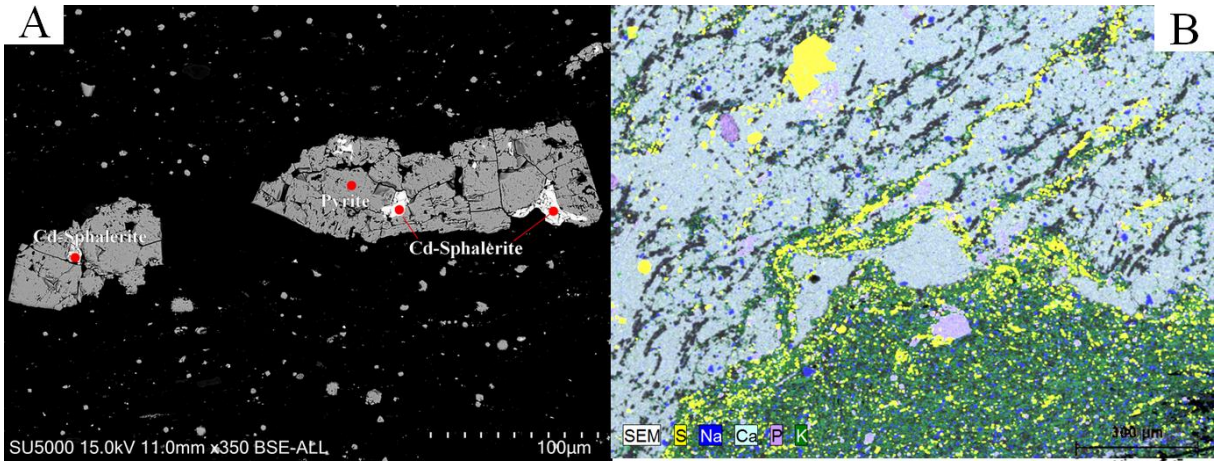

Figure 17: SEM scans of Cd-bearing Sphalerite together with Pyrite in AT3K (A) and an element mapping in AT4K (B) with S (yellow), K (green), Na (dark blue), Ca (light blue) and P (purple).

Jevnaker (E16) Alum Shale

The thick sections from the BH1N samples that contain alum shale were investigated, and regularly feature a matrix that consists mainly of quartz, mica and feldspar. The carbonate-, sulphide- and phosphate minerals occur in larger grains and veins (Figure 18) rather than for instance framboidal pyrite. Quantification of Fe and S implies both pyrite and pyrrhotite are present in samples BH1N-3m and BH1N-7m. An U-bearing phosphate mineral is observed in the BH1N-7m sample, and is often found inside larger apatite grains which are commonly surrounded by sulphides (Figure 18).

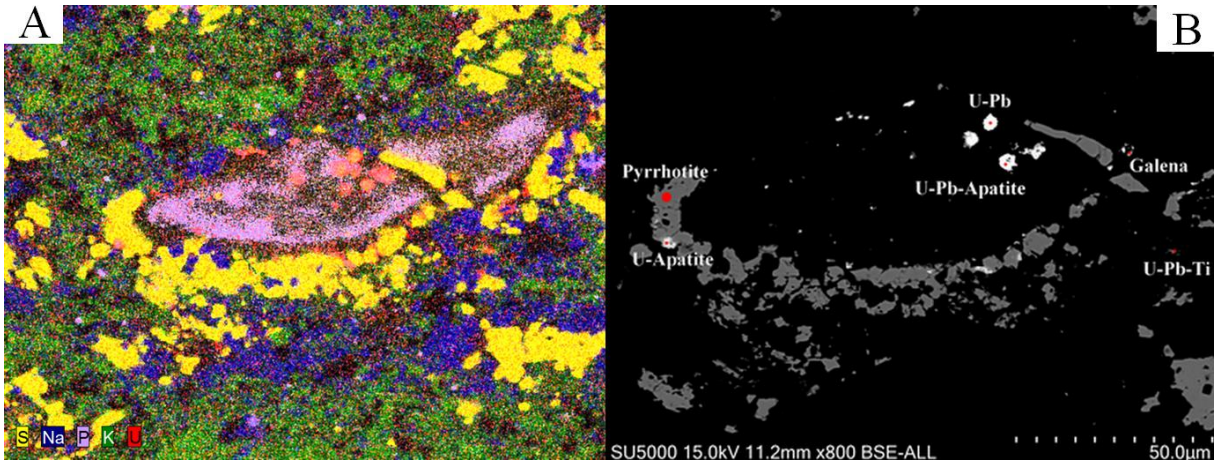

Figure 18: SEM scans with same scale of an apatite grain in BH1N-7m. A: Element mapping with S (yellow), Na (blue), K (green), U (red). B: Identification of pyrrhotite, U- and Pb- bearing apatite and galena.

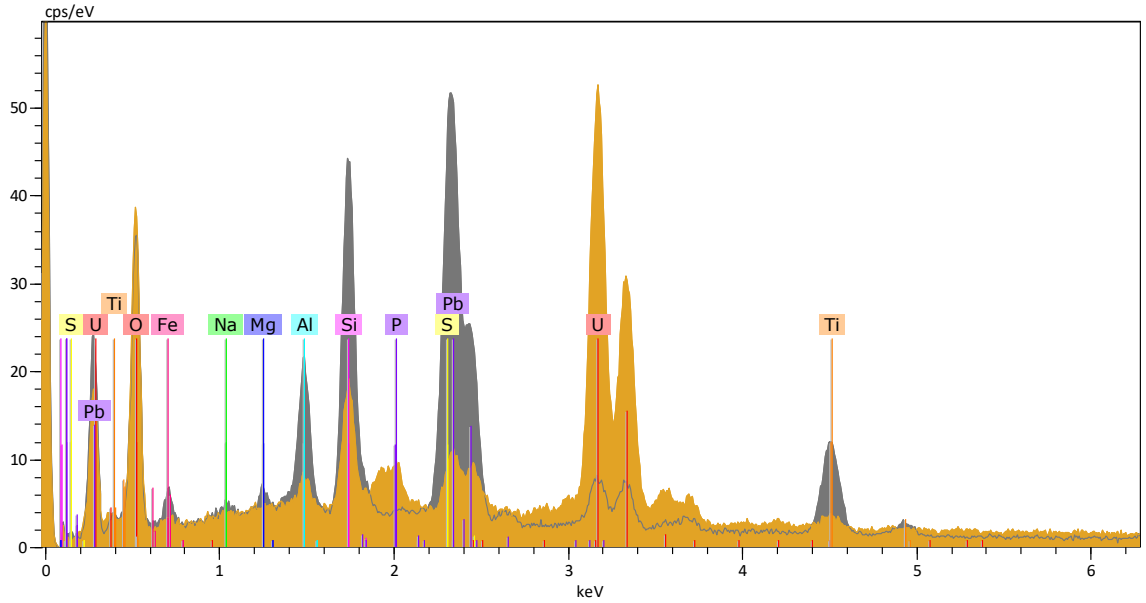

Figure 19: Spectrum of a U-bearing mineral (orange) and a Pb-bearing mineral (grey). All other mineral identifications have been conducted with similar spectrums (Appendix 3).

The As and Co bearing sulphide minerals arsenopyrite and cobaltite as well as galena are observed as heavy minerals in both the BH1N-3m and BH1N-7m samples, often visible in relation to pyrrhotite (Figure 20b). An REE-bearing silicate mineral identified as allanite $(Ca, Mn, Ce, La, Y, Th)_2Al(Al, Fe^{3+})(Fe^{2+}, Fe^{3+}, Ti)OOH[Si_2O_7][SiO_4]$ was observed next to pyrrhotite in both BH1N-3m and BH1N-7m (Figure 20a).

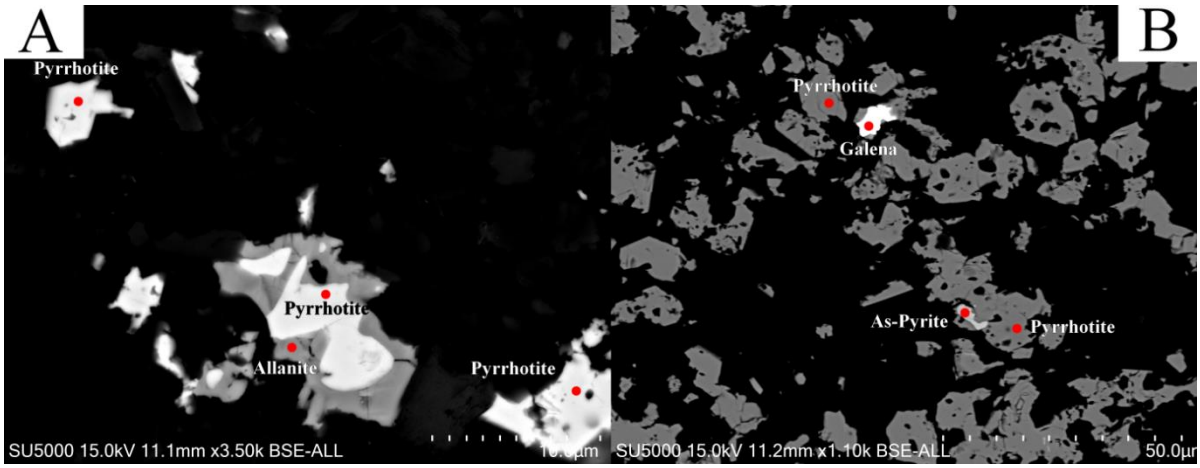

Figure 20: SEM scanning of sample BH1N-7m showing minerals occurring with pyrrhotite.
A: Pyrrhotite and allanite in relation to each other.
B: Identification of pyrrhotite, arsenopyrite and galena in sulphide veins.

In places in BH1N-3m the sulphide grains are seemingly weathered (Figure 21), where the weathering rim has the composition of a Fe-sulphate such as copiapite $(Fe^{2+}Fe^{3+}(SO_4)_6(OH)_2)$. These areas with the weathering rim are surrounded with calcite, and not necessarily the shale matrix. The composition of the sulphide was not quantified here, and it may be both pyrite and pyrrhotite.

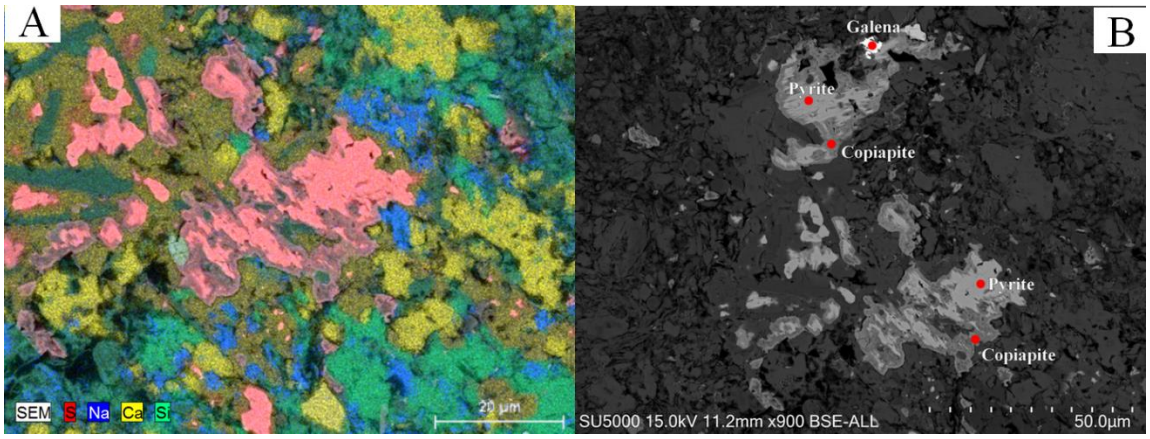

Figure 21: SEM scanning of sample BH1N-3m showing weathering of sulphides
A: Element mapping with S (red), Na (blue), Ca (yellow), Si (green).
B: Identification of Fe-sulphate weathering rim around pyrite or pyrrhotite.

BH2S-0-1m and BH2S-9-10m has a light mineral matrix and heavier minerals concentrated in veins (Figure 22). Some of the sulphide minerals have a clearly visible rim (Figure 23a) which gives a slightly different spectrum (Appendix 3). A mapping of element content reveals that other sulphides than pyrite and pyrrhotite are common in the sulphide veins, as the Fe and S map do not fully overlap (Figure 22a).

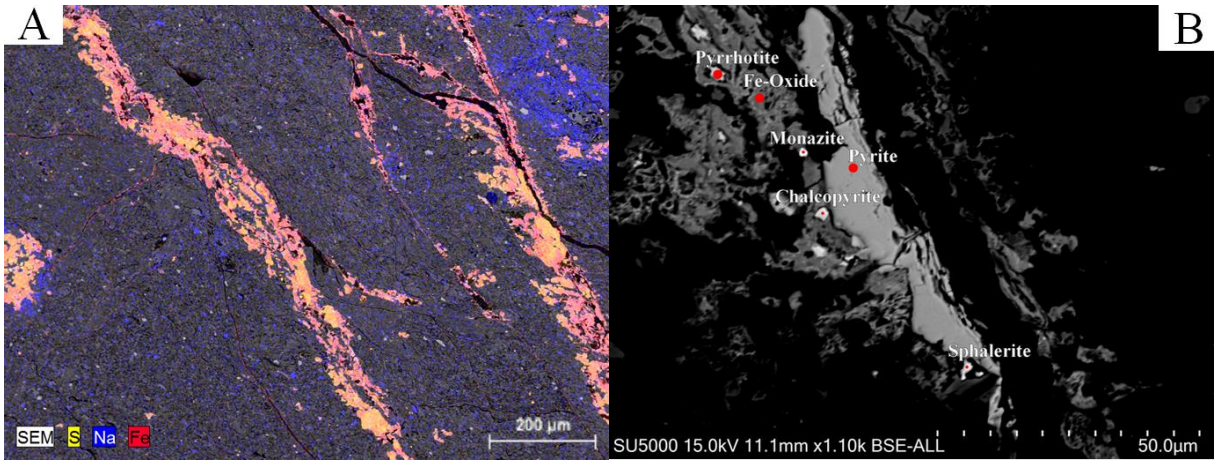

Figure 22: SEM scanning from BH2S-0-1m, showing the sulphide veins characteristic for the E16 shale.
A: Element mapping of sulphide veins, with S (yellow), Na (blue), Fe (red).
B: Pyrrhotite, pyrite, chalcopyrite, sphalerite, monazite and Fe-oxides in and around a sulphide vein.

Several accessory minerals such as Fe-oxides, sulphides and phosphates were identified. The sulphides identified were pyrite and pyrrhotite, sphalerite, chalcopyrite, arsenopyrite and cobaltite (Figure 22b, Figure 23b). Monazite and allanite were identified here, occurring around sulphide minerals.

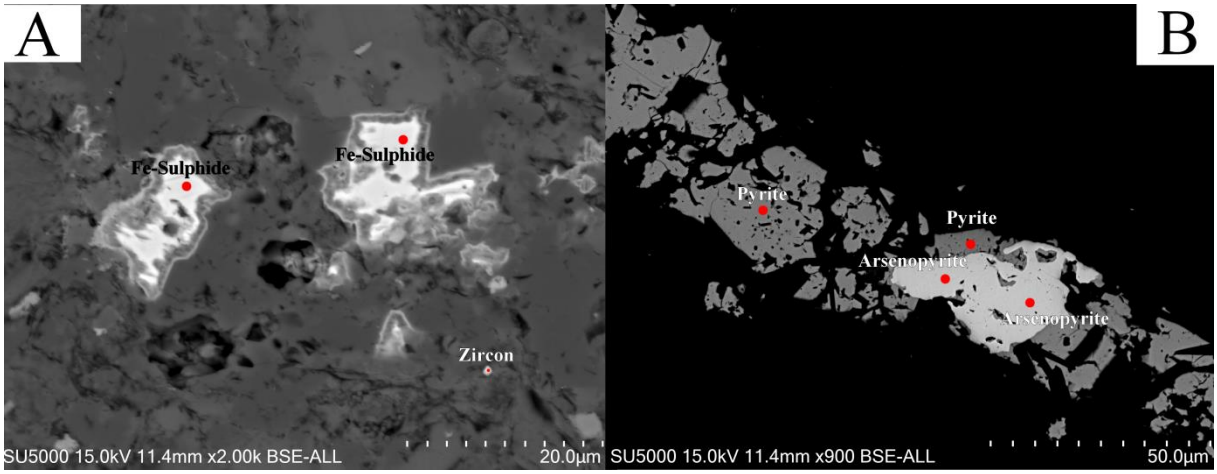

Figure 23: SEM scanning of BH2S-9-10m, showing different occurrence of sulphide minerals seemingly weathered (A) and unweathered (B).

Galgeberg shale (Rv. 4)

The thick sections of the Galgeberg shale show a rock with more clay minerals, with both muscovite and chlorite common in the thick sections. Sulphide minerals are present in the sample where they are mostly scattered around as framboidal grains or gathered in smaller groups (Figure 24a). F-apatite is present in the samples.

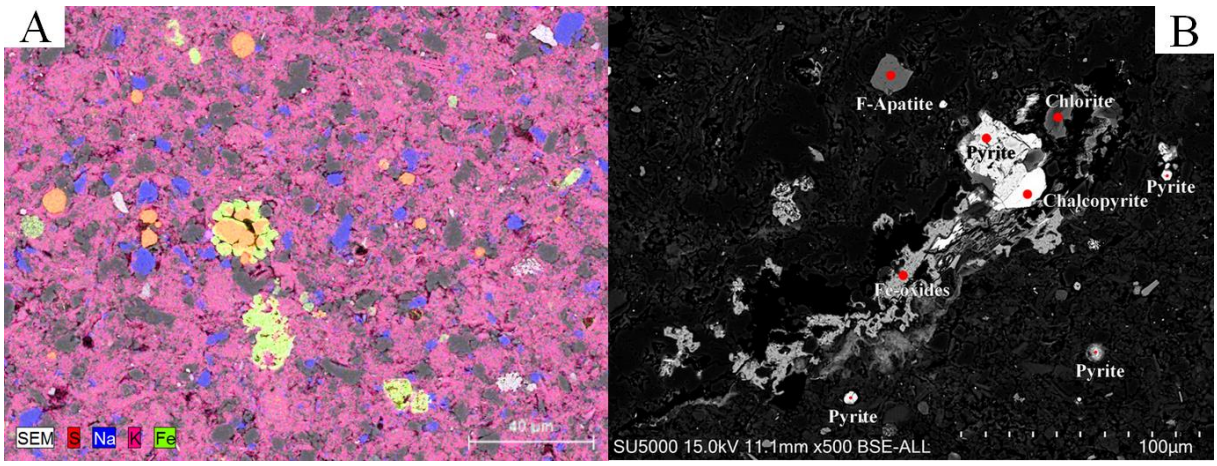

Figure 24: SEM scanning of sample G2, showing general trends of the sample and identification of minerals.
A: Element mapping with S (red), Na (blue), K (pink) and Fe (green).
B: Identification of pyrite, chalcopyrite, apatite and chlorite in addition to Fe-oxides.

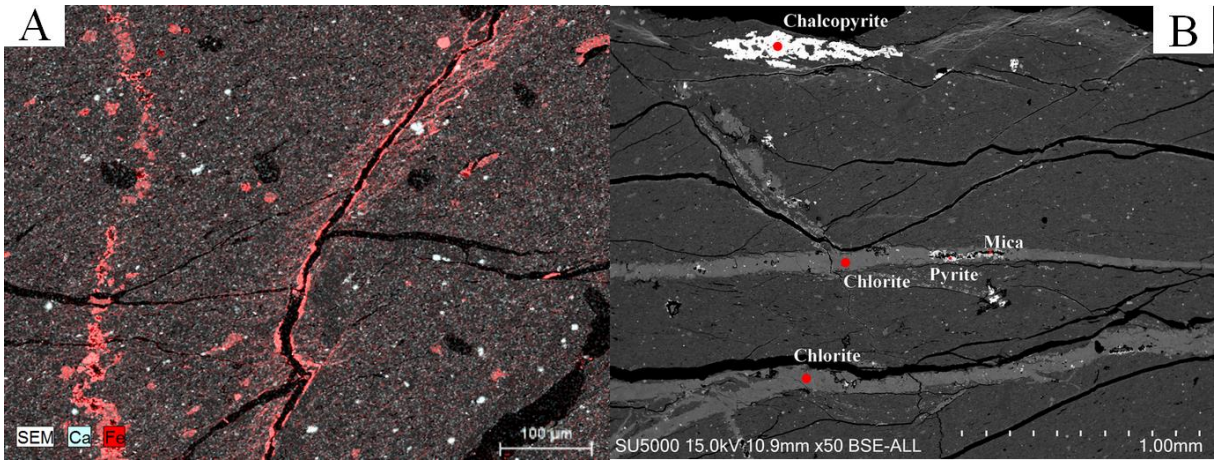

Figure 25: SEM scan of sample G3K, showing chlorite veins in the shale.
A: Element mapping with Ca (light blue) and Fe (red).
B: Identification of chlorite, pyrite, mica and chalcopyrite.

The sulphides found in the Galgeberg shale include framboidal and euhedral pyrite, pyrrhotite, chalcopyrite and sphalerite. The sulphides are often weathered and with a rim of iron oxides (Figure 24b), but in lower quantities than the alum shale samples. Chlorite is often found around the sulphide minerals too, and not all of the Fe in the sample is associated with

sulphides. As seen in Figure 25a, the Fe in the sample is often found in higher amounts in cracks and chlorite veins. Sulphate minerals such as Barite and a Fe-sulphate were present in the samples, while phosphate minerals found with monazite in both samples and xenotime found in G2. Rutile and zircon was found in both the Galgeberg samples.

Table 6: Composition of the different identified sulphide minerals in alum shale samples from Rv. 4 and E16, given as percentage of the element in the measured mineral phase.

Sample	O	Si	Ca	S	Fe	Zn	Ni	Cd	Co	Cu	As	Se	Re	Pb	Mineral
A1	4.83	0.59		60.58	34.01										Pyrite
BH1N-7m	4.51	0.55	1.08	47.55	47.55										Pyrrhotite
AT4K	4.47	0.78		43.65	1.67	48.73		0.53					1.07		Sphalerite
BH1N-7m	3.01	1.60		33.47	6.90		4.52		27.24		23.27				Cobaltite
BH2S-0-1m	3.10	0.83		31.27	31.72				4.93		28.15				As-Pyrite
BH2S-0-1m	4.64	0.65		42.33	26.54					25.84					Chalcopyrite
BH1N-3m	14.73			35.48								1.38	1.07	47.34	Galena

5.2 Water Sample Chemistry

5.2.1 Pallet experiments

The water sampled from the pallet experiments generally show a pH between 6.5 and 8.1 (Figure 26a). The lowest pH values are observed in the pallets containing the AT alum shale, while the A samples give the highest measured pH. The EC values vary greatly for AT, and spans from just above 500 µS/cm to over 4000 µS/cm (Figure 26b). The values for A and G are less variable, and G has most of its samples between 2000-3200 µS/cm. All the Eh values indicate oxidising conditions with values between 150 and 300 mV (Figure 26c).

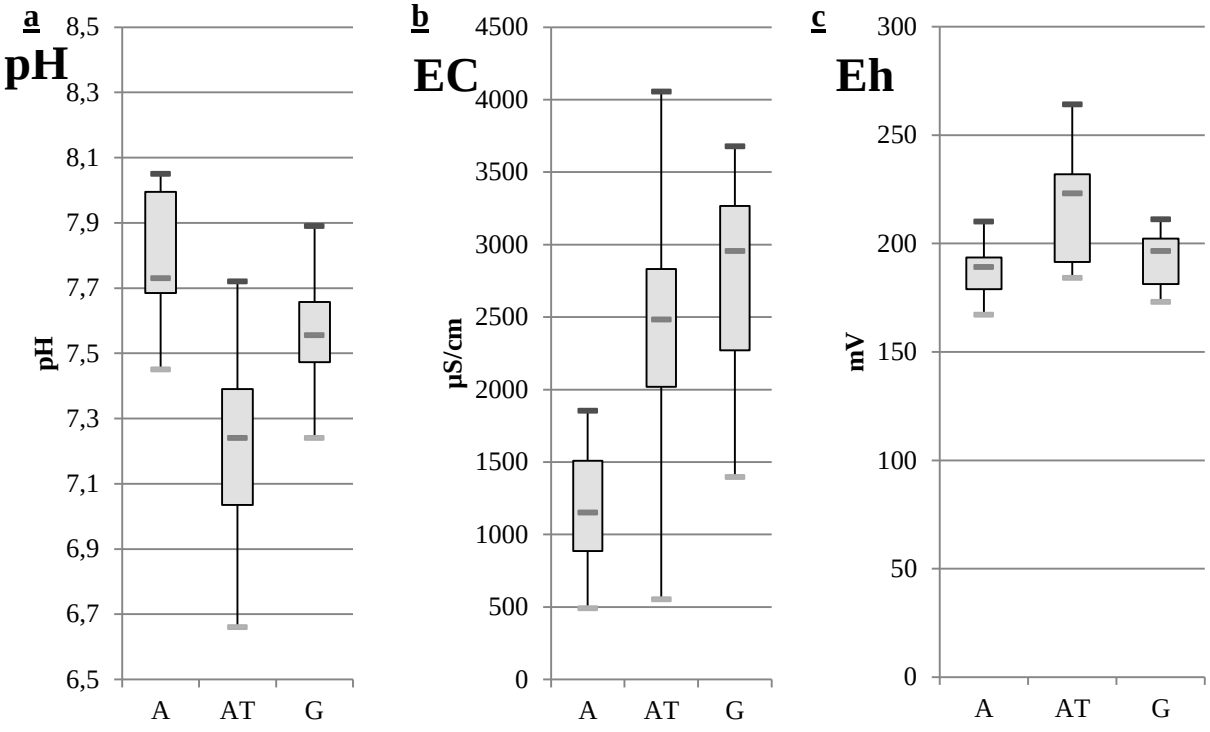

Figure 26: Box plots showing the general water characteristics of the water samples from the pallet experiments measured during sampling, with a: pH, b: EC and c: Eh. The boxes represent the middle 50 % of the data, while the top and bottom indicators indicate the maximum and minimum values measured.

Light ions

The light ion concentrations measured in the water samples are similar in both A, G and AT samples, as the dominating anion is SO_4^{2-} in all cases (Figure 27). In A the concentration varies between 500-4000 mg/l, in G between 2600-5900 mg/l, and in AT between 1300-7500 mg/l. The major cation is Ca^{2+} in A, while Mg^{2+} and Ca^{2+} have similar concentrations in G and AT. The sum of Mg and Ca is in all cases lower than the concentration of SO_4^{2-}. The concentrations of Na^+, K^+, F^-, and Cl^- are low relative to the previously mentioned elements for all samples, while PO_4^{3-}, NO_3^- and Br^- show concentrations below the detection limit in most of the samples. They are for this reason not included in the overview/figure below, but results can be found in Appendix 4.

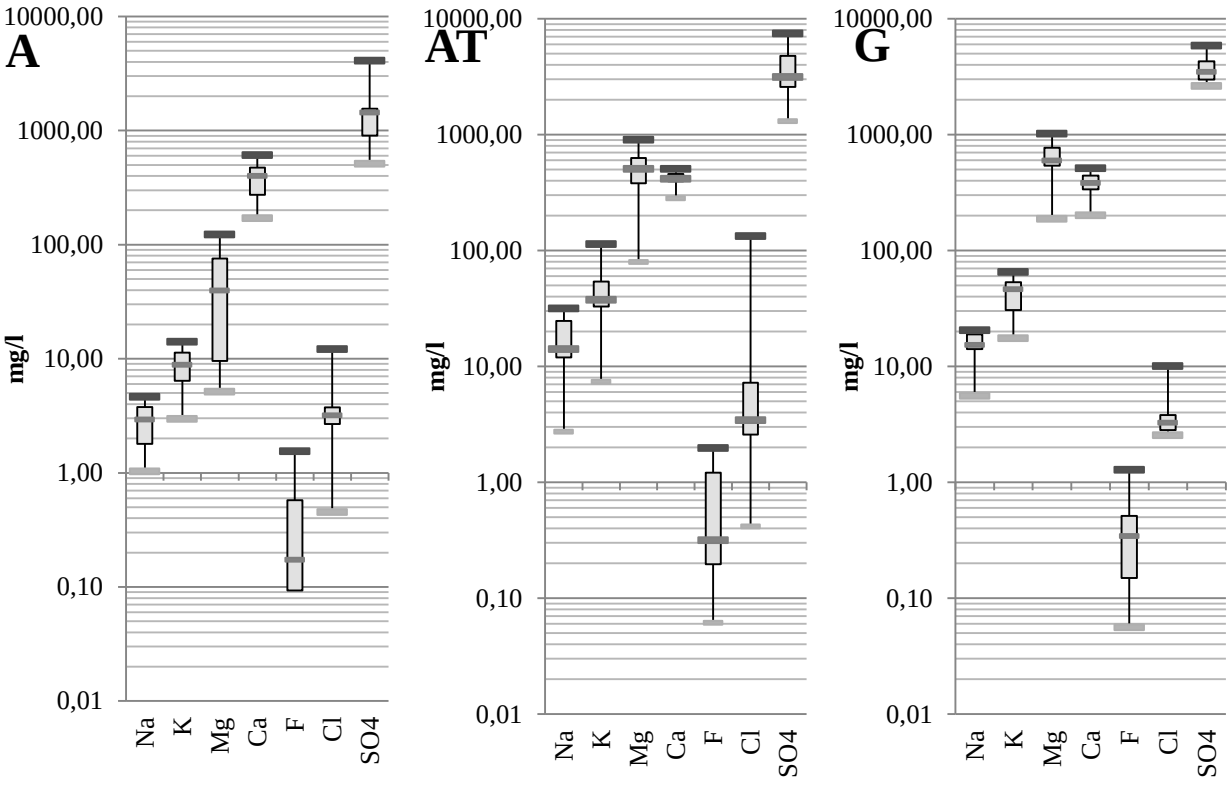

Figure 27: Box plots of the light ion concentrations in the water samples taken from the pallet experiments in the sampling period, grouped as A, AT and G. The boxes represent the middle 50 % of the data, while the top and bottom indicators indicate the maximum and minimum values measured. Note: Logarithmic scale.

Trace elements

Trace element concentrations vary in the samples, both in terms of which trace elements are abundant and their concentration values. In the A samples Sr has the highest concentrations, with Fe, Ni, Zn, Mo and U being abundant in the leached water (Figure 28). Al, Cr, Co and Cu are released in concentrations between 2-50 µg/l while V, Cd and Pb have very low concentrations (0-3 µg/l, Table 7).

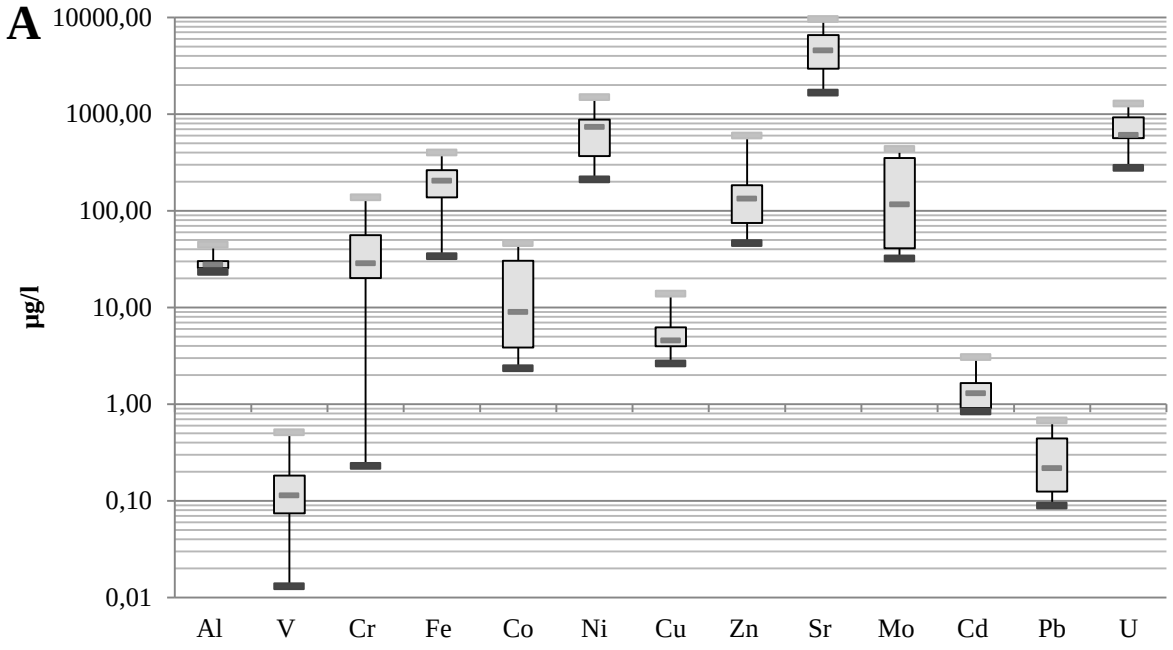

Figure 28: Box plot of the trace element concentrations in the water samples taken from the A pallets in the experiment at Gran. The boxes represent the middle 50 % of the data, while the top and bottom indicators indicate the maximum and minimum values measured. Note: Logarithmic scale.

For AT both Ni and Zn exhibit higher but more variable concentrations between samples than Sr (Figure 29), and the lowest concentration for Sr is higher than the lowest concentrations for Ni and Zn (Table 7). Uranium is abundant, but with a concentration that is commonly 10 times lower than those of Ni, Zn and Sr. Fe, Co and Cd show similar concentration spans, while Al, Cr and Mo have slightly lower concentrations (2-284 µg/l). Vanadium and lead have very low concentrations (0-2 µg/l).

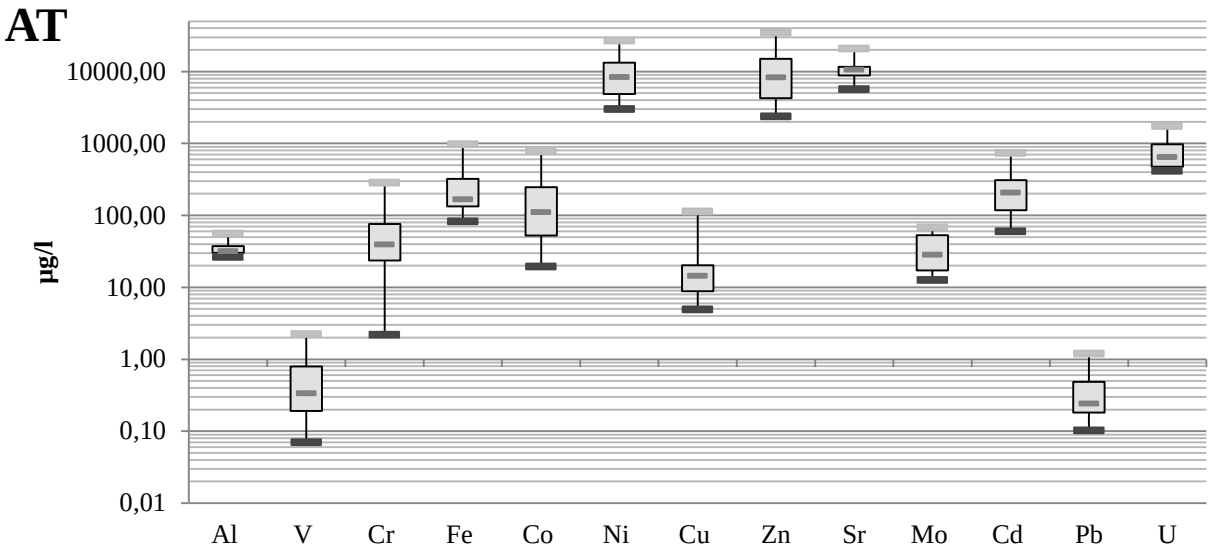

Figure 29: Box plot of the trace element concentrations in the water samples taken from the AT pallets in the experiment at Gran. The boxes represent the middle 50 % of the data, while the top and bottom indicators indicate the maximum and minimum values measured. Note: Logarithmic scale.

G has Sr as its major trace element (Figure 30), with concentrations in the water samples measured to be around 10 times the concentrations found for Ni and Zn (Table 7). Iron has relatively high concentrations compared to the other elements analysed. Al, Cr, Co, Cu and U all have concentrations between 0-74 µg/l, while Mo is slightly higher at 55-172 µg/l. V, Cu, Cd and Pb have very low concentrations.

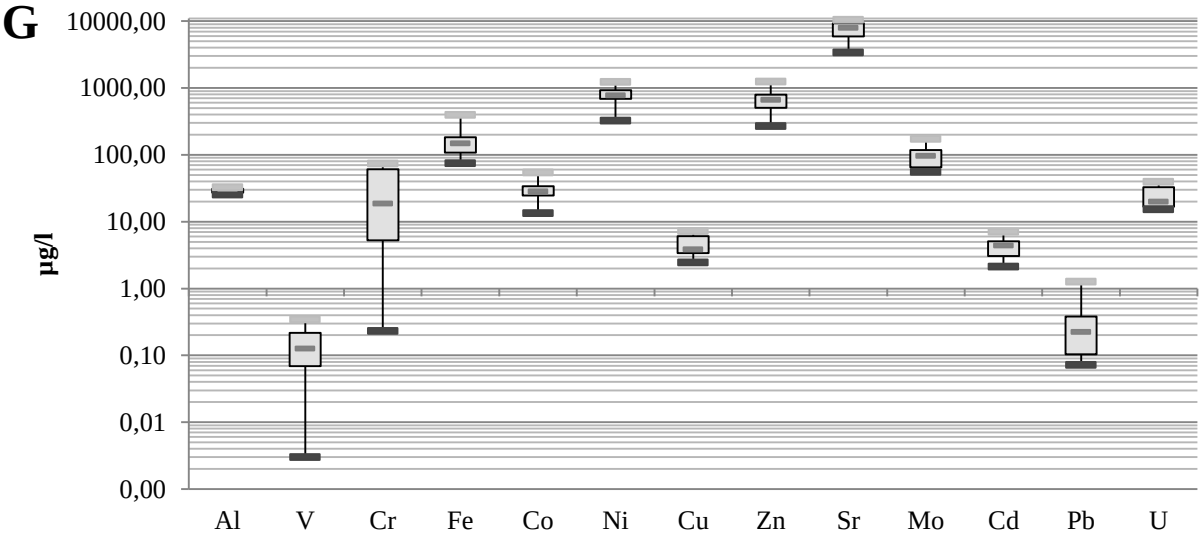

Figure 30: Box plot of the trace element concentrations in the water samples taken from the G pallets in the experiment at Gran. The boxes represent the middle 50 % of the data, while the top and bottom indicators indicate the maximum and minimum values measured. Note: Logarithmic scale.

Table 7: Minimum, average and maximum trace element content in the water samples from the pallet experiments at Gran, Hadeland.

Samples	A			AT			G		
µg/l	Min	Avg	Max	Min	Avg	Max	Min	Avg	Max
Al	25.53	28.92	44.19	26.39	35.79	55.48	25.36	29.52	32.71
V	0.01	0.18	0.51	0.07	0.70	2.23	0.00	0.15	0.34
Cr	0.23	46.63	137.2	2.18	69.57	284.4	0.23	30.04	73.86
Fe	33.65	201.2	399.4	81.68	274.0	967.9	74.48	173.5	392.6
Co	2.33	16.79	46.03	19.28	218.1	774.3	13.33	30.47	54.30
Ni	210.5	730.6	1492.1	2988	10808	26685	322.0	775.0	1227
Cu	2.62	5.79	13.76	4.90	22.61	112.2	2.43	4.50	7.18
Zn	45.91	168.7	594.4	2357	11466	34719	267.2	663.0	1239
Sr	1654	4705	9569	5632	11341	20804	3384	7440	10409
Mo	32.05	180.2	434.3	12.56	33.93	67.16	55.31	102.5	172.3
Cd	0.84	1.52	3.04	59.39	248.6	737.3	2.12	4.31	7.01
Pb	0.09	0.30	0.67	0.10	0.37	1.19	0.07	0.34	1.26
U	275.8	713.1	1281	414.7	795.3	1735	15.21	24.39	39.40

5.2.2 Column experiments

General characteristics of the water samples taken from the columns were not measured for all the samples. Measurements of individual samples show near neutral pH with very low EC.

The major cation in the water samples from the column experiment in all four setups is Ca^{2+}, with values up to 25.87 mg/l. Mg^{2+} and K^{+} have a similar range of concentrations, with 0.31-11.85 mg/l and 0.19-9.98 mg/l respectively. Na^{+} exhibits the lowest concentrations, with a range of 0.20-3.34 mg/l. The control column containing sand released Na^{+}, and 19 out of 42 samples from alum shale showed 70 % or more of the Na^{+} to probably originate from the sand. For K^{+}, Mg^{2+} and Ca^{2+} the contribution from the sand is in most cases less than 70 %, and considered to be minor. The highest concentrations are generally measured in the first and the last sample taken. There are only minor differences between the individual columns, but column 3 has a slightly lower average K^{+} release (0.61 mg/l compared to 1.06-1.35 mg/l).

The heavier elements are in general released in minor amounts. Fe (1.21-31.1 µg/l), Al (6-126 µg/l), Ni (below detection limit of 4.63 ppb to 80.5 µg/l) and Zn (2.22-121 µg/l) show low to medium concentrations, while Sr (12.98-498 µg/l), Mo (2.39-381 µg/l) and U (1.92-288 µg/l) have very variable concentrations. V, Cr, Cd, Co, Cu, Pb, all have concentrations less than 7 µg/l. The control column releases Zn, Cu and Cd in quantities similar or higher than the alum shale samples. Results from individual water samples can be found in Appendix 5.

Table 8: Average concentrations of elements in water samples from the column experiment.

Column	1	2	3	4	K
Na^+ (mg/l)	0.83	0.89	0.77	0.72	0.67
K^+ (mg/l)	1.35	1.33	0.61	1.06	0.29
Mg^{2+} (mg/l)	1.85	0.84	0.90	0.87	0.54
Ca^{2+} (mg/l)	9.68	10.29	8.16	9.98	2.15
Al (µg/l)	24.79	44.76	35.28	32.05	5.45
V (µg/l)	1.29	1.18	1.17	1.89	0.13
Cr (µg/l)	0.16	0.20	0.13	0.14	0.05
Fe (µg/l)	5.38	3.88	3.89	3.72	1.19
Co (µg/l)	0.41	0.25	0.46	0.33	0.02
Ni (µg/l)	9.32	6.03	6.03	9.65	4.63*
Cu (µg/l)	1.41	0.76	0.75	0.81	3.48
Zn (µg/l)	35.20	15.64	10.63	13.21	15.06
Sr (µg/l)	77.55	54.75	58.47	52.68	7.70
Mo (µg/l)	58.70	35.79	32.81	19.63	0.09
Cd (µg/l)	0.13	0.07	0.07	0.06	0.23
Pb (µg/l)	0.06	0.04	0.04	0.04	0.05
U (µg/l)	44.87	43.46	32.98	37.07	0.08

*Detection limit

The highest measured concentrations for different elements spread out over several sampling dates, and are not necessarily the dates with the lowest pumping velocity. Molybdenum and Cobalt have the highest concentration in water with a water velocity of 0.0395 ml/s, from the first sampling in column 1 (Table 9). Aluminium, Vanadium and Chromium have their highest concentration the day after with a water velocity of 0.0175 ml/s, while Zn has its highest concentration at 13.12 with a similar water velocity. Lead has its maximum during this period, with a water velocity of 0.0253 ml/s. The rest of the elements analysed for have their highest concentration after the experiment was left standing still for 26 days, comparable to a water velocity of 1.15 ml/d. It is worth noting that the sand used for permeability seemingly contributed Cu, Zn, Cd and Pb in comparable quantities to the alum shale.

Table 9: Maximum concentrations of trace elements and date of occurrence in the column experiments. Influence from the sand used for permeability and water velocity and residence time is included. Note the different units for water velocity (ml/s and ml/d) amd residence time (min and days).

Element	Max (µg/l)	Column	K(%)	Date	Water velocity	Residence time
Al	125.60	2	2.45	08.12.16	0.0175 ml/s	27 min
V	6.83	4	1.16	08.12.16	0.0175 ml/s	27 min
Cr	0.33	2	8.30	08.12.16	0.0175 ml/s	27 min
Fe	31.13	1	1.26	16.01.17	1.15 ml/d	26 days
Co	4.60	3	0.73	16.01.17	1.15 ml/d	26 days
Ni	80.53	4	3.48	16.01.17	1.15 ml/d	26 days
Cu	3.39	1	19.67	16.01.17	1.15 ml/d	26 days
Zn	121.02	1	13.54	13.12.16	0.0172 ml/s	27 min
Sr	498.26	1	0.59	16.01.17	1.15 ml/d	26 days
Mo	381.39	1	0.07	07.12.16	0.0395 ml/s	12 min
Cd	0.71	1	28.48	07.12.16	0.0395 ml/s	12 min
Pb	0.18	3	29.99	09.12.16	0.0253 ml/s	18 min
U	288.28	1	0.00	16.01.17	1.15 ml/d	26 days

5.3 Statistical Analysis and Modelling

5.3.1 Correlation Analysis

The correlation analysis of the water sample chemistry from the pallet experiments (Section 5.2.1) revealed that there were two distinct groups of trace elements that had either strong or moderate correlation to each other. Ni, Zn, Sr, Cd and Co can be grouped as these elements are correlated to two or more of the other elements (Figure 31), and Fe, Cr, V and Cu can be grouped as these elements correlate to one or more of the other elements. Uranium and Molybdenum did not have strong correlation to any of the other elements, and only a moderate correlation to each other in G and to cobalt in AT. The full correlation matrices can be found in Appendix 6

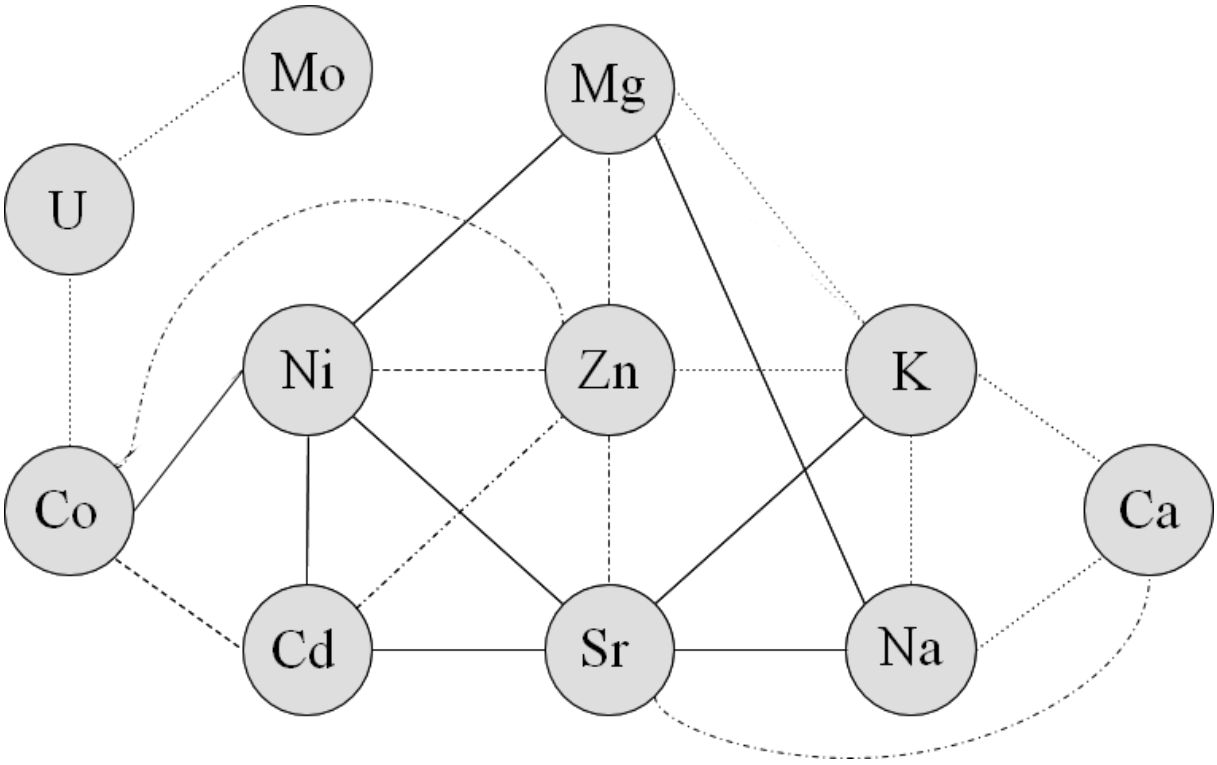

Figure 31: Correlation of different elements in water samples from the pallet experiment. A continuous line implies a strong correlation between the elements for sample groups A, AT and G, while the dotted lines indicate strong correlation in only one or two sample groups. The weakest lines only represent a moderate correlation in either A, AT or G.

The most important correlations are those between Co, Ni, Cd, Sr and Zn, as these are either strong or moderate in more than one group of shale samples. Ni is strongly correlated with Zn in both AT and G (Table 10), and show strong correlation with Cd and Sr in all three experiments. Nickel has a strong correlation to Cobalt in AT. Cd has a strong correlation to Co and Zn in AT and G, but only a moderate correlation in A. Sr and Zn is strongly correlated in A, AT and G.

Table 10: Correlation factors between selected elements in the different pallet experiments, forming the basis of Figure 31.

Element 1	Element 2	A	AT	G
Ni	**Zn**	-0.12	0.98	0.96
Ni	**Cd**	0.86	0.92	0.70
Ni	**Co**	0.66	0.90	0.82
Ni	**Sr**	0.94	0.81	0.79
Cd	**Co**	0.58	0.71	0.82
Cd	**Zn**	-0.01	0.98	0.82
Sr	**Zn**	0.73	0.76	0.71

5.3.2 PHREEQC Groundwater Modelling

The inverse modelling of the water sample average gave two models for A (A-A and A-B), two models for AT (AT-A and AT-B) and two models for G (G-A and G-B) (Table 11). The values from PHREEQC are given in mol/l over a 14 day period, with positive values indicating dissolution and negative values indicating precipitation (Table 11). A-A and A-B are nearly the same, as the only difference is it the model is using either O_2 or CO_2 in the weathering reactions. Both options are expected, though CO_2 contributes C to the system. The same occurs for AT-A and AT-B, though AT-B takes chalcopyrite into account as well. G-A and G-B is similar, as G-B includes chalcopyrite.

The largest amount of pyrite dissolution occurs in G, marginally larger than that in AT which in turn is about 10 times larger than that in A. Illite, calcite and CO_2 or O_2 dissolution follows the same trend, while more albite weathers in AT than G and A. Weathering of sphalerite follows the trend AT>G>A, while for chalcopyrite the case is AT>A>G according to the inverse model simulation.

Table 11: Results from the inverse modelling calculation in PHREEQC, with two results for A (A-A and A-B), one results for AT (AT-A) and two results for G (G-A and G-B).

Model	A-A	A-B	AT-A	AT-B	G-A	G-B
Pyrite (mol/l)	4.587e-02	4.587e-02	4.747e-01	4.747e-01	5.942e-01	5.942e-01
Illite (mol/l)	2.585e-02	2.585e-02	2.657e-01	2.657e-01	3.320e-01	3.320e-01
Albite (mol/l)	1.216e-04	1.216e-04	7.709e-04	7.709e-04	6.635e-04	6.635e-04
Sphalerite (mol/l)	2.585e-06	2.585e-06	1.762e-04	1.762e-04	1.019e-05	1.019e-05
Chalcopyrite (mol/l)				3.575e-07	0	1.541e-07
Calcite (mol/l)	6.117e-02	6.117e-02	6.336e-01	6.336e-01	7.933e-01	7.933e-01
CO2(g) (mol/l)		1.109e-01		1.147e+00		1.435e+00
O2(g) (mol/l)	1.109e-01		1.147e+00		1.435e+00	
Gypsum (mol/l)	-4.946e-02	-4.946e-02	-6.005e-01	-6.005e-01	-7.555e-01	-7.555e-01
Jarosite (mol/l)	-1.529e-02	-1.529e-02	-1.582e-01	-1.582e-01	1.981e-01	-1.981e-01
Kaolinite (mol/l)	-1.859e-02	-1.859e-02	-1.911e-01	-1.911e-01	-2.389e-01	-2.389e-01
Montmor-Ca (mol/l)	-1.342e-02	-1.342e-02	-1.375e-01	-1.375e-01	-1.715e-01	-1.715e-01
C (mol/l)	-6.117e-02	-1.720e-01	-6.335e-01	-1.780e+00	-7.933e-01	-2.228e+00

6 Discussion

6.1 Characteristics of Alum Shale at Hadeland compared with other reports

6.1.1 Mineralogy

Simply by comparing the XRD and SEM results of the alum shale samples from Rv. 4 and E16, one can observe that samples classified as alum shale are not necessarily rocks with the same composition. The variation in the samples is thought to be due to the variation of the mineral content, both through matrix variations but also through inclusions of pure quartz and especially calcite in concretions and veins. This variation is observed both regionally between sampling sites and locally at each site. A difference between the amount of organic carbon and accessory minerals between samples may affect the distribution of primary minerals and elements. The amount of pyrite and pyrrhotite in the samples may seem overestimated compared to previous studies, but it is possible that underestimation of these minerals have occurred in previous studies (Nyland and Teigland, 1984).

The alum shale from Rv. 4 has a very similar composition between the samples, even if these have been taken at different locations. The differences between the samples here are often only reflected in the calcite content, contrary to what is observed at E16 where changes between alum shale and limestone composition is observed on a meter scale. BH1N varies from a similar relationship between quartz, feldspars and sulphides as A and AT to almost pure calcite between the BH1N-7m and 8m samples. This can be observed in BH1N-1m, where the calcite content is larger in the thick section than what was measured in XRD (Figure 13c). More calcite is generally measured with XRD in the BH2S samples, but while the XRD of BH2S-9-10m has the most calcite from this core the thick section has almost no calcite (Figure 13d, Figure 23). This means that part of a rock sample can be classified as limestone, while another part can be classified as alum shale. Limestone breccia was mentioned in the core log (Multiconsult, 2014), but these results show that almost pure calcite veins are common on a cm scale at Jevnaker compared to Gran.

The mineralogy of the alum shale samples from Hadeland is consistent with the information found in literature, though the feldspar and clay mineral selected in other XRD analyses varies compared to this study where microcline and albite is chosen as the most probable feldspars. Abreham (2007) reported orthoclase and sanidine, both feldspars that can be considered polymorphs of microcline (Goldsmith and Laves, 1954). It can be assumed that the distinctions between the different feldspar and mica minerals are of minor significance in this context, as the chemical composition will be similar. It is implicated that microcline represents feldspars, muscovite/illite represents micas and pyrite or pyrrhotite represents sulphides. The XRD measurements show a clear distinction between pyrite and pyrrhotite, as they are never identified in the same sample.

Phosphate minerals were found in the thick section analysis with SEM, but not identified in the XRD analysis. Apatite (some containing U) and monazite were the most common phosphates, with xenotime also observed. The phosphate content in alum shale is rarely mentioned, but Bjørlykke (1974a) and Bjørlykke and Englund (1979) give a concentration of about 0.1 % P_2O_5 in the lower Palaeozoic shales while Allard et al. (1991) has a PO_4^{3-} concentration of 0.25 % in Swedish alum shale. These values confirm that the detection of phosphate minerals in alum shales through XRD analysis is unlikely with a detection limit of 1-2 %. Even if the phosphate mineral content would be higher than the XRD detection limit, the occurrence of different phosphate minerals may mean that the concentration of each of them are lower than the detection limit. This could be why previous studies rarely mention phosphates, as XRD has been the most common method for identifying minerals in the alum shale.

Indications of Contact Metamorphism

Microcline is considered to be stable against weathering, and according to Nesse (2012) normal in sedimentary rocks. As the core logs from E16 Jevnakerveien show (Figure 9, Figure 10), the alum shale samples have been taken close to intrusives (Multiconsult, 2014). Albite is commonly found in low-grade metamorphic pelitic rocks (Nesse, 2012), which is a description that fits the alum shale from E16 due to the possible contact metamorphism from the intrusive dikes found in the core log (Multiconsult, 2014). This transition from microcline to albite could be a good indication of contact metamorphism, as albitisation is a common process (Starkey, 1959) where K^+ is replaced by Na^+ (Smith, 1974). The source of sodium is unknown and it is unclear if metasomatic fluid migration can be the source for such a trans-

formation. Na might originate from the intrusives, but it could come from phases initially present in the alum shale (pers. comm. K. Bjørlykke, 09.05.2017), such as Na-rich alkali-feldspar. The Na content has not been measured in the rock samples used in this study, but Armands (1972) gives values of 0.170 % Na and 3.645 % K in unmetamorphosed Swedish shale. Similar values are observed by Snäll (1988) in altered allocthonous alum shale, though that is in Jämtland far away from the Oslo rift. The brecciation in the samples from Jevnaker is most likely related to the intrusions, and may allow or even be a sign of fluid migration due to increased pore pressure (Figure 8).

Albitisation can occur at temperatures over 65°C in diagenetic environments (Saigal et al., 1988), but this is unlikely with alum shale as microcline is detected as the major feldspar in the relatively unmetamorphosed shale at Gran. Partially albitisised feldspars similar to those observed from diagenetic processes are not observed in this study. It can be assumed that the difference between the shale at Gran and the shale at Jevnaker is due to post-diagenetic processes (pers. comm. P. Aagaard, K. Bjørlykke, 09.05.2017). Simultaneously to alibitisation, pyrite to pyrrhotite metamorphism may occur (Antun, 1967), though this process may require temperatures of at least 90-180°C (Truche et al., 2010). Pyrite and albite is found in samples further away from the intrusives (BH1N-1m, BH2S-9m), indicating that albitisation can be more extensive than pyrrhotitisation. The disilicate mineral allanite is mentioned to occur in metamorphosed carbonate rocks (Smith et al., 2002), and is found in relation to pyrrhotite in these samples (Figure 20). Allanite may contain U and Th in addition to REE's (Smith et al., 1956). Albite can thus be an important indicator in terms of alum shale contact metamorphism and possible pyrrhotite presence, as the sulphide mineral itself is hard to identify with XRD (Bastiansen et al., 1957). Chlorite or biotite content may be related to contact metamorphism (Nyland and Teigland, 1984), which may explain presence of this mineral in E16 samples.

The distribution of calcite and sulphide minerals and in general larger variation in mineral content implies that the rock is more complex at E16 than at Rv. 4, and it is likely that recrystallization of calcite, pyrite and quartz has happened. This is evident in the samples where the core log (Figure 9, Figure 10) shows limestone breccias (Multiconsult, 2014), as the XRD results usually show calcite as the dominant mineral in samples taken from these sections. The E16 samples are perhaps even more similar to the samples described by Snäll (1988), which is deformed, recrystallised, folded and penetrated by irregular calcite or pyrite veins,

though pyrrhotite is not mentioned in relation to the mineralogy. As with the Jämtland allochtonous shale, the origin of the calcite and pyrite veins can be attributed to stinkstones and dispersed framboidal pyrite in less metamorphosed shale (Snäll, 1988).

6.1.2 Trace elements

Trace elements may substitute for common cations in abundant rock-forming minerals or occur in accessory minerals with concentrations lower than the detection limit of XRD. The valence of the trace element in its ionic form is essential information in terms of determining which cations may be substituted. The crystal structure and composition of the mineral gives certain boundaries to the dimensions and valence to the element substituting. In alum shale it is thought that trace elements may occur in three major categories; Substituting in rock-forming minerals, in sulphides and other accessory minerals, and together with organic material (Nyland and Teigland, 1984).

The trace element content in the samples used in this study were measured by H. Fjermestad and made available through personal communication (E-Mail, 07.09.2016) as raw data sorted after sample set. The average content of the elements investigated in this study was calculated and is presented in Table 12. Compared to the average alum shale in Table 1, the A samples have a higher amount of S, Ni, Sr, Co, U and Mo, but lower amount of Zn. The AT samples have a similar amount of S, U and Mo, while Ni, Zn, Sr and Co is higher compared to the average alum shale. Sample set G has a lower amount of S, Ni, U and Mo, but high values of Ni, Zn and Sr.

Table 12: Average measured content of selected elements in the rock samples used in the pallet experiments. Values were calculated from the data provided by H. Fjermestad (E-Mail, 07.09.2016), measured using handheld XRF according to the method described by Hagelia and Fjermestad (2016)

Sample set	S (%)	Ni (ppm)	Zn (ppm)	Co (ppm)	Sr (ppm)	U (ppm)	Mo (ppm)
A	6.3	207	64	99	219	185	256
AT	4,5	285	331	265	253	124	185
G	1,4	97	203	201	144	29	55

Iron is usually related to pyrite or pyrrhotite in alum shale samples. However as the G samples contain chlorite and biotite, iron could be derived from these minerals. Zinc was found in pyrite similar to the results of Armands (1972), but more interestingly in a separate

sphalerite phase that contained trace amounts of Cd in AT. Bjørlykke (1974a) mentioned that Zn must occur outside pyrite, and this sphalerite explains part of that occurrence. It is uncertain if the sphalerite observed can account for all of the Zn in the sample, but it is likely as an average Zn concentration of 331 ppm (Table 12) requires less than 0.1 % sphalerite. Zinc may be situated in organic matter (Rashid, 1974), but the presence of sphalerite makes this less likely. Sphalerite may account for much of the Cd in alum shale, as Cd-bearing sphalerite was found during SEM analysis and Cd is commonly found in sphalerite (Cook et al., 2009). Cadmium was related to sulphides by Lavergren et al. (2009a), though the presence of Cd in sphalerite makes Cd-sulphide such as greenockite (CdS) unlikely. The presence of sphalerite could be related to processes occurring during the Caledonian orogeny (Lecomte et al., 2017).

Nickel is often assumed to be bound to sulphides similar to Zn, but is only found in a sulphide in cobaltite in the E16 alum shale and not found in sulphides at all in the Rv. 4 alum shale. This is interesting since Ni generally occurs in similar concentrations as Zn in the shale (Table 1 and Table 12). Nickel is not thought to be enriched in pyrite (Armands, 1972), but is generally associated with sulphides in leaching studies (Fjermestad, 2013). Cobalt shows a similar behaviour as it is often associated with sulphides in previous studies, but is only identified in cobaltite during the SEM analysis in this study. The Co concentrations are higher than Ni in cobaltite, which may suggest that Ni might be bound elsewhere such as in organic material (Rashid, 1974). Arsenic, cobalt and nickel in arsenopyrite and cobaltite are only found in the contact metamorphosed shale at Jevnaker. These minerals may be the result of pyrite metamorphosis as they can be associated with hydrothermal vein systems and metamorphic rocks (Nold, 1990). Arsenic and Cobalt may be enriched in alum shale pyrite (Armands, 1972, Lecomte et al., 2017). Similarly to Ni, Co could be related to organic matter (Rashid, 1974). Arsenic has been found to be enriched in pyrite in alum shale (Armands, 1972), further supporting the hypothesis of cobaltite as a product of pyrite metamorphosis.

Strontium and molybdenum were not found in any minerals. Considering the low concentrations of Sr previously found in alum shale (Table 1) this may not seem surprising, but the samples used in the pallet experiment (Table 12) have concentrations of Sr and Mo on the same level as Ni and Zn. An explanation of this could be Mo complexation to organic matter that is either water soluble or allows transformation to molybdate ions (MoO_4^{2-}) (Lavergren et al., 2009a), and Sr exchanging with K in feldspar (Cherniak and Watson, 1992).

Uranium was observed in phosphate minerals during SEM analysis. Both U and P content in the Rv. 4 alum shales were measured by H. Fjermestad, but a quick correlation analysis (similar to section 4.3.1) on the raw data received 07.09.2016 (E-Mail) reveals that the two elements have a correlation coefficient of 0.34, which is not considered a good correlation.

Figure 32 shows the two elements plotted against each other, and there is no relationship between the two. Lecomte et al. (2017) found a positive correlation for U towards P and TOC, though the correlation coefficients are not available for comparison. The positive correlation between U and P found by Lecomte et al. (2017) is related to apatite, though a better correlation than that in Figure 32 would be expected if all apatite in alum shale contained U.

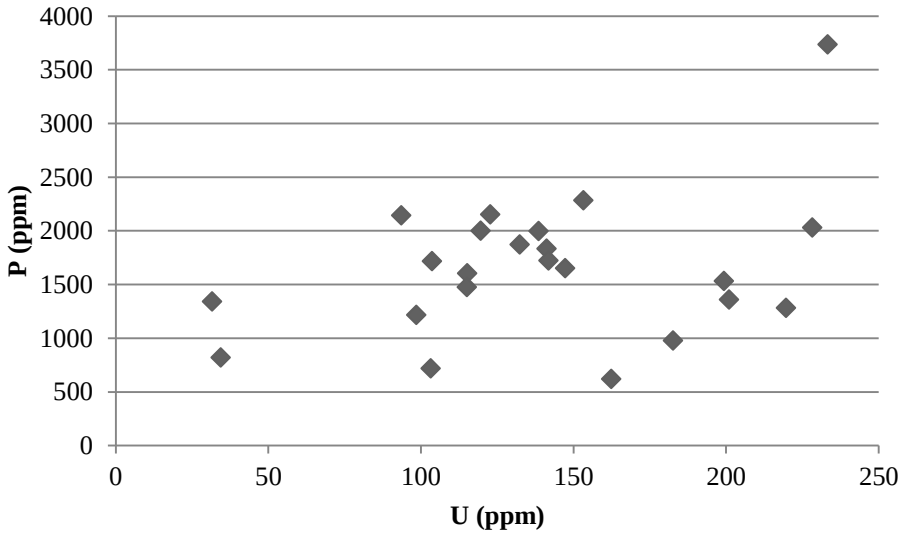

Figure 32: U (ppm) plotted against P (ppm) using measurements of the chemical content of the Gran alum shale samples by H. Fjermestad (E-Mail 07.09.2016). There is no relationship between the two elements.

Armands (1972) mentions that U could be associated to the detrital minerals zircon, titanite and phosporite, or associated with the sulphide phase. The results from SEM analysis in this study confirm that U is present in phosphates, but it is uncertain if the U in phosphates can account for all the U in alum shale as not all phosphate minerals in the samples contain U. Uranium was probably reduced from U^{6+} to U^{4+} in the alum shale depositional environment, and U^{4+} is the most probable form of U to occur in apatite where it is substituting for Ca (Altschuler et al., 1958). Uranium is not very soluble in a reducing environment such as the alum shale depositional environment, and it is likely that U was coupled to apatite formation during scavenging and deposition of marine phosphorus (März et al., 2008).

Uranium could also be associated with phosphate due to remobilization during metamorphosis (Lecomte et al., 2017), backed by the SEM results in this study. The contact metamorphosed shale at Jevnaker see higher U concentrations in some phosphate grains, and mobilization of U from other phases to the phosphate phase replacing other cations may have occurred during metamorphosis. Lavergren et al. (2009a) found most of the U in the residual fraction from leaching studies, implying that it primarily resides in weathering resistant minerals. It is mentioned by Armands (1972) that U is well correlating with Na-K-feldspar, though he explains that the correlation may be due to feldspar formation during sedimentation. Uranium fixation in the alum shale occurred simultaneously, and the U is most likely bound to organic material and phosphates present in the depositional environment (Lecomte et al., 2017). In a study published in April 2017, Lecomte et al. (2017) detected two types of U-bearing minerals in altered alum shale: 1) uraninite and U-titanate micro-inclusions in synmetamorphic pyrite and 2) complex assemblages of U, Ti and Y phospho-silicates. This is similar results as those observed in Figure 18, though here Pb is present in a larger amount. Uraninite is not observed in this study, though U can be related to both P, Ti and in coexistence with pyrite in metamorphic shale.

McKelvey (1955) proposed that the uraniferous organic "kolm" material is dispersed throughout the shale in addition to the larger lenses observed in Sweden, and that only 4 % "kolm" would account for the U content of the shale. Uranium being related to more than one phase is supported by observed radiation from alum shale following the primary lamination (Bjørlykke, 1974a). The increased mineralization of U in the contact metamorphosed alum shale at Jevnaker further supports the assumption of U to be present in organic matter. Organic matter may be the source of the higher concentrations of U in phosphate grains in contact metamorphic shale.

6.2 Mineral to Water Reactions

Alum shale is different from most other lithologies due to the rapid weathering rate where the rock changes character and affects the environment on a 10-50 year timescale. This is reflected in this study, where a minor amount of alum shale stored in an oxidizing environment leads to relatively high mineral weathering rates and subsequently high concentrations of trace elements in percolating water.

6.2.1 Water Sample Quality

The water sampling quality was checked using PHREEQC, and the electrical balance error percentage is in general ±5 %. This can be considered acceptable, but in the case of larger errors the analytical procedures should be examined (Appelo and Postma, 2013). Some samples show an error of 40-50 %. These are all samples where the sulphate concentration is very high, especially compared to the cation concentrations. Looking at the rock composition, it is unlikely that there are any unmeasured cations occurring in large enough concentrations to balance the solution. The sulphate concentrations were however so high in some samples that they fell outside the calibration curve unless diluted 1000 times, adding uncertainty (pers. comm. M. Naoroz, 26.10.2016). The electrical balance results are available in Appendix 4 together with the rest of the water sample data. The uncertainty in the measured sulphate concentration is thought to be the reason for the high error in these samples, which is why the solutions used for the PHREEQC inverse modelling have balanced the charge using sulphate.

6.2.2 General Water Sample Features

The pallet experiments had been running for a while before samples were taken for this thesis. Early sampling by Fjermestad et al. (2017) shows high variation between pH and leaching of elements in the A samples. The measured pH varies between 6.8-8.2 for the A samples, 9.0-9.5 for the G samples and 7-12 for the AT samples. The AT samples start out with high pH (above 10), but this is thought to be related to residuals from concrete used during the tunnel excavation (Fjermestad et al., 2017). All the pallets have seemingly stabilised into a steady state situation before samples were taken for this study, and any effects related to the road construction and adding of lime can be considered negligible at this point. The pH values measured in this paper are in general slightly lower than those found by Fjermestad et al. (2017). The EC are in general varying between the samples, but for the A and G samples there are no large changes between the early and later samples. The AT samples generally have an increase in EC, though the AT experiment was only measured four weeks initially. The Eh has decreased from the initial measurements, though there are some uncertainties in terms of the measurement methods here as different equipment and techniques have been used. The Eh is still well inside the oxidizing environment.

The lowest concentration of both the light ions and heavy elements being measured in the A samples can be attributed to lower surface area of the alum shale in pallet A1. Container A1 generally exhibits lower concentrations than A2K and A3, and confirms that increased surface area may give an increased reactivity for alum shale on this scale. It is likely that lower evapotranspiration, increased permeability, and thus lower residence time and a diluting effect due to more water in the container contributes to the lower concentrations. The A samples generally feature lower concentrations than the AT samples, but that cannot be explained by the similar phenomenon observed with A1 compared to A2K and A3. Values measured by Fjermestad et al. (2017) show that concentrations of most elements have large variation during the first few weeks, especially for the A samples but in some cases G as well. This indicates that the elements are loosely bound to the rock mass, and could imply that the rock was partly weathered before the experiment started. The A samples were taken from a traditional roadcut, and has been more susceptible to weathering before sampling because of less protection from overlying material. Due to possible soil weathering and acid production with CO_2 input from soil respiration (Hanson et al., 2000), the water weathering the alum shale before sampling may be slightly acidic and increase the weathering rate. It is uncertain if this can explain the varying concentrations, or if it is due to the sampling process

6.2.3 Mineral Weathering Rates

As the average of the water samples have been testes in PHREEQC, one can effectively quantify the weathering of alum shale. Assuming a constant rate and using the inverse modelling results from AT, one can estimate the amount of time until the all the sulphides have dissolved by dividing the amount of the sulphide mineral by the rate of weathering. Assuming a pyrite content of 20 % based on the XRD results (Figure 13), the pyrite will be completely weathered in approximately 16 years. Sphalerite takes considerably longer at approximately 135 years, assuming a concentration of 0.05% based on what is observed under SEM. This concentration gives the same temporal range as when the calculation is based on the Zn concentration measured using handheld XRF (Table 12). As the concentrations of Ni are similar to Zn both in terms of rock and water samples, it can be assumed that Ni is released on a similar timescale. Cobalt can have a similar concentration in rock samples, but since it is released in lower concentrations it can be assumed to be released over a longer period. With a lower initial concentration of U in the rock samples (Table 12) it can be interpreted that release of U will decrease quicker than Zn and Ni, but is not backed by any modelling results.

The presence of calcite in the alum shale inhibits acidification as mentioned by Jeng (1991a), but weathering of the rock still occurs with high release of Zn, Ni and sulphate. Jeng (1991b) added calcite in a lab experiment and demonstrated an effective removal of trace elements from solution as well as an observed increase in pH. The pH is already near neutral in the samples taken in this study, but Zn, Ni and sulphate are still released with high concentrations from the pallet experiments. The large amount of calcite dissolution in the PHREEQC model is probably related to buffering reactions (Appelo and Postma, 2013), and all the calcite will be weathered in approximately 11 years. This is based on a calcite content of 15 %, derived from the results of the XRD analysis (Figure 13). Pyrite weathering following the depletion of calcite will lead to acidification due to a lower acid reducing potential of the rock, and increased weathering and release of elements more soluble in acid solutions such as Fe and Al may occur.

The G samples show a weathering rate similar to the A samples, despite having less sulphides. This can be related to the higher specific surface area in the G samples, especially as the grey shale has a matrix that will disintegrate easily due to it consisting of mainly mica instead of weathering resistant quartz and feldspars (Figure 13b). A lack of carbonate will give a lower buffering capacity which could accelerate the sulphide weathering process (Jeng, 1991a, Jeng, 1991b). This is visible as the pH in the water samples from G pallets often are lower than in samples from A pallets (Figure 26). As the sulphide content is significantly lower in Galgeberg shale than in alum shale, it does not pose such a risk for long term acidification. Inverse models in PHREEQC are far less common than forward models utilizing the same program, and the modelling results obtained in this study has due to this reason not been compared to any other study.

A high weathering rate can be explained by a high surface area of the common framboidal pyrite in this relatively unmetamorphosed alum shale (as suggested by Jeng (1990)), but also with ideal weathering conditions with aerobic conditions. If the weathering rate is controlled mainly by the high surface area, one could expect the Jevnaker alum shale to have a slower weathering rate of pyrite as the sulphides are concentrated in veins of euhedral pyrite with lower surface area. Pyrrhotite has been mentioned as a possible catalyst for alum shale reactivity (Bastiansen et al., 1957), and pyrrhotite is as common as pyrite in the Jevnaker alum shale. The high weathering rate of pyrrhotite is often attributed to the large surface area compared to pyrite (Janzen et al., 2000), but it is uncertain if this will still be the case for the

Jevnaker alum shale due to larger grains. Weathering of chalcopyrite may be underestimated due to the low mobility of Cu in groundwater, and larger concentrations may be released with further decrease in pH (Appelo and Postma, 2013).

6.2.4 Trace Element Mobilization and Transport

The correlation analysis shows that concentrations of Zn, Ni, Sr, Co and Cd are likely to exhibit a similar release pattern in water that has percolated through alum shale in an oxidising environment. These elements are situated in phases that are weathered in such an environment, and they have similar transport characteristics. It cannot be interpreted from the correlation analysis alone that these elements are situated in the same minerals or phases, and results from XRD and SEM as well as earlier sampling must be taken into account.

When comparing the results from the early sampling by Fjermestad et al. (2017) with the results in the assumed steady state situation in Oct-Nov 2016 there are two patterns that emerge. The elements are either released in relatively high concentrations in the early part of the experiment and decreases in the samples taken for this study, or the opposite distribution with increasing concentrations measured. The elements showing the first trend are Al and Mo in all cases and Ni, Co, Cd and U only for the A experiments. As for Fe, Zn and Sr in all three experiments and Ni, Co, Cd and U in AT, they start out with relatively low concentrations and show higher concentrations in the latest samples. The different behaviour of Ni, Co, Cd and U between the A and AT samples could be another indicator of pre-sampling weathering of the A samples. If the behaviour of an element is similar in both the A and AT experiments, the pattern can be related to weathering processes inside the experiment. Release is then likely to be related to the water transport characteristics of the elements. If the elements show high concentrations in water runoff during this experiment, it is either situated in a reactive mineral or loosely bound through sorption or ion-exchange.

While analysing the elements showing similar behaviour in all experiments, it is clear that Al and Fe are controlled more by factors concerning water solubility and transport than mineral reactions. Aluminium is situated in both mica and feldspar present in alum shale, but in near-neutral waters the Al^{3+} concentrations is often very low (May et al., 1979). The higher Al concentrations in the start of the experiment may reflect only the loosely bound Al, which may have been transported together with colloidal- and organic material. The concentrations of K^+ and Na^+ are thought to reflect the feldspar and mica weathering better than Al, as these

elements are more soluble and thus more mobile in the environment (Berner, 1980). In the Hadeland alum shale Fe is mainly related to pyrite, but the concentrations of Fe in the water samples are very low compared to the sulphate concentrations. Ferric iron is only stable in water solution in low pH solutions, while Fe^{2+} requires a low redox potential (Appelo and Postma, 2013). Since the Fe^{2+} in pyrite is easily oxidised to less soluble Fe^{3+} creating Fe-(oxyhydr)oxides and iron sulphates in higher pH ranges, the mobility of Fe is limited. The water samples taken at Hadeland are around the boundary between Fe^{2+} and $Fe(OH)_3$ (Figure 6), mostly due to the lower temperature lowering the pe.

Fjermestad (2013) assigns most of the Mo to more stable phases, while the results in this study combined with the results from Fjermestad et al. (2017) show the highest Mo release at the start of the experiment. This may represent only an ion-exchange fraction of Mo in alum shale, but the quantities released may suggest that most of the Mo is released quickly after exposure. Karlsson et al. (2012) saw that heating increased the leachability of Mo from alum shale, meaning that contact metamorphosed shale could release Mo at a higher rate. This supports that Mo is situated in the organic fraction, which is modified during heating.

Strontium and zinc is both considered mobile in the environment, and both show a similar leaching pattern throughout this experiment. Since Zn is found in sphalerite in alum shale, this mineral is thought to be the main source for this element. The pattern exhibiting release after 1-2 years both in shale from the roadcut and the tunnel means that weathering of this mineral occurs in the pallet experiments, and not to a large degree before sampling. Release and transport of Sr in water can be attributed to mineral surface reactions, though with a higher reaction rate compared to Zn as the concentrations are relatively high to start with.

Ni, Co, Cd and U show different behaviour between the A and the AT samples. Cadmium has been measured in sphalerite, and release increases with time in AT. The concentrations measured in A in this study are lower than those measured by Fjermestad et al. (2017). That might indicate that Cd is released easily, though concentrations in AT samples of both Cd and Zn increase from the initial samples by Fjermestad et al. (2017) to the samples taken for this study, indicating a release depending on mineral dissolution. The similarities between Cd and Zn are another indication of the occurrence and release of both elements from sphalerite. A quick cross-plot of the two elements visualise the relationship between the two elements (Figure 33). Similarities between Cd and Zn in terms of release from alum shale were recognised by Lavergren et al. (2009a). The lower concentrations of Zn in the A samples

could either be due to lower overall release of Zn, or that the peak concentrations of Zn have already occurred. The Zn content in the rock is lower in A compared to AT (Table 12), and a lower overall release of Zn is the more likely option.

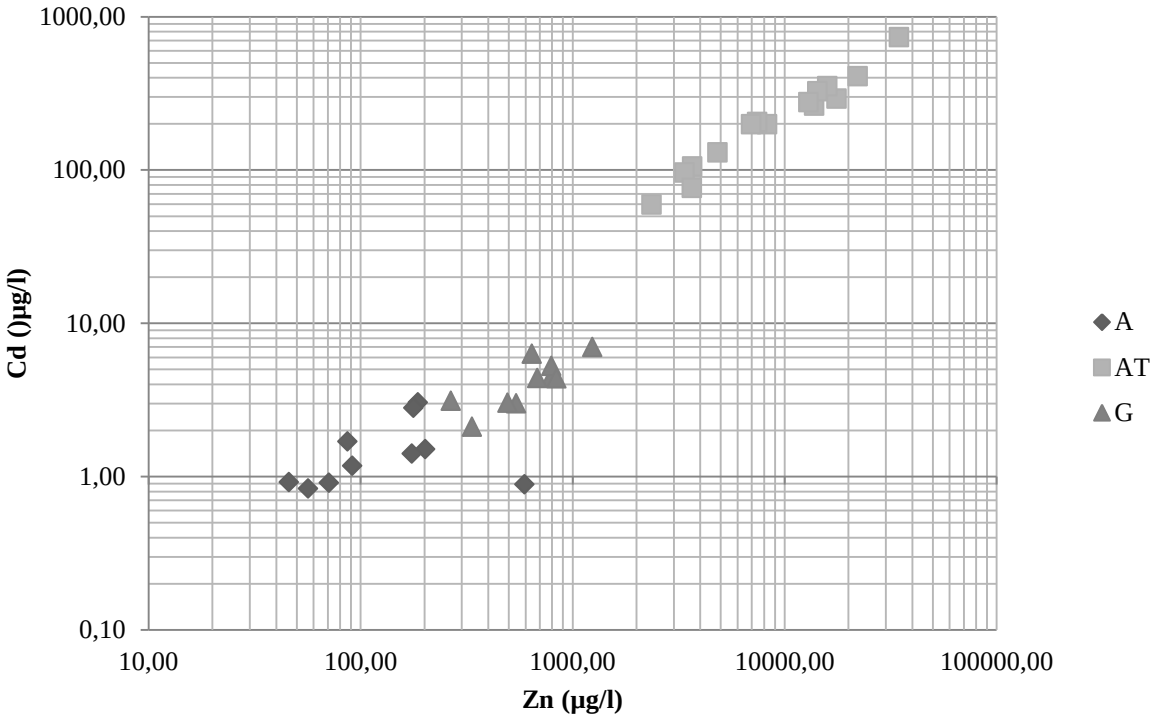

Figure 33: Cross plot between Zn and Cd measured in water samples from the pallet experiments, indicating a linear relationship. Note: Both axes are logarithmic in order to visualise the relationship in samples with both high and low concentrations

Nickel and cobalt have relatively high concentrations in some early samples in A measured by Fjermestad et al. (2017), and shows less spread in the samples taken in this study. The AT samples taken for this study have a lot higher concentration than the earlier samples. As the A rock samples have a similar amount of Ni as the AT samples (Table 12), it could be interpreted that the peak release of Ni already occurred in the A pallets (Figure 34). This is though not measured, and there might be a difference in release between the two pallet groups. Nickel is considered to be less mobile than Zn, and if release of Ni at a higher rate has occurred it implies that Ni is loosely bound in the Hadeland alum shale. That means Ni release could be related to ion-exchange processes or oxidation and dissolution of organic matter rather than sulphide oxidation, and that Ni is not necessarily bound primarily to sulphides. This is in disagreement with Jeng (1991b), who regards Ni to mainly be in a form requiring aggressive treatment before dissolving. In his experiments the release of Ni are low relative to the total Ni content, though it is explained that some portion of the Ni is easily

soluble or already present in an oxidised form. Falk et al. (2006) connects Ni to Cd and Zn as the most mobile elements, similarly to what is observed in the pallet experiments. For Ni and other elements that may be associated with organic matter, different grainsize in small scale leaching experiments may not give a systematic difference (pers. comm. H. Hellevang, 27.04.2017). The lack of an observed Ni-bearing mineral increases the likelihood of Ni to be present with organic matter.

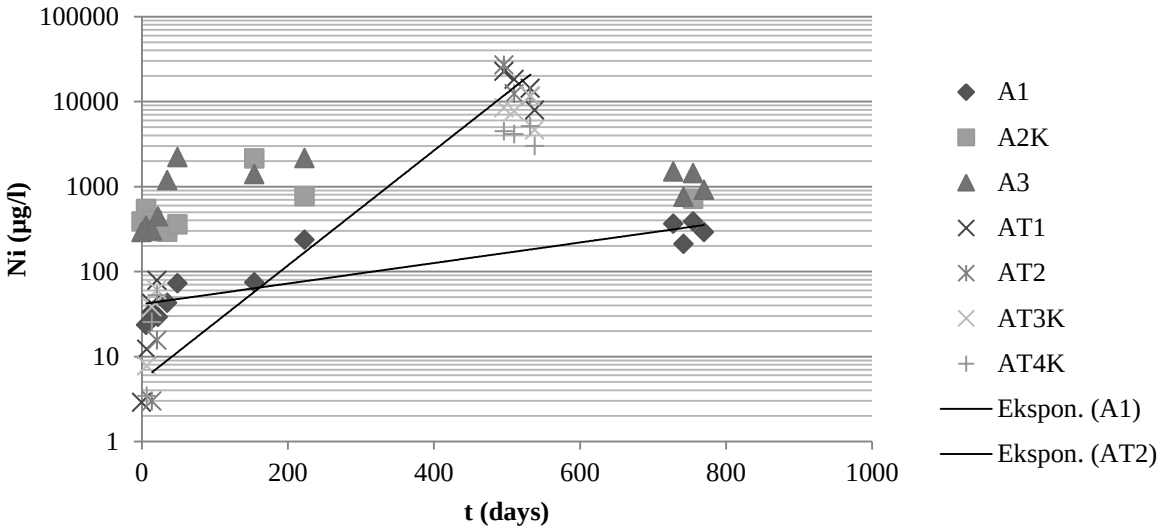

Figure 34: Temporal distribution of Ni release, using results from both A and AT water samples. A possible peak release of Ni between 400 and 600 days may occur, but it could be related to a difference between the weathering rate of the shale samples indicated by the added trend-lines for A1 and AT2.

The Co content in rock samples is lower in A compared to AT (Table 12), and it is reflected in the water samples as the AT samples taken for this study have higher concentrations than measured in the A samples. With a significant initial release measured by Fjermestad et al. (2017), Co is easily available for transport from the partly weathered A shale, but also released in a pattern similar to that of Zn in AT. The higher Co concentrations observed in runoff from AT can be attributed to the higher Co concentration in the rock samples. Lavergren et al. (2009a) describes leaching of Co as similar to Cd, Zn and Ni, and Co is less susceptible for adsorption than Zn (Abd-Elfattah and Wada, 1981).

The release of U from the pallets follow a similar distribution as Ni and Co with a decrease in A and G and an increase in AT, though here the initial water sample concentrations in A are higher than the later concentrations from AT. This could indicate that the shale at A have a higher initial release due to weathering before the experiment started, and weathering of the

phase containing U happens at a higher rate. Uranium must be in a form that is easily transported in near neutral aqueous solutions. That will in most cases be hexavalent uranium, either as a separate ion or as the uranyl complexion. Helmers (2013) mentions carbonate as a possible mobilization agent through complexation with U, though it is uncertain how much dissolved carbonate is present in the water samples taken for this study. Complexation with carbonate is supported by Akcay (1998), who found that hexavalent uranium had the strongest sorption and complexation around pH 7. The correlation analysis does not show a clear relationship between U and Ca (Appendix 6, Figure 31). Fjermestad (2013) mentions apatite as a possible mineral from which U can be released in reducing conditions. If U is situated as tetravalent ions substituting for Ca^{2+} in apatite (Altschuler et al., 1958), it would need to be oxidised from tetravalent U to hexavalent U before significant transport could occur. Apatite is not considered redox sensitive, and may dissolve in similar quantities regardless of oxygen availability (Goyne et al., 2006). As U is also related to organic material (McKelvey, 1955, Leventhal, 1991, Schovsbo, 2002), dissolution and transport of organic material may contribute to transport of U. This could especially be the case if the organic matter dissolving exists as a nonadsorbable compound (Davis, 1982).

6.2.5 Comparison to Water Regulations

Comparing with the water regulations in Table 2, it is obvious that Ni and Zn are of the largest concern. Zinc is in Class IV only in two A1 alum shale samples; otherwise the concentrations are in Class V with a considerable margin for both A, AT and G samples. Cadmium has quite low threshold values, and has concentrations in Class V for all AT samples, Class IV for all A samples and both Class IV and V for the G samples. Uranium do not have such a classification scheme despite the possible radiation health effects (Banks et al., 2000), but all the alum shale samples give values well above the EPA (2009) drinking water threshold. It is likely that the U levels measured in this study are of environmental concern in terms of radioactive decay and radon degassing from water as well as settlement of radioactive polonium dust (Skipperud et al., 2016). Cobalt and molybdenum often show values above the given threshold, while Sr show one value corresponding to class II in an AT sample that generally gives large concentrations.

6.2.6 Comparison of Experiments

The column laboratory experiment shows similarities with the results from the pallet experiments. Since the shale in the laboratory experiment were crushed and mixed, it is hard to estimate effects related to grainsize and mineral distribution in the rock without conducting a similar pallet experiment. The smaller grainsize and thus higher specific area in the columns most likely contribute to a higher reaction rate (Aagaard and Helgeson, 1982), and relative trends can be compared instead of absolute value.

Mo is released quite quickly with high concentrations in early samples from the columns, as measured by Fjermestad et al. (2017) in the pallet experiments. The results from this study are insufficient to identify and quantify any effect of contact metamorphosis on Mo release, as is observed with heating in other studies (Karlsson et al., 2012). Zn, Sr, Ni, Co and U show similar patterns in the column experiment, with higher concentrations often related to high water residence time and probably controlled by the mineral reaction rate as in the pallet experiments. Similar to the pallet experiments, Cd has high concentrations both at the start of the experiment and with longer residence times later. The Fe values in the column experiment are low, while the Al values are similar to those observed from the pallet experiment. The Al values could be influenced by sample containers releasing the element to the samples (pers. comm. S. Simonsen, 25.01.2017), as different containers were used for the samples from the column experiments compared to the samples from the pallet experiments. Despite not being measured, it can be assumed that sulphate were the major anion in the column experiment due to the extended similarities to the pallet experiment. As for the pallet experiments calcite buffers the acidity produced by sulphide weathering, evident as Ca is the major cation. Due to the high calcite content and the presence of pyrrhotite instead of pyrite, acid runoff may not occur to a large extent.

6.2.7 Factors Controlling Release of Elements

Release of elements can be controlled by either the reaction rate or transport of the elements. The results from the column experiments can be used to estimate what controls the release of an element, especially if one disregards the loosely bound elements that flush out immediately. Since Fe, Co, Ni, Sr and U all show their highest concentration in the last sample, release of these elements are probably controlled by the weathering reaction rate. Zinc has high release in general, and could be controlled by transport.

Mo, Cd and Al all show their highest concentration in the first or second sample, and this release can be attributed to a loosely bound fraction that is transport dependent. The size of this fraction relative to the total amount of the element is unknown.

Contribution of Al, Zn, and Cd from the sand used to create permeability is assumed to occur, but the amount contributed for Al is uncertain as the near-neutral pH mobility of this element is low due to low solubility (May et al., 1979). In terms of Zn and Cd it seems that these are present and loosely bound in the sand, as the highest concentrations of these elements are measured coincide with relatively low residence time (Table 9) and significant release from the control column. The higher concentrations of these elements observed in the samples with a lower water flow velocity can be attributed to weathering of sphalerite from the shale, as both of these elements were observed in this mineral in the E16 alum shale.

Deciding between a rate- or transport controlled release cannot be done with the pallet experiments, as the water flow through the pallets is not continuous over the 14 day periods. Days with high and low transport may occur within the same sampling period, and without continuous sampling and measurement of precipitation the effect cannot be accounted for. Unsaturated conditions may occur in the pallets, which could enhance the reaction rate and concentration of elements in the pore water due to higher oxygen availability. The column experiment shows that the E16 alum shale has a potential for leaching elements of environmental concern in near-neutral solutions, possibly with a similar pattern as the Rv. 4 alum shale.

Previous leaching studies have usually targeted different mineral phases using sequential extraction (Fjermestad, 2013), which do not necessary reflect weathering with longer water residence time and thus the conditions in an alum shale depot. It is uncertain if the sequential extraction methods used can thoroughly distinguish between different phases that may dissolve or oxidise in alum shale, and in that case in which order the different phases are released. During personal communication, H. Hellevang mentioned how a leaching study experiment may be rate controlled, and that the system may not be in equilibrium when samples are taken. As an example, all the sulphides may not be dissolved by the added hydrogen peroxide, and the remaining sulphides will be dissolved in the residual fraction. The SEM analysis in this study shows that most of the Fe in alum shale are situated in sulphides, though the results from Fjermestad (2013) have most of the Fe released in the residual fraction.

6.2.8 Comparison With Alum Shale Depot

Groundwater samples from the alum shale depot at Hadeland taken during 2016 were analysed by Fjermestad (2017), and raw data from 2016 were made available through personal communication (H. Fjermestad, E-Mail 27.02.2017). Water samples were collected from three wells with different depths referred to as Well 1 (5m), Well 2 (10m) and Well 3 (15m) (Fjermestad, 2017), with the last sample available taken 13.12.16. The raw data only includes the chemical analysis for major and trace elements, and while the water flow in the depot is unknown the water table is described as stable by Fjermestad (2017). One of the arguments for allowing such a depot was little to no groundwater flow, and it is assumed that the residence time is at least as long as in the pallet experiments. The characteristics of the depot material vary, and individual particle size can range from boulders to silt.

In terms of release of elements from the shale Zn and Ni exhibit the same trend (Figure 35), with concentrations increasing throughout the period in Well 1 while being stable in Well 2 and 3. The concentrations in the last sample from Well 1 reach 175 µg/l and 221 µg/l Zn and Ni respectively. This is similar to the pallet experiments, where Ni is thought to be released at a higher rate than Zn. Cobalt has a similar development in between the wells, and the highest concentration from is 5,81 µg/l in the last sample from Well 1. Strontium has rather stable concentrations between 2500-3500 µg/l in two wells, levels about 1000 µg/l lower than the values observed from pallet A. Release of U is rather large initially and reaches over 900 µg/l before stabilizing around 400 µg/l in Well 1 (Figure 35). These are quantities similar to what is observed from the pallet experiments, and implies that a more mobile fraction is leached before release continue due to weathering of more resistant U-bearing phases. This could be similar behaviour as what Fjermestad (2013) and Helmers (2013) describes from sequential extraction studies. Molybdenum follows a similar pattern as U, and is released quickly after the measurements started in similar fashion to the pallet experiments. Cadmium concentrations are in general low with no clear pattern, with values similar to those measured in the A samples. Concentrations generally decrease between December 2016 and March 2017 (Fjermestad, 2017).

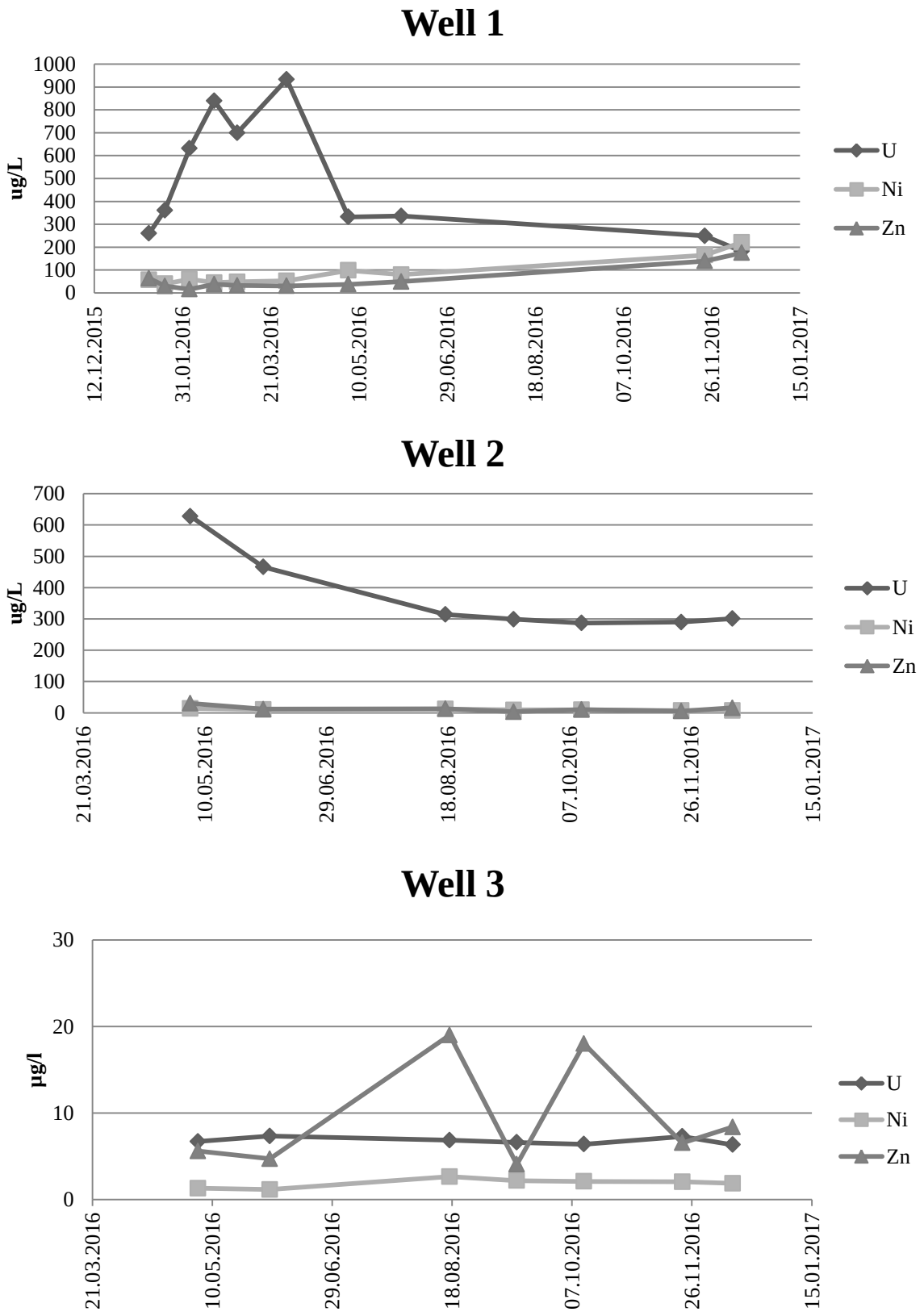

Figure 35: Development of U, Ni and Zn concentrations in the alum shale depot at Hadeland, with water samples taken from Well 1 (5 m depth), Well 2 (10 m depth) and Well 3 (15 m depth). Lower concentrations are observed with depth. Modified from Fjermestad (2017).

The sulphate concentrations in the water samples from the alum shale depot are usually lower than those measured from the pallet experiment. The samples from AT can have concentrations up to 10 times as high, while A has only slightly higher concentrations. Similarly to the Zn, Ni and Co values the sulphate concentration increases in one well while being stable in two. As observed from the results of the pallet experiment the Fe concentration do not follow the sulphate concentration, and there is no obvious pattern when it comes to the Fe concentration. A similar alum shale depot studied by Allard et al. (1991) has a weathering rate of about 15 g Fe m^{-2} y^{-1}, observed in a functioning depot. A similar value for the pallet experiments can be estimated to 0.3 to 3-4 kg Fe m^{-2} y^{-1} assuming an alum shale volume of 0,2 m^3 and using the weathering rate obtained for A and AT respectively in PHREEQC. As the results from the PHREEQC inverse model shows, one could expect sulphide weathering and growth of gypsum with either O_2 or CO_2. CO_2 may be present as a proton donor through dissolution and reaction with groundwater, and increase the weathering. The likeliness of the reaction using CO_2 in the alum shale depot is uncertain. The excess sulphate in the water samples may originate from dissolution of secondary gypsum (Hecht and Kölling, 2002), but the mineral was not measured during XRD. Fjermestad et al. (2017) identified secondary gypsum on the alum shale, indicating that precipitation and dissolution of gypsum also affects the sulphate concentrations.

The PHREEQC model was applied to a water sample taken at 13.12.2016 from Well 1 in the alum shale depot, and the results were very similar to the results for the A samples. On average 5.50 and 5.48 g pyrite, 6.12 and 6.08 g calcite as well as 0.25 and 0.26 mg sphalerite were calculated to dissolve with CO_2 present in the A samples and in the well sample respectively. Surprisingly the pyrite dissolution in the well sample is controlled by the iron concentration, which is similar in both the well- and pallet samples. Since sulphate is the major anion, it is used for charge balancing here as well. The only clear difference between the two results is the albite weathering, which is higher in the depot by a factor of 16.5 due to a higher Na concentration. The concentrations of Fe, Ni, Zn and sulphate from the last four well samples and the samples from A1 are comparable (Figure 36), though the pallet experiment sees more variation. This can be attributed to a larger variation in water input. Formation of secondary minerals is similar to A, and could cause a volume increase in the alum shale depot.

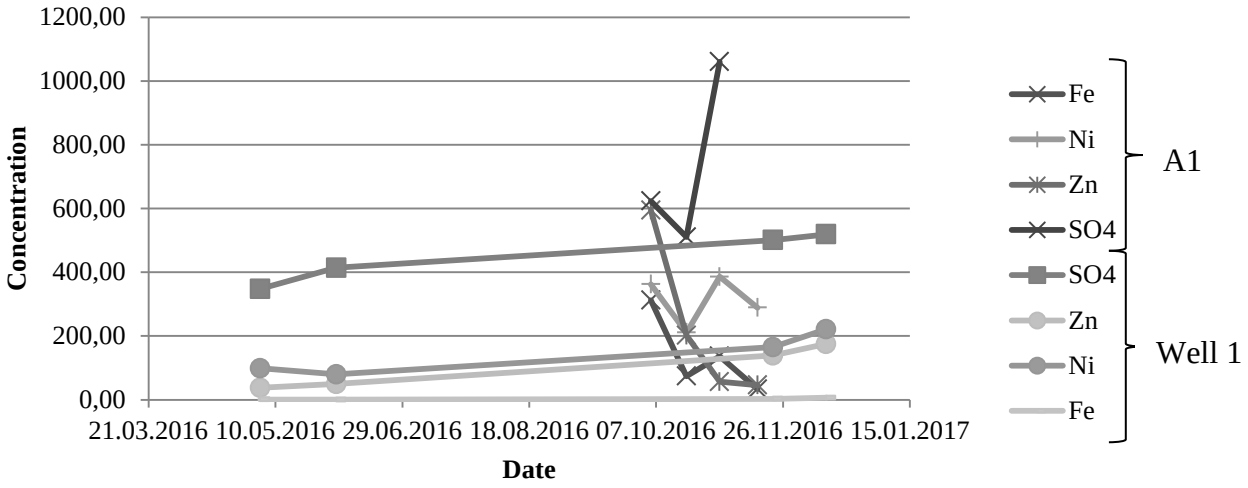

Figure 36: Comparison of water sample concentration development of Fe, Ni, Zn (µg/l) and SO4 (mg/l) from Well 1 in the alum shale depot from May 2015 to December 2016 and A1 from the pallet experiment (October-November 2016). The pallet experiment sees more variation, but the values are comparable.

One of the key differences between the pallet experiments and the alum shale depot is the water saturation. In order to maintain reducing conditions in the depot, transport of oxygen to the depot cannot occur to a large degree (Skipperud et al., 2016). Oxygen is present in the atmosphere, and infiltrating water will contain O_2 due to contact with the atmosphere. In the unsaturated zone the O_2 concentration is controlled by gas diffusion from the atmosphere, which occurs at a rate 10^4 higher than diffusion through groundwater (Appelo and Postma, 2013). Increasing water saturation will thus reduce the diffusion of oxygen. This is not well controlled in the pallet experiments, and a larger influx of oxygen in the pallets compared to the depot could lead to a higher weathering rate of pyrite (Equation 1) (Hecht and Kölling, 2002) and the shale. The PHREEQC inverse model comparison between the A samples and the depot well water sample show very similar results, but other factors may cancel out the effect of lower oxygen availability in the depot. One factor could be grainsize, as one of the A pallets contained coarser material which has led to lower concentrations. A period without sampling open up for the possibility of a weathering peak and higher release of weathering products from the A samples, while water from the well has been continuously sampled. Fjermestad (2017) assign the weathering observed in Well 1 to contact with surface water.

Well conditions may change with time as precipitation of weathering products may increase the permeability, and thus water transport due to opening of cracks. The same weathering products may cement pore space and decrease permeability. The water budget for the depot is critical to monitor in order to limit increased transport of elements with depot development.

Temperature will vary with the season for the pallets, but be rather stable in the depot. During winter the shale and water in the pallets will freeze, while the depot will only freeze in the top layers. Frost wedging of the shale may lead to a lower grainsize and higher specific area of the material with time, but release of trace elements to the environment will not occur when the percolating water is frozen. A frost wedge effect was not observed by Karlsson et al. (2012), but the crushing and sieving of the alum shale material before the freezing process as done in that study could reduce the possible effect of frost wedging compared to the pallets with a highly variable grain size. Accumulation of snow and ice on top of the pallets may lead to higher flow through the pallets during spring, but a short residence time implies that it will not lead to higher release of trace elements. It is observed that higher temperatures and inflow of water during spring may affect the redox conditions in the alum shale depot (Fjermestad, 2017), possibly explaining the lowering of concentrations during winter 2017.

6.2.9 Implications for new projects

The E16 alum shale has different mineralogy and more heterogeneous composition compared to the Rv. 4 alum shale due to contact metamorphosis, and may give a different potential in terms of acidification of surface water together with release of trace elements of environmental concern. It may be challenging to classify rocks from roadworks, as the core samples used in this study show large variations on a cm scale. Identical rock samples may thus be classified differently depending on the method, and a chemical analysis may not give large differences between these rocks with respect to trace element content (Nyland and Teigland, 1984).

Sulphides are not as dispersed and have a smaller surface area in the contact metamorphosed shale as they are concentrated in veins, but are often a combination of pyrrhotite and pyrite together with accessory sulphide minerals. The larger calcite content will give a larger buffer capacity, but as observed in the pallet experiment elements such as U, Zn, Ni and Mo are still mobile in near neutral conditions buffered by calcite. A higher potential production of gypsum and other sulphates compared to the Rv. 4 alum shale may occur due to more calcite in the E16 alum shale. It may be an advantage to locate an alum shale depot in an area where volume changes can occur without larger consequences.

In addition to the elements analysed in this study the E16 alum shale contains arsenopyrite, which through weathering may release As and Co to groundwater. Intake of As through drinking water may lead to cancer, and the No Observed Adverse Effect (Class II) concentration is 0.5 µg/l (Miljødirektoratet, 2016). For that reason weathering and mobility of arsenic from alum shale should be included in future work regarding alum shale, especially in cases where contact metamorphosis occurs.

7 Summary

7.1 Conclusion

The mineral content in relatively unmetamorphosed shale found using XRD in samples taken for this study is similar to previous studies, and the primary mineral content of alum shale is well established with quartz, feldspars, illite/muscovite, pyrite and veins of calcite. The mineral quantification conducted in this study however measured a larger sulphide content than previous studies. Sphalerite is found during SEM analysis, and accounts for the zinc and cadmium in the shale. Accessory minerals such as phosphates are not identified in XRD, but contain uranium and rare earth elements.

Low grade contact metamorphic shale was studied, and pyrrhotite and albite were identified as indicators of metamorphism. The formation process of these minerals is unclear, but the contact metamorphic alum shale clearly has coarser mineral grains indicating recrystallization.

Alum shale weathering is dominated by pyrite oxidation and production of acidity, which is subsequently buffered by dissolution of calcite. The mineral reactions can be identified by analysing water samples, where high concentrations of sulphate indicate weathering of sulphides and elevated concentrations of Ca^{2+} indicate calcite dissolution. The presence of both these ions in solution may lead to precipitation of gypsum, though this was not measured during mineralogical analysis of the shale. Calcite dissolution was found to occur at a higher rate compared to pyrite oxidation, and acidification may occur in the future depending on the amount of calcite.

The conducted experiments reveal that water percolating through alum shale in an oxidising environment release Zn, Ni and U in concentrations that are of environmental concern. A large release of Zn implicates a significant release of Cd as well, since both are measured to be situated in sphalerite. Nickel was not found in sulphides to the same extent as Zn, and it is uncertain if Ni is related to sulphides in relatively unmetamorphosed shale. Cobalt was found in arsenopyrite and cobaltite in contact metamorphosed shale. Strontium and molybdenum was not measured in a mineral phase.

It is measured that coarser alum shale material release lower concentrations of elements, and exhibit less mineral weathering. This is thought to be related to a lower residence time of percolating water and a lower specific surface area of the rock fragments leading to a lower weathering rate. In order to limit the environmental impact of alum shale weathering, it can be recommended that future depot masses are not crushed. Unsaturated conditions may also be unfortunate, as a larger input of oxygen through gas diffusion can be expected.

7.2 Further Studies

It is recommended that the Gran experiment are continued in order to monitor long term exposure in a natural environment. Concentrations have not gone down for several elements of environmental concern, and some elements may not yet have leached at all. If acidification occurs after calcite is completely dissolved, one may release elements that are now sorbed in the alum shale material. Even if the alum shale weathering represents a quick process on a geological timescale, it is reported that changes happen on a 10 year scale.

A similar pallet experiment with the Jevnaker alum shale could be conducted, in order to compare the effect between the low specific surface area of pyrite in alum shale and the high reported reactivity of pyrrhotite in contact metamorphosed alum shale.

Another possibility is to do a similar long term laboratory leaching test with deionised water or other weak solutions, on a 1 ½ year period with less leaking potential and measurement of content before and after leaching. Columns with oxidising and reducing conditions should be compared.

In terms of where the different studied elements are situated in alum shale, it is still uncertain where Ni, Mo and Co are situated. Additionally it is uncertain if the amount of U found in phosphate minerals are sufficient to account for all the U in alum shale. A chemical analysis of trace elements in the organic fraction of alum shale would probably give further insight into the location of these elements. An accurate measurement of the chemical composition of the rock using XRF is recommended for any future study.

References

AAGAARD, P. & HELGESON, H. C. 1982. Thermodynamic and kinetic constraints on reaction rates among minerals and aqueous solutions. I. Theoretical considerations. *American Journal of Science,* 282**,** 237-285.

ABD-ELFATTAH, A. L. Y. & WADA, K. 1981. Adsorption of Lead, Copper, Zinc, Cobalt, and Cadmium by Soils That Differ in Cation-Exchange Materials. *Journal of Soil Science,* 32**,** 271-283.

ABREHAM, A. Y. 2007. *Reactivity of alum and black shale in the Oslo region, Norway.* Master, University of Oslo.

AKCAY, H. 1998. Aqueous speciation and pH effect on the sorption behavior of uranium by montmorillonite. *Journal of Radioanalytical and Nuclear Chemistry,* 237**,** 133-137.

ALLARD, B., ARSENIE, I., HAKANSSON, K., KARLSSON, S., AHLBERG, A. C., LUNDGREN, T., COLLIN, M., RASMUSON, A. & STRANDELL, E. 1991. Effects of Weathering on Metal Releases from an Engineered Deposit for Alum Shale Leaching Residues. *Water Air and Soil Pollution,* 57-8**,** 431-440.

ALTSCHULER, Z. S., CLARKE JR., R. S. & YOUNG, E. J. 1958. The Geochemistry of Uranium in Apatite and Phosporite. *Shorter Contributions to General Geology.* Washington: USGS.

ANDERSON, G. & PARKHURST, D. L. 2015. LLNL. USGS.

ANDERSSON, A., DAHLMAN, B. & GEE, D. G. 1982. Kerogen and uranium resources in the Cambrian alum shales of the Billingen—Falbygden and Närke areas, Sweden. *Geologiska Föreningen i Stockholm Förhandlingar,* 104**,** 197-209.

ANTUN, P. 1967. Sedimentary Pyrite and its Metamorphism in the Oslo Region. *Norsk Geologisk Tidsskrift,* 47**,** 25.

APPELO, C. A. J. & POSTMA, D. 2013. *Geochemistry, groundwater and pollution,* Amsterdam, A.A. Balkema Publishers.

ARMANDS, G. 1972. *Geochemical studies of uranium, molybdenum and vanadium in a Swedish alum shale.* Stockholm Contributions in Geology 27, University of Stockholm.

ASSARSSON, G. & GRUNDULIS, V. 1961. Chemical Investigations of upper Cambrian shales at Hynneberg, Närke. *Geologiska Föreningen i Stockholm Förhandlingar,* 83**,** 9.

BANKS, D., FRENGSTAD, B., SKREDE, A. K., KROG, J. R., STRAND, T., SIEWERS, U. & LIND, B. 2000. Grunnvann - ikke bare vann. *Gråsteinen, NGU,* 6**,** 65.

BASTIANSEN, R., MOUM, J. & ROSENQVIST, I. T. 1957. *Bidrag til belysning av visse bygningstekniske problemer ved Oslo-områdets alunskifere,* Oslo, Norges geotekniske institutt.

BEKTURSUNOVA, R. & L'HEUREUX, I. 2011. A reaction-transport model of periodic precipitation of pyrite in anoxic marine sediments. *Chemical Geology,* 287**,** 158-170.

BELZILE, N., CHEN, Y.-W., CAI, M.-F. & LI, Y. 2004. A review on pyrrhotite oxidation. *Journal of Geochemical Exploration,* 84**,** 65-76.

BERNER, R. A. 1980. *Early Diagenesis: A Theoretical Approach,* Princeton University Press.

BERNER, R. A. 1984. Sedimentary Pyrite Formation - an Update. *Geochimica Et Cosmochimica Acta,* 48**,** 605-615.

BHATTI, T. M., BIGHAM, J. M., CARLSON, L. & TUOVINEN, O. H. 1993. Mineral Products of Pyrrhotite Oxidation by Thiobacillus-Ferrooxidans. *Applied and Environmental Microbiology,* 59**,** 1984-1990.

BJØRLYKKE, K. 1974a. Depositional History and Geochemical Composition of Lower Palaeozoic Epicontinental Sediments from the Oslo Region. *Norges Geologiske Undersøkelse,* 305**,** 81.
BJØRLYKKE, K. 1974b. Geochemical and mineralogical influence of Ordovician Island Arcs on epicontinental clastic sedimentation. A study of Lower Palaeozoic sedimentation in the Oslo Region, Norway. *Sedimentology,* 21**,** 251-272.
BJØRLYKKE, K. & ENGLUND, J. O. 1979. Geochemical response to Upper Precambrian rift basin sedimentation and Lower Palaeozoic epicontinental sedimentation in south Norway. *Chemical Geology,* 27**,** 271-295.
BOGGS, S. J. 2014. Silisiclastic Sedimentary Rocks. *In:* BOGGS, S. J. (ed.) *Principles of Sedimentology and Stratigraphy.* 5 ed. London: Pearson Education Limited.
CHERNIAK, D. J. & WATSON, E. B. 1992. A Study of Strontium Diffusion in K-Feldspar, Na-K Feldspar and Anorthite Using Rutherford Backscattering Spectroscopy. *Earth and Planetary Science Letters,* 113**,** 411-425.
CHI FRU, E., HEMMINGSSON, C., CALLAC, N., PEREZ, N., PANOVA, E. G., BROMAN, C. & EL ALBANI, A. 2016. Atmospheric weathering of Scandinavian alum shales and the fractionation of C, N and S isotopes. *Applied Geochemistry,* 74**,** 94-108.
CHRISTENSEN, J. B. & CHRISTENSEN, T. H. 2000. The effect of pH on the complexation of Cd, Ni and Zn by dissolved organic carbon from leachate-polluted groundwater. *Water Research,* 34**,** 3743-3754.
COLLINS, R. N. & KINSELA, A. S. 2010. The aqueous phase speciation and chemistry of cobalt in terrestrial environments. *Chemosphere,* 79**,** 763-71.
COOK, N. J., CIOBANU, C. L., PRING, A., SKINNER, W., SHIMIZU, M., DANYUSHEVSKY, L., SAINI-EIDUKAT, B. & MELCHER, F. 2009. Trace and minor elements in sphalerite: A LA-ICPMS study. *Geochimica et Cosmochimica Acta,* 73**,** 4761-4791.
DAVIS, J. A. 1982. Adsorption of Natural Dissolved Organic-Matter at the Oxide Water Interface. *Geochimica Et Cosmochimica Acta,* 46**,** 2381-2393.
DAVIS, J. A. & KENT, D. B. 1990. Surface Complexation Modeling in Aqueous Geochemistry. *Reviews in Mineralogy,* 23**,** 177-260.
DEPARTMENT OF GEOSCIENCES. 2011a. *Scanning Electron Microscope laboratory* [Online]. University of Oslo. Available: http://www.mn.uio.no/geo/english/research/about/infrastructure/sem/ [Accessed 27.02 2017].
DEPARTMENT OF GEOSCIENCES. 2011b. *X-Ray Diffraction Laboratory* [Online]. Oslo: University of Oslo. Available: http://www.mn.uio.no/geo/english/research/about/infrastructure/x-ray-diffraction/index.html [Accessed 06.02 2017].
DYPVIK, H. 1984. Uran, Thorium, Kalium Fordeling og Naturlig Radioaktivitet i Slilisiklastiske Sedimenter, Leirsteiner og Skifre Spesielt. *Intern skriftserie.* Oslo: Institutt for Geologi.
EIDSTUEN, B. 2014. Morstad gård i forgrunnen sett nordfra i Viggadalen. Nye Riksvei 4 tar form - Gjøvik: Oppland Arbeiderblad.
EPA 2007. Drinking water standards and health advisories table. San Francisco: United States Environmental Protection Agency.
EPA 2009. Table of Regulated Drinking Water Contaminants. United States Environmental Protection Agency.
ERLSTRÖM, M. 2014. Skiffergas och biogen gas i alunskiffern i Sverige, förekomst och geologiska förutsättningar - en översikt. Uppsala: Sveriges geologiska undersökning.

FALK, H., LAVERGREN, U. & BERGBÄCK, B. 2006. Metal mobility in alum shale from Öland, Sweden. *Journal of Geochemical Exploration,* 90**,** 157-165.
FJERMESTAD, H. 2013. *Mobilitet av uran og andre metall i bergartar i ny vegtrase på Gran, Hadeland* MSc, Norwegian University of Life Sciences.
FJERMESTAD, H. 2014. Rv4 Gran grense - Alunskifer og miljøutfordringer i byggeprosjektet. *Statens Vegvesen***,** 16.
FJERMESTAD, H. 2017. Svar på forespørsel fra Statens strålevern om tilsyn i forbindelse med avslutning av vegprosjektet Rv. 4 Gran. Statens Vegvesen, 35.
FJERMESTAD, H., HAGELIA, P. & THOMASSEN, T. 2017. Utlekkingsforsøk med svartskifer fra Rv. 4, Hadeland. Statens Vegvesen.
FOSLIE, S. 1919. Kulskiferen ved Gjøvik. *Tidsskrift for Bergvæsen,* 7**,** 5.
FRANCIS, C. A., FLEET, M. E., MISRA, K. & CRAIG, J. R. 1976. Orientation of Exsolved Pentlandite in Natural and Synthetic Nickeliferous Pyrrhotite. *American Mineralogist,* 61**,** 913-920.
GAUTIER, D. L., SCHOVSBO, N. H. & NIELSEN, A. T. 2014. Resource Potential of the Alum Shale in Denmark. *Unconventional Resources Technology Conference.* Denver.
GOLDSMITH, J. R. & LAVES, F. 1954. The Microcline-Sanidine Stability Relations. *Geochimica Et Cosmochimica Acta,* 5**,** 1-19.
GOYNE, K. W., BRANTLEY, S. L. & CHOROVER, J. 2006. Effects of organic acids and dissolved oxygen on apatite and chalcopyrite dissolution: Implications for using elements as organomarkers and oxymarkers. *Chemical Geology,* 234**,** 28-45.
HAGELIA, P. & FJERMESTAD, H. 2016. Bruk av XRF på bergartar for vurdering av miljørisiko. Statens Vegvesen.
HANSON, P. J., EDWARDS, N. T., GARTEN, C. T. & ANDREWS, J. A. 2000. Separating root and soil microbial contributions to soil respiration: A review of methods and observations. *Biogeochemistry,* 48**,** 115-146.
HECHT, H. & KÖLLING, M. 2002. Investigation of pyrite-weathering processes in the vadose zone using optical oxygen sensors. *Environmental Geology,* 42**,** 800-809.
HELMERS, T. A. 2013. *The mobility of uranium from U-containing bedrock materials as a function of pH - implications for tunnel construction.* MSc, Norwegian University of Life Sciences.
HILLIER, S. 2000. Accurate quantitative analysis of clay and other minerals in sandstones by XRD: comparison of a Rietveld and a reference intensity ratio (RIR) method and the importance of sample preparation. *Clay Minerals,* 35**,** 291-302.
HÖFLINGER, G. 2013. *Brief Introduction to Coating Technology for Electron Microscopy* [Online]. Science Lab: Leica Microsystems. Available: http://www.leica-microsystems.com/science-lab/brief-introduction-to-coating-technology-for-electron-microscopy/ [Accessed 20.03 2017].
JAMTVEIT, B., DAHLGREN, S. & AUSTRHEIM, H. 1997. High-grade contact metamorphism of calcareous rocks from the Oslo Rift, Southern Norway. *American Mineralogist,* 82**,** 1241-1254.
JANZEN, M. P., NICHOLSON, R. V. & SCHARER, J. M. 2000. Pyrrhotite reaction kinetics: Reaction rates for oxidation by oxygen, ferric iron and for nonoxidative dissolution. *Geochimica Et Cosmochimica Acta,* 64**,** 1511-1522.
JENG, A. S. 1990. Morphology of Pyrite in Alum Shale, Oslo, Norway. *Acta Agriculturae Scandinavica,* 40**,** 11-21.
JENG, A. S. 1991a. Weathering of Some Norwegian Alum Shales .1. Laboratory Simulations to Study Acid Generation and the Release of Sulfate and Metal-Cations (Ca, Mg and K). *Acta Agriculturae Scandinavica,* 41**,** 13-35.

JENG, A. S. 1991b. Weathering of Some Norwegian Alum Shales, 2. Laboratory Simulations to Study the Influence of Aging, Acidification and Liming on Heavy Metal Release. *Acta Agriculturæ Scandinavica* 4**,** 76-87.
JERSTAD, A., JENSEN, C. L., RAMBERG, G. B., RUDEN, L., ÅNESTAD, K. & STRAND, T. 2005. Kartlegging av radon i Gran kommune. *RaMAP*. Statens Strålevern.
KARLSSON, L., BACKSTRÖM, M. & ALLARD, B. 2012. Leaching of Sulfidic Alum Shale Waste at Different Temperatures. *9th International Conference on Acid Rock Drainage.* Ottawa.
KIM, J. H., GIBB, H. J. & HOWE, P. D. 2006. Cobalt and inorganic cobalt compounds. *Concise International Chemical Assessment Document.* International Programme on Chemical Safety.
KIRBY, C. S. & BRADY, J. A. E. 1998. Field determination of Fe2+ oxidation rates in acid mine drainage using a continuously-stirred tank reactor. *Applied Geochemistry,* 13**,** 509-520.
LARSEN, B. T. & GABRIELSEN, R. H. 2013. Lagene foldes og skyves. Kaledonidene i Oslofeltet. *In:* RAMBERG, I., BRYHNI, I., NØTTVEDT, A. & RANGNES, K. (eds.) *Landet blir til - Norges geologi.* Trondheim: Norsk Geologisk Forening.
LAVERGREN, U., ASTROM, M. E., BERGBACK, B. & HOLMSTROM, H. 2009a. Mobility of trace elements in black shale assessed by leaching tests and sequential chemical extraction. *Geochemistry-Exploration Environment Analysis,* 9**,** 71-79.
LAVERGREN, U., ASTROM, M. E., FALK, H. & BERGBACK, B. 2009b. Metal dispersion in groundwater in an area with natural and processed black shale - Nationwide perspective and comparison with acid sulfate soils. *Applied Geochemistry,* 24**,** 359-369.
LECOMTE, A., CATHELINEAU, M., MICHELS, R., PEIFFERT, C. & BROUAND, M. 2017. Uranium mineralization in the Alum Shale Formation (Sweden): Evolution of a U-rich marine black shale from sedimentation to metamorphism. *Ore Geology Reviews,* 88**,** 71-98.
LEHNER, S., SAVAGE, K., CIOBANU, M. & CLIFFEL, D. E. 2007. The effect of As, Co, and Ni impurities on pyrite oxidation kinetics: An electrochemical study of synthetic pyrite. *Geochimica et Cosmochimica Acta,* 71**,** 2491-2509.
LEVENTHAL, J. 1991. Comparison of organic geochemistry and metal enrichment in two black shales: Cambrian Alum Shale of Sweden and Devonian Chattanooga Shale of United States. *Mineralium Deposita,* 26**,** 104-112.
MAY, H. M., HELMKE, P. A. & JACKSON, M. L. 1979. Gibbsite solubility and thermodynamic properties of hydroxy-aluminium ions in aqueous solution at 25 C. *Geochimica Et Cosmochimica Acta,* 43**,** 861-868.
MCKELVEY, V. E. 1955. Uranium in the Upper Cambrian Black Shale of Sweden. *Trace Elements Investigations Report,* 495**,** 19.
MILJØDIREKTORATET 2016. Grenseverdier for klassifisering av vann, sediment og biota.
MORLEY, C. K. 1986. The Caledonian Thrust Front and Palinspastic Restorations in the Southern Norwegian Caledonides. *Journal of Structural Geology,* 8**,** 753-765.
MULTICONSULT 2014. Kjernelogging, kartlegging av alunskifer - E16 Eggemoen-Olum. 7.
MÄRZ, C., POULTON, S. W., BECKMANN, B., KÜSTER, K., WAGNER, T. & KASTEN, S. 2008. Redox sensitivity of P cycling during marine black shale formation: Dynamics of sulfidic and anoxic, non-sulfidic bottom waters. *Geochimica et Cosmochimica Acta,* 72**,** 3703-3717.

NAKREM, H. A. & WORSLEY, D. 2013. Havet oversvømmer landet. *In:* RAMBERG, I., BRYHNI, I., NØTTVEDT, A. & RANGNES, K. (eds.) *Landet blir til - Norges geologi.* 2 ed. Trondheim: Norsk Geologisk Forening.
NAOROZ, M. S. 2013. Ion Chromatography of Sodium, Magnesium, Potassium and Calcium with Suppression of Eluent. *Laboratory Document.* Department of Geosciences: University of Oslo.
NAOROZ, M. S. 2016. Ion Chromatography of Fluoride, Chloride, Bromide, Nitrate, Sulfate, and Phosphate with Suppression of Eluent. *Laboratory Document* Department of Geosciences: University of Oslo.
NESSE, W. D. 2012. *Introduction to Mineralogy,* New York, Oxford University Press.
NGI 2015. Identifisering of karakterisering av syredannende bergarter. *In:* MILJØDIREKTORATET (ed.). Oslo: Miljødirektoratet.
NGU. 2017. *Berggrunn N50*. http://geo.ngu.no/kart/berggrunn_mobil/: NGU.
NHM. 2007. *Waldemar C. Brøggers hus (tidl. Geologisk museum)* [Online]. Oslo: Natural History Museum - University of Oslo. Available: http://www.nhm.uio.no/om/bygninger/geologisk-museum/ [Accessed 06.02 2017].
NOLD, J. L. 1990. The Idaho Cobalt Belt, Northwestern United-States - a Metamorphosed Proterozoic Exhalative Ore District. *Mineralium Deposita,* 25**,** 163-168.
NYLAND, B. & TEIGLAND, J. 1984. *En Sedimentologisk og Geokjemisk Undersøkelse av de Kambriske og Underordoviciske Marine Sedimenter i Oslofeltet.* MSc, University of Oslo.
OFTEDAHL, C. 1955. On the Sulphides of the Alum Shale in Oslo. *Norsk Geologisk Tidsskrift,* 35**,** 117-120.
OWEN, A. W., BRUTON, D. L., BOCKELIE, J. F. & BOCKELIE, T. G. 1990. The ordovician successions of the Oslo region, Norway. *Norges Geologiske Undersøkelse Special Publication,* 4**,** 58.
PABST, T., SØRMO, E. & ENDRE, E. 2016. Geochemical characterisation of Norwegian Cambro-Ordovician black mudrocks for building and construction use. *Bulletin of Engineering Geology and the Environment*.
PARKHURST, D. L. & APPELO, C. A. J. 2013. Description of Input and Examples for PHREEQC Version 3-A Computer Program for Speciation, Batch-Reaction, One-Dimensional Transport, and Inverse Geochemical Calculations. *Modeling Techniques and Methods.* USGS.
PARKS, G. A. 1990. Surface Energy and Adsorption at Mineral-Water Interfaces: An Introduction. *Reviews in Mineralogy,* 23.
PERKINELMER 2011. The 30-Minute Guide to ICP-MS. 8.
PRASAD, A. S. 2013. *Essential and Toxic Element: Trace Elements in Human Health and Disease*, Elsevier Science.
PUURA, E., NERETNIEKS, I. & KIRSIMAE, K. 1999. Atmospheric oxidation of the pyritic waste rock in Maardu, Estonia. 1 field study and modelling. *Environmental Geology,* 39**,** 1-19.
RAMBØLL. 2006a. *R206,* 1:2000. www.vegvesen.no: Statens Vegvesen.
RAMBØLL. 2006b. *R207,* 1:2000. www.vegvesen.no: Statens Vegvesen.
RASHID, M. A. 1974. Adsorption of Metals on Sedimentary and Peat Humic Acids. *Chemical Geology,* 13**,** 115-123.
SAIGAL, G. C., MORAD, S., BJØRLYKKE, K., EGEBERG, P. K. & AAGAARD, P. 1988. Diagenetic Albitization of Detrital K-feldspar in Jurassic, Lower Cretaceous, and Tertiary Clastic Reservoir Rocks From Offshore Norway I. Textures and Origin. *Journal of Sedimentary Petrology,* 58**,** 1003-1013.

SANTOS, S. H. 2014. *Potential Mobility of Radionuclides and Trace Elements in Bedrock Materials and in the deposition area at a tunnel construction site RV4 Gran Hadeland.* Master, Norwegian University of Life Sciences.
SCHOVSBO, N. H. 2002. Uranium enrichment shorewards in black shales: A case study from the Scandinavian Alum Shale. *GFF,* 124**,** 107-115.
SCOTT, P. W. & MIDDLETON, R. 1983. Captonite and Maenaite Sills near Gran, Hadeland, Oslo Region. *Norges Geologiske Undersøkelse,* 389**,** 1-26.
SJÖBLOM, R. 2014. Long-term developments in residues from the processing of alum shale and possible remedies. *Energy Production and Management in the 21st Century,* 1**,** 789-800.
SKIPPERUD, L., ALVARENGA, E., LIND, O. C., TEIEN, H.-C., TOLLEFSEN, K. E., SALBU, B. & WÆRSTED, F. M. 2016. Effekter og miljørisiko knyttet til inngrep i områder med sulfidrike mineraler. *NORWAT.* Ås: Norwegian University of Life Sciences - Center for Environmental Radioactivity.
SMITH, J. V. 1974. *Feldspar Minerals v. 2, Chemical and Textural Properties,* New York, Springer-Verlag.
SMITH, M. P., HENDERSON, P. & JEFFRIES, T. 2002. The formation and alteration of allanite in skarn from the Beinn an Dubhaich granite aureole, Skye. *European Journal of Mineralogy,* 14**,** 471-486.
SMITH, W. L., FRANCK, M. L. & SHERWOOD, A. M. 1956. Uranium and Thorium in the accessory allanite of igneous rocks. *Trace Elements Investigations Report,* 398**,** 20.
SNÄLL, S. 1988. Mineralogy and maturity of the alum shales of south-central Jämtland, Sweden. *Sveriges geologiska undersökning,* Ser. C**,** 1-46.
SOPP, O. I. 1966. *Bidrag til belysning av alunskiferens svellingsmekanisme.* Master, University of Oslo.
STARKEY, J. 1959. Chess-board Albite from New Brunswick, Canada. *Geol. Mag. ,* 96**,** 141-145.
STATENS VEGVESEN. 2016a. *E16 Eggemoen-Olum* [Online]. Statens Vegvesen. Available: http://www.vegvesen.no/Europaveg/e16nymoenolum/delprosjekter/e16-eggemoen-olum [Accessed 12.04 2017].
STATENS VEGVESEN. 2016b. *NORWAT* [Online]. Available: http://www.vegvesen.no/fag/Fokusomrader/Forskning+og+utvikling/pagaende-FoU-program/NORWAT [Accessed 14.10 2016].
STATENS VEGVESEN. 2016c. *Rv. 4 Lunner grense-Jaren* [Online]. Statens Vegvesen. Available: http://www.vegvesen.no/vegprosjekter/rv4hadeland/Delprosjekter/Lunnergr-Jaren [Accessed 12.04 2017].
TAYLOR, S. R. 1964. Abundance of Chemical Elements in the Continental Crust - a New Table. *Geochimica Et Cosmochimica Acta,* 28**,** 1273-1285.
TEREFE, D. 2016. *Swelling properties of Alum Shale as a function of its mineralogy.* MSc, University of Oslo.
TRUCHE, L., BERGER, G., DESTRIGNEVILLE, C., GUILLAUME, D. & GIFFAUT, E. 2010. Kinetics of pyrite to pyrrhotite reduction by hydrogen in calcite buffered solutions between 90 and 180°C: Implications for nuclear waste disposal. *Geochimica et Cosmochimica Acta,* 74**,** 2894-2914.
UPTON, G. & COOK, I. 2016. A Dictionary of Statistics. 3 ed.: Oxford University Press.
VANLOON, G. W. & DUFFY, S. J. 2011. *Environmental Chemistry - A Global Perspective,* New York, Oxford University Press.
WHO 1996. Molybdenum in Drinking-water. *Guidelines for drinking-water quality.* 2 ed. Geneva: World Health Organization.

YOUNGER, P. L., BANWART, S. A. & HEDIN, R. S. 2002. *Mine Water - Hydrology, Pollution, Remediation,* Dordrecht, Kluwer Academic Publishers.

Appendix 1 - Standards

Standards for IC

Ion	Stock (mg/l)	Calibration Levels (mg/)		
		1	**2**	**3**
Na^+	1000	2,5	5	10
K^+	1000	5	10	20
Mg^{2+}	1000	5	10	20
Ca^{2+}	1000	5	10	20

Calibration levels for anions varied with each analysis.

Standards for ICP-MS

	Etalon	TMDW-B	6020-5ppb	6020-50ppb	68A
Al (ppb)	30	125		50	
V (ppb)	30	35		50	
Cr (ppb)	30	20		50	
Fe (ppb)	30	100		50	
Co (ppb)	30	25		50	
Ni (ppb)	30	60		50	
Cu (ppb)	30	20		50	
Zn (ppb)	30	75		50	
Sr (ppb)	30	300			30
Mo (ppb)		110			
Cd (ppb)		10	5		
Pb (ppb)		20	5		
U (ppb)					30

Appendix 2 – XRD

XRD Results:

Sample	Quartz	Feldspar	Muscovite/Illite	Sulphides	Calcite	R	LGCS
A1	36,4	7,9	13,9	29,3	12,5	0,161	2,89
A3	30,5	6,9	13,0	24,9	24,7	0,160	2,98
AT1	23,6	9,9	11,7	21,7	33,1	0,173	3,07
AT2	29,6	21,4	17,8	28,9	2,2	0,157	2,95
AT3K	30,1	17,4	18,6	33,1		0,168	2,59
AT4K	32,0	19,7	18,0	28,0	2,4	0,160	2,91
BH1N-1m	23,6	19,7	26,5	12,8	17,4	0,129	2,24
BH1N-3m	40,8	9,6	29,4	20,2		0,142	2,60
BH1N-7m	39,4	21,0	16,7	17,8	5,2	0,132	2,40
BH1N-8m	5,5				94,5	0,209	3,19
BH2S-1m	45,3		38,5	16,2		0,167	3,08
BH2S-5m	13,9	15,5		8,7	63,2	0,152	2,52
BH2S-9m	5,3	9,3		11,9	73,4	0,178	2,88
BH2S-15m	18,1	13,2	Biotite 0,7	9,0	59,0	0,146	2,48
G1	33,3		63,2	3,5		0,185	3,35
G3K	40,1		34,7 (Muscovite) 25,2 (Chlorite)			0,165	3,05

XRD Diffractograms analysed in DIFFRAC.EVA

Due to a limited amount of coloured pages available, the diffractograms are shown without colour.

A1

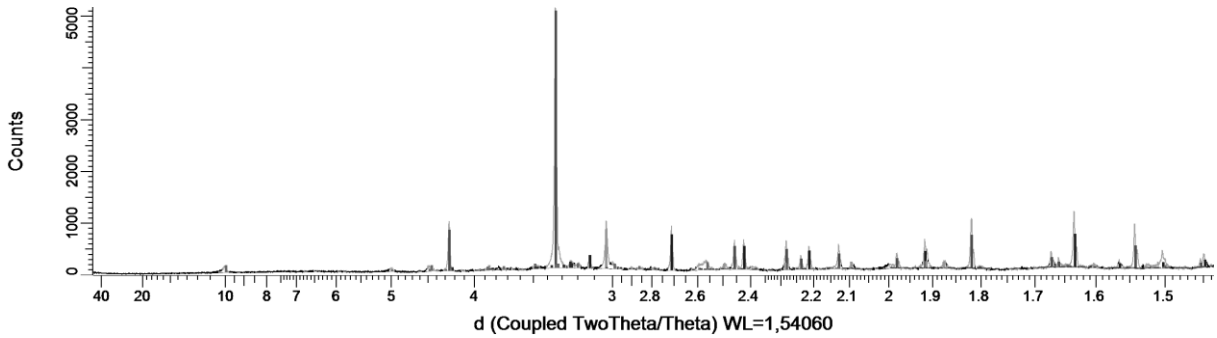

A3:

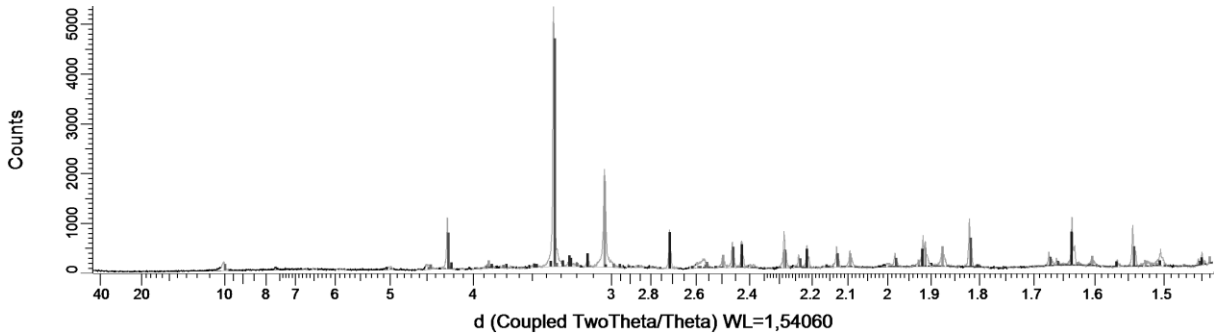

AT1

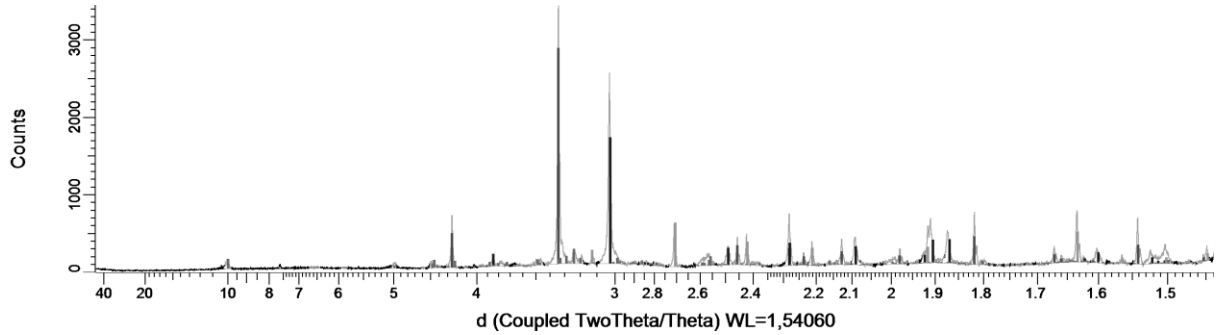

AT2:

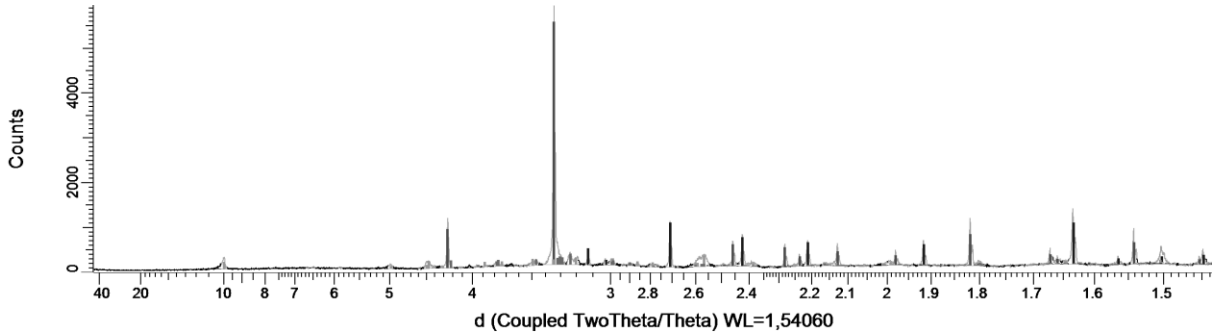

AT3K:

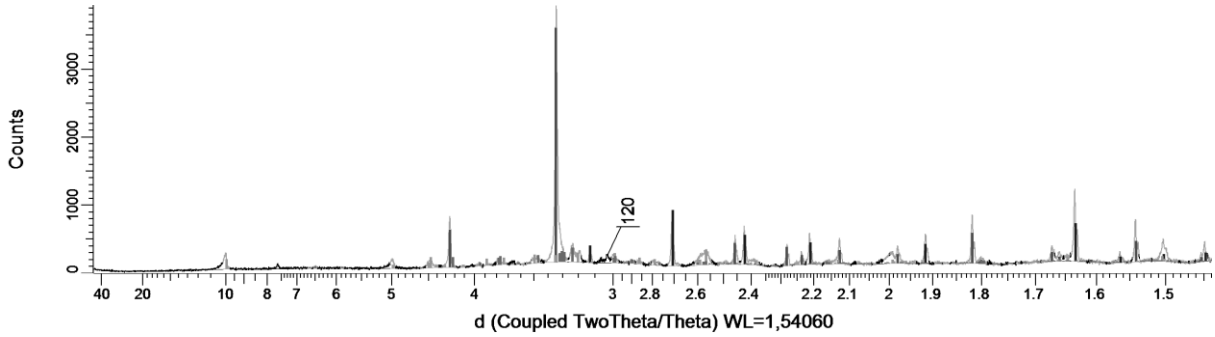

AT4K:

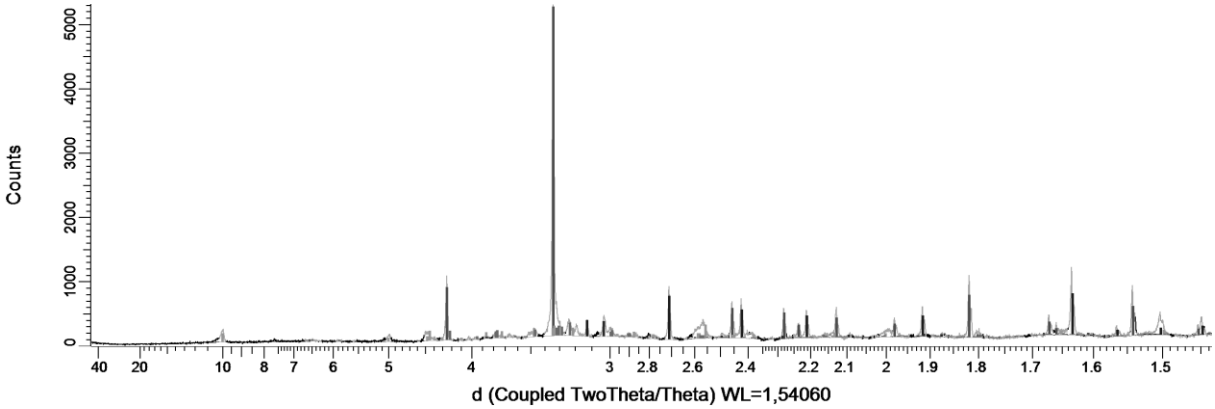

BH1N-1m:

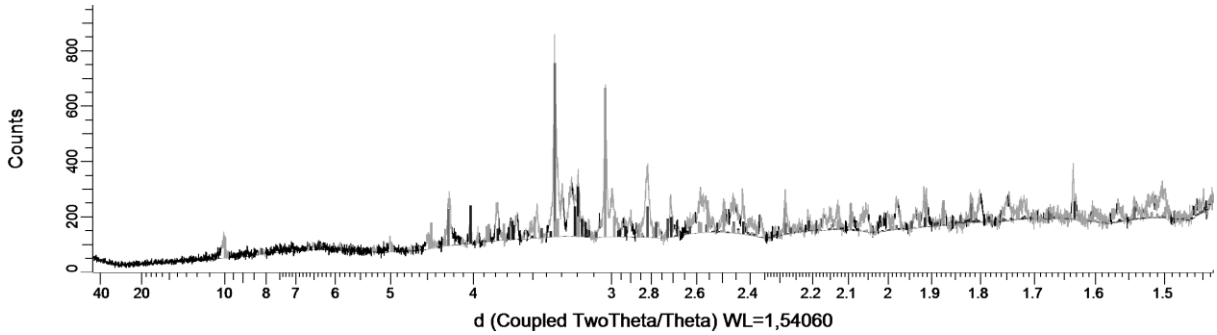

BH1N-3m:

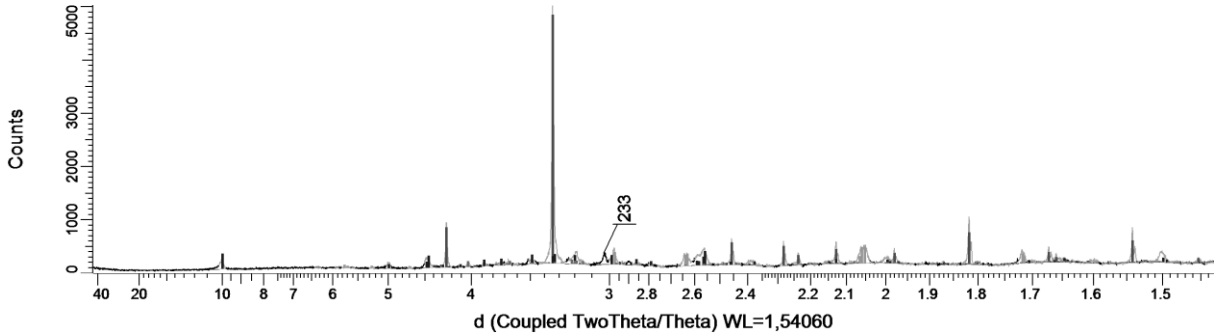

BH1N-7m:

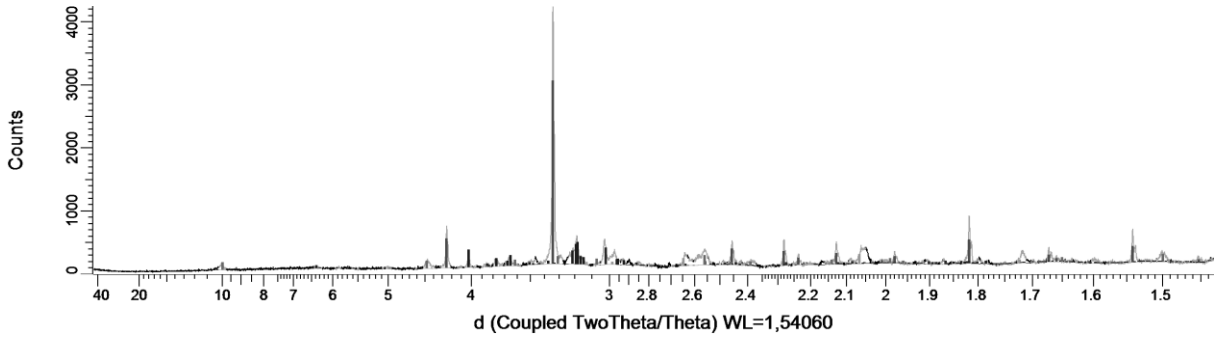

BH1N-8m:

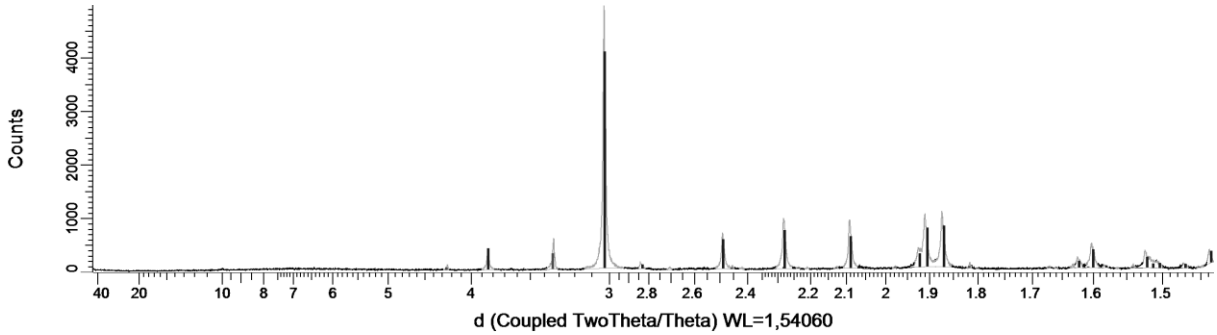

BH2S-1m:

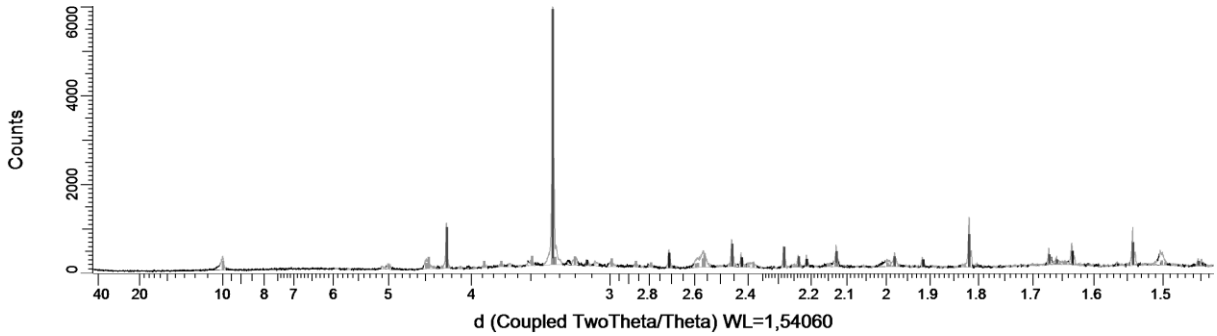

BH2S-5m:

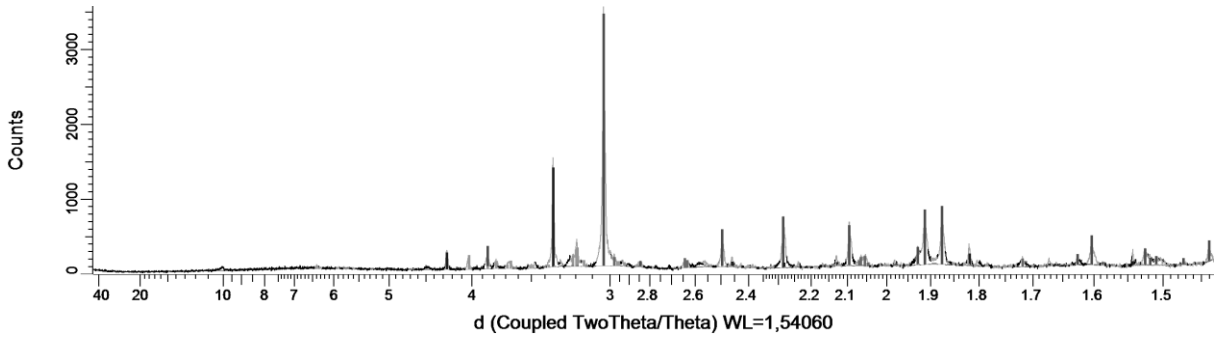

BH2S-9m

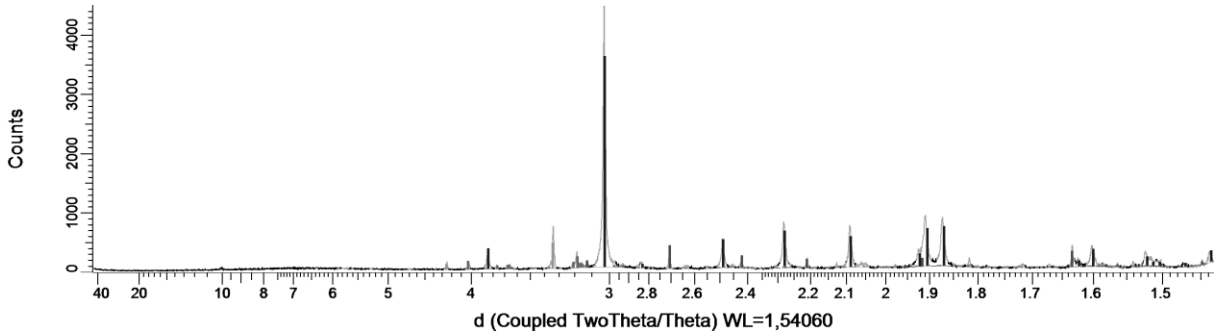

BH2S-15m:

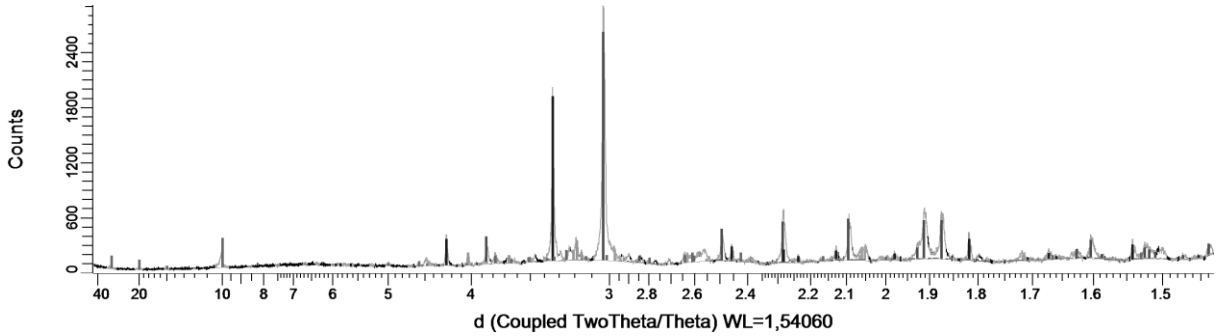

G1:

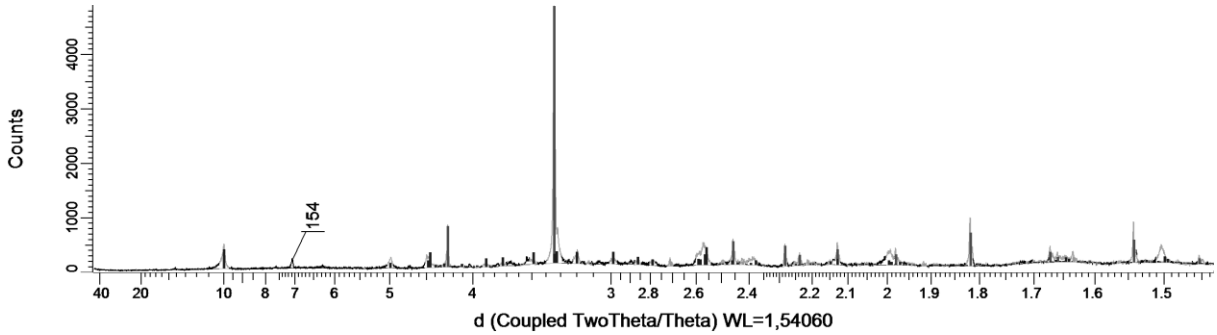
Counts
0
1000
2000
3000
4000
154
40
20
10
8
7
6
5
4
3
2.8
2.6
2.4
2.2
2.1
2
1.9
1.8
1.7
1.6
1.5
d (Coupled TwoTheta/Theta) WL=1,54060

G3K:

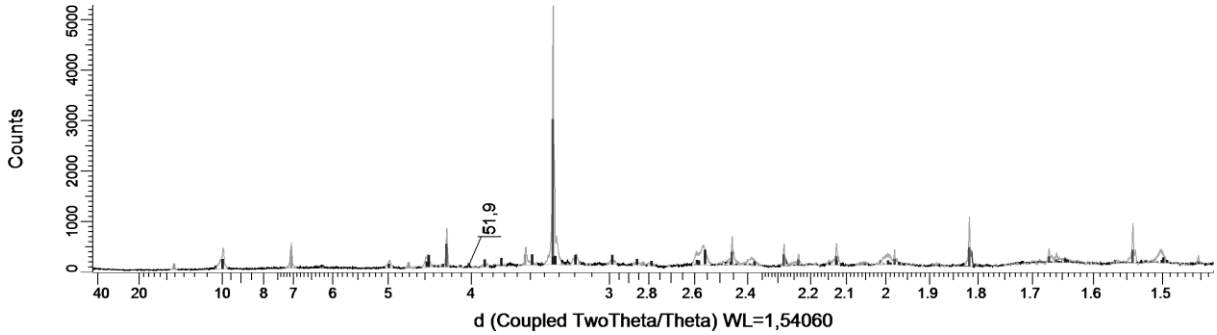
Counts
0
1000
2000
3000
4000
5000
51,9
40
20
10
8
7
6
5
4
3
2.8
2.6
2.4
2.2
2.1
2
1.9
1.8
1.7
1.6
1.5
d (Coupled TwoTheta/Theta) WL=1,54060

Appendix 3 – SEM

Quantification of element content in different minerals sorted after thick section and figure. Sample group A

Sample	Scan	O	F	Al	Si	P	S	Ca	Fe	La	Ce	Nd	Th	U	Mineral
A1	A1 1	63,47			1,28	16,67		0,69		4,45	9,62	3,57		0,26	Monazite
A1	A1 1	62,68		0,44	1,18	16,61		0,87		4,66	9,54	3,57	0,27	0,20	Monazite
A1	A1 1	53,47	6,72		0,46	13,12		25,98							F-Apatite
A1	A1 1	4,83			0,59		60,58		34,01						Pyrite

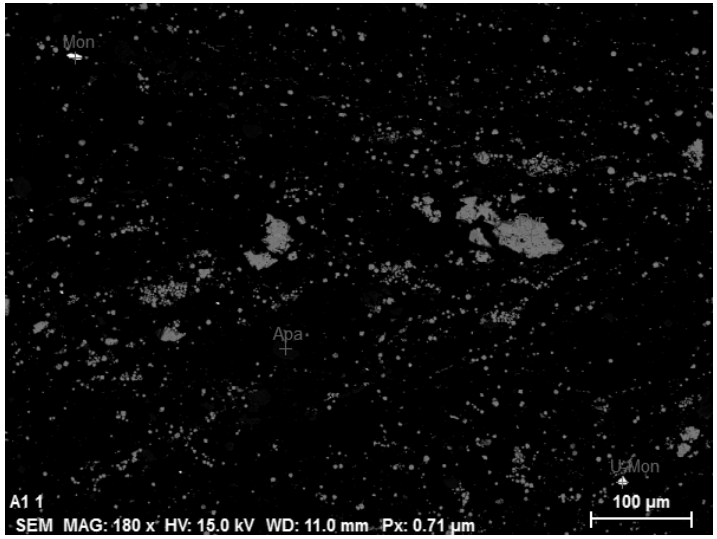

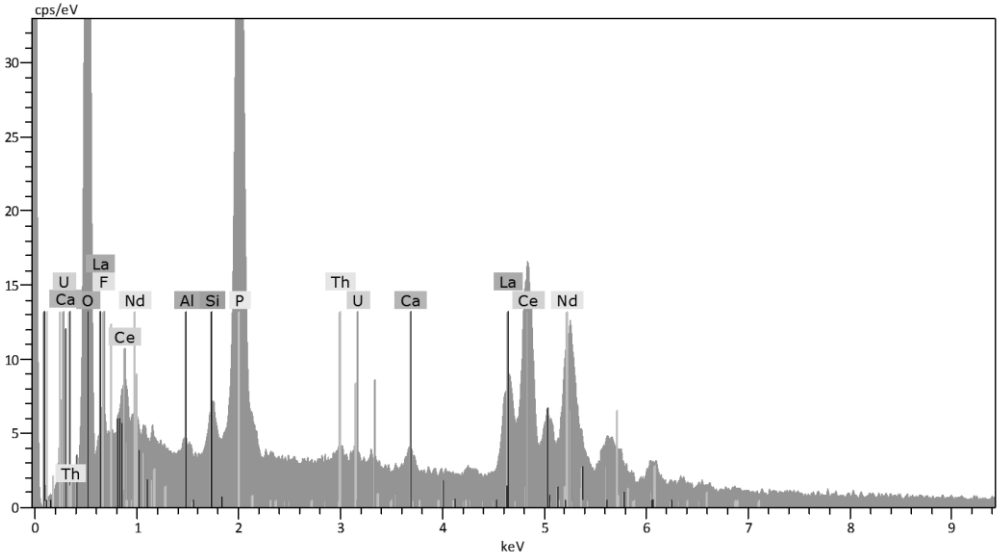

Quantification of element content in different minerals sorted after thick section and figure. Sample Group AT and BH1N.

Sample	Scan	O	Al	Si	P	S	Ca	Mg	Fe	Zn	Cd	La	Ce	Nd	Th	Mineral
AT4K	AT4K 16	4,47		0,94		43,65			1,67	48,73	0,53					Sphalerite
AT4K	AT4K 14	4,51		0,78		60,41			34,30							Pyrite
AT4K	AT4K 14	62,40		1,67	16.50		1.45					5,01	9,07	2,87	1,04	Monazite
AT4K	AT4K 15	62,17	0,80	1,78	16,40							6,69	8,44	3,54	0,19	Monazite
AT4K	AT4K 15	64,74	0,05	0,91	14,50							5,23	9,77	4,22	0,57	Monazite
AT4K	AT4K 16	62,65	0,38	1,36	17,41		0,53					4,85	8,79	3,41	0,61	Monazite

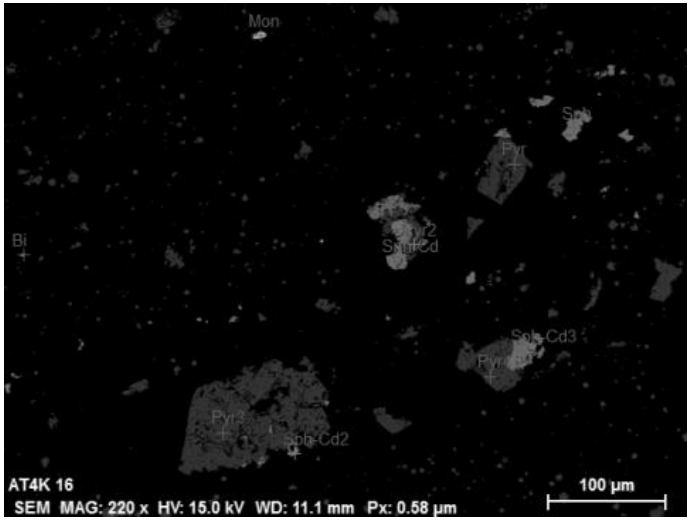

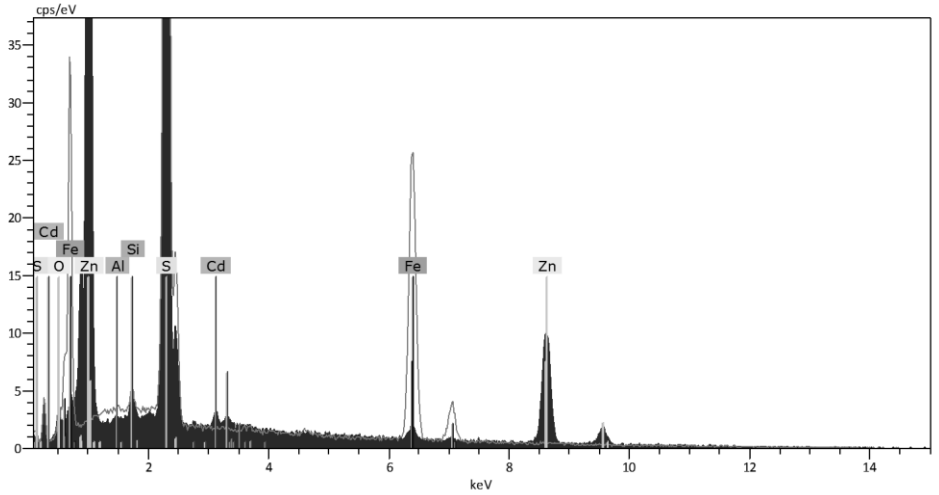

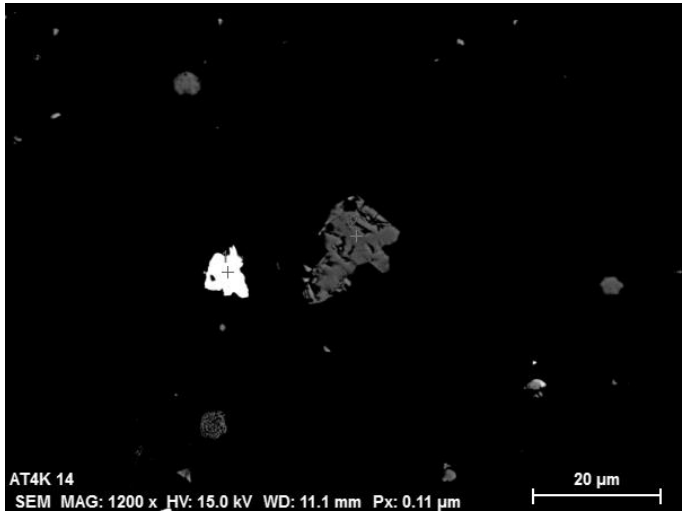
AT4K 14
SEM MAG: 1200 x HV: 15.0 kV WD: 11.1 mm Px: 0.11 µm
20 µm

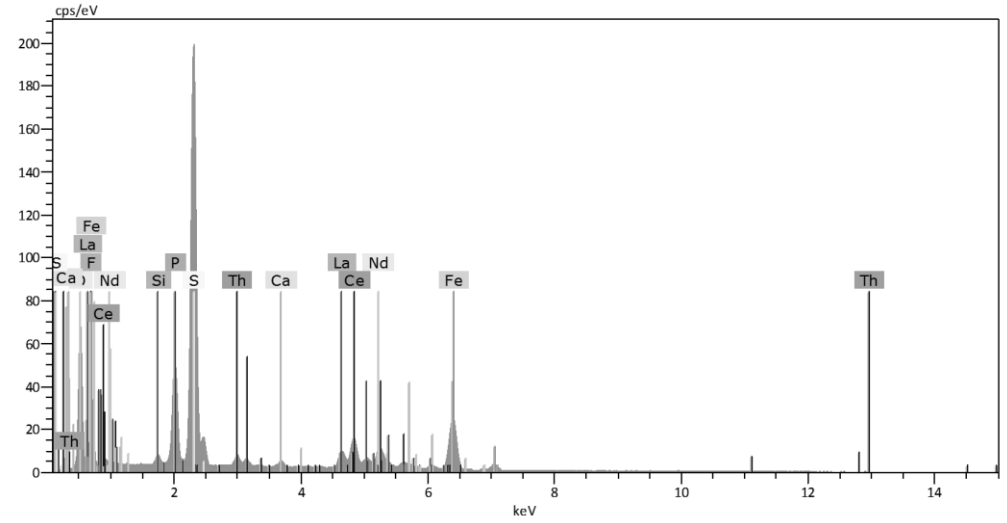
cps/eV
keV
Fe
La
F
S
Ca
Nd
Si
P
S
Th
Ca
La
Nd
Ce
Fe
Th
Ce
Th

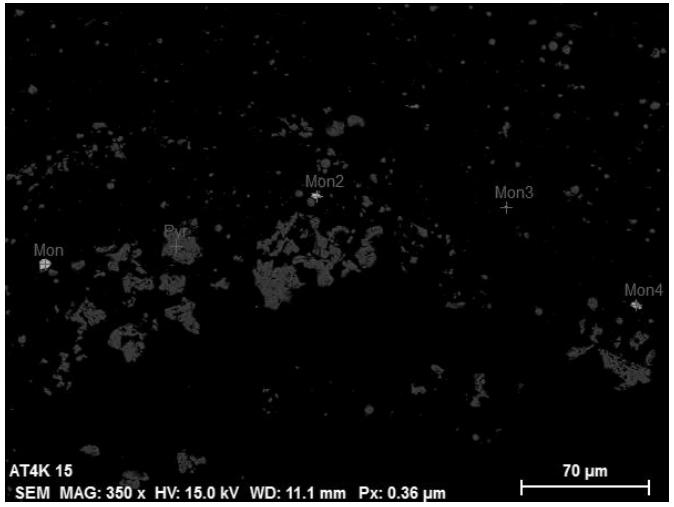
Mon2
Mon3
Mon
Mon4
AT4K 15
SEM MAG: 350 x HV: 15.0 kV WD: 11.1 mm Px: 0.36 µm
70 µm

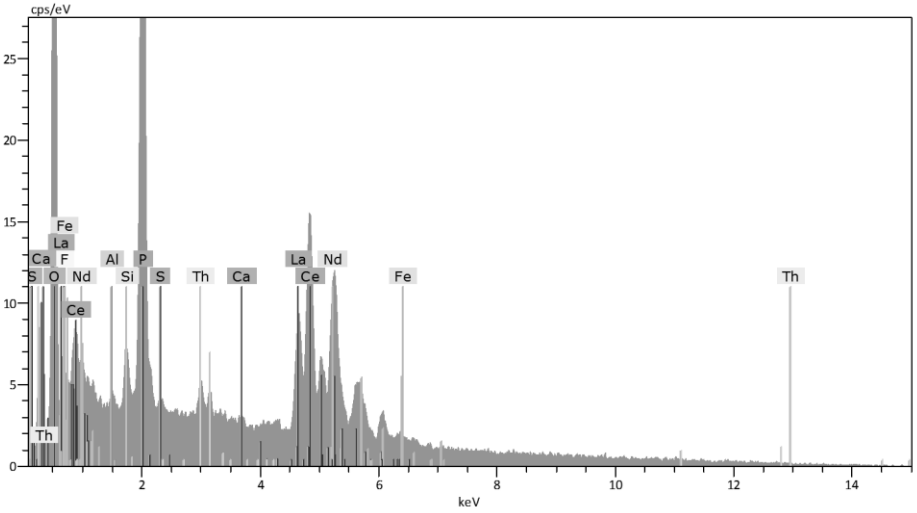
cps/eV
keV
Fe
La
Ca
F
Al
P
S
O
Nd
Si
S
Th
Ca
La
Nd
Ce
Fe
Th
Ce
Th

Quantification of element content in different minerals sorted after thick section and scan, BH1N.

Sample	Scan	O	F	Al	Si	P	S	Ca	Mg	Fe	Se	Re	La	Ce	Nd	Th	U	Pb	Mineral
BH1N-3m	BH1N-3m 1	14,73					35,48				1,38	1,07						47,34	Galena
BH1N-3m	BH1N-3m 1	39,87					19,49			3,94	0,94	1,72						34,04	Galena (Oxidised)
BH1N-3m	BH1N-3m 5	9,53		0,44			43,03			12,80		2,36						31,84	Galena
BH1N-3m	BH1N-3m 5	15,26					35,27			4,01		0,41						45,06	Galena (Oxidised)
BH1N-3m	BH1N-3m 5	3,88			0,58		60,64			34,89									Pyrite
BH1N-3m	BH1N-3m 7	3,47					48,17			48,36									Pyrrhotite
BH1N-3m	BH1N-3m 7	57,68		11,19	15,36			7,14	1,10	3,80			1,08	2,10	0,55				Allanite
BH1N-7m	BH1N-7m 5	4,51			0,55		47,55	1,08		47,55									Pyrrhotite
BH1N-7m	BH1N-7m 5	59,62	1,35	3,88	7,95	8,58		13,86		1,56						1,13	2,07		U-Apatite
BH1N-7m	BH1N-7m 5	52,90	3,78	2,13	5,23	10,82		21,22	0,74							0,94	2,24		U-Apatite

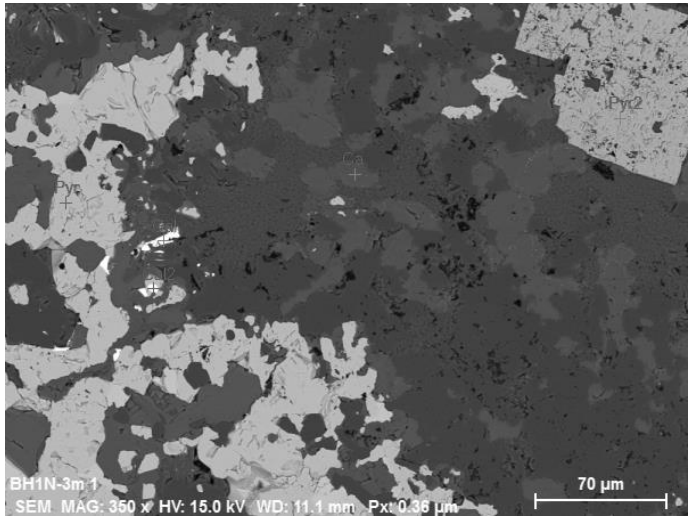
Pyr2
Ca
Pyr
Gal
Gal2
BH1N-3m 1
SEM MAG: 350 x HV: 15.0 kV WD: 11.1 mm Px: 0.36 µm
70 µm

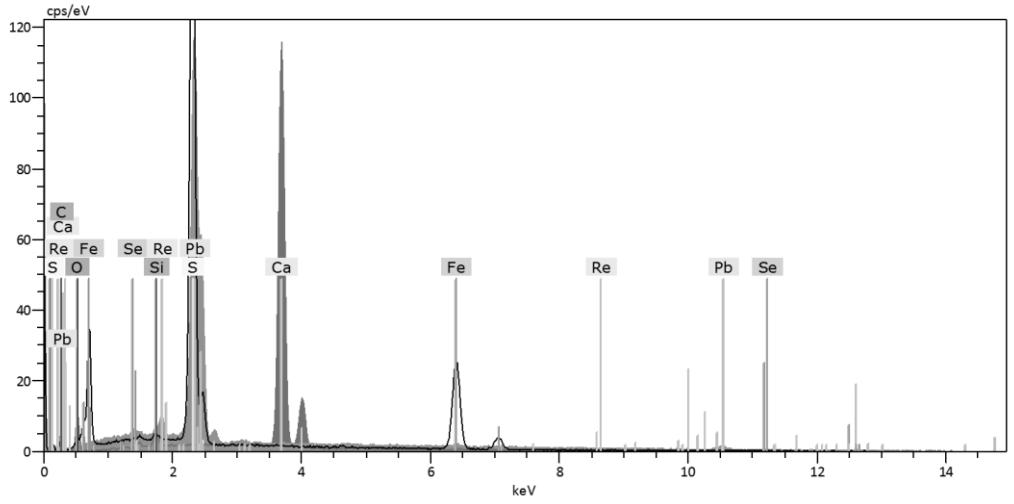
cps/eV
C
Ca
Re Fe
S O
Se Re Pb
Si S
Ca
Fe
Re
Pb Se
Pb
keV

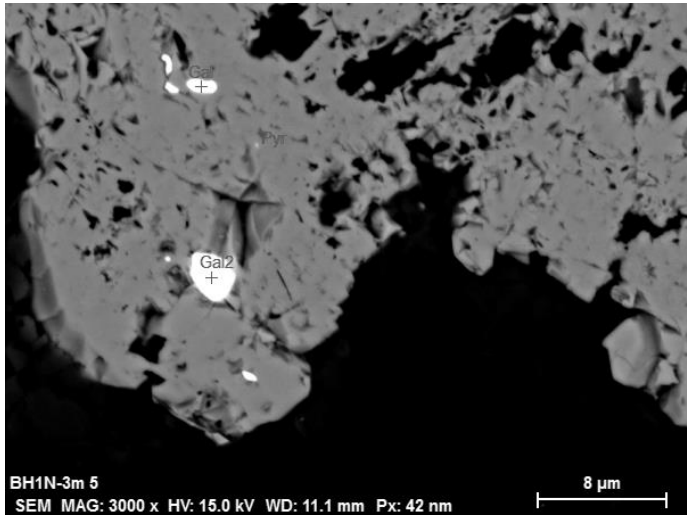
Gal
Pyr
Gal2
BH1N-3m 5
SEM MAG: 3000 x HV: 15.0 kV WD: 11.1 mm Px: 42 nm
8 µm

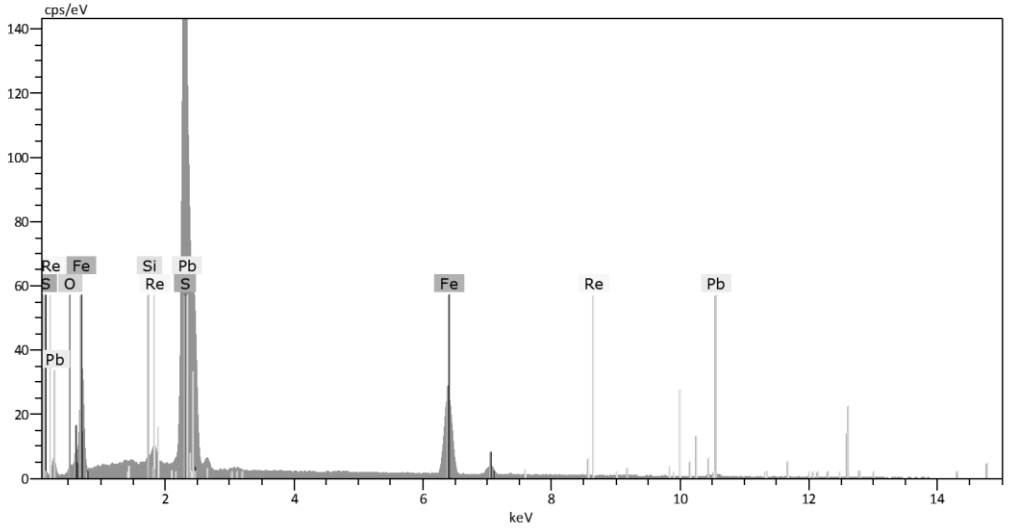
cps/eV
Re Fe
S O
Si Pb
Re S
Fe
Re
Pb
Pb
keV

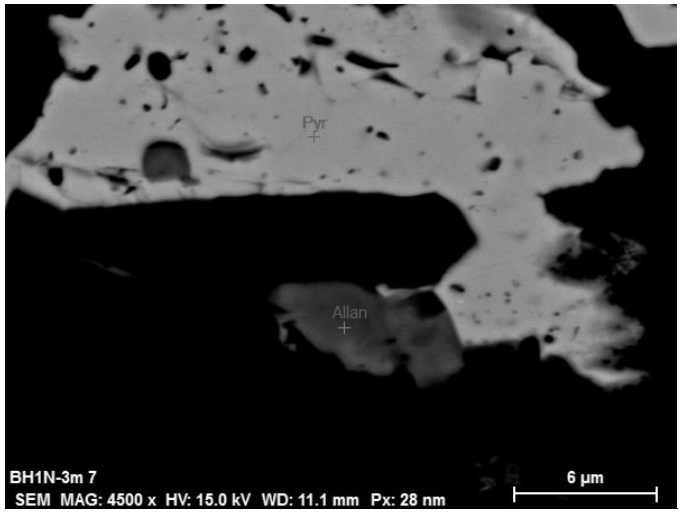
Pyr
Allan
BH1N-3m 7
SEM MAG: 4500 x HV: 15.0 kV WD: 11.1 mm Px: 28 nm
6 µm

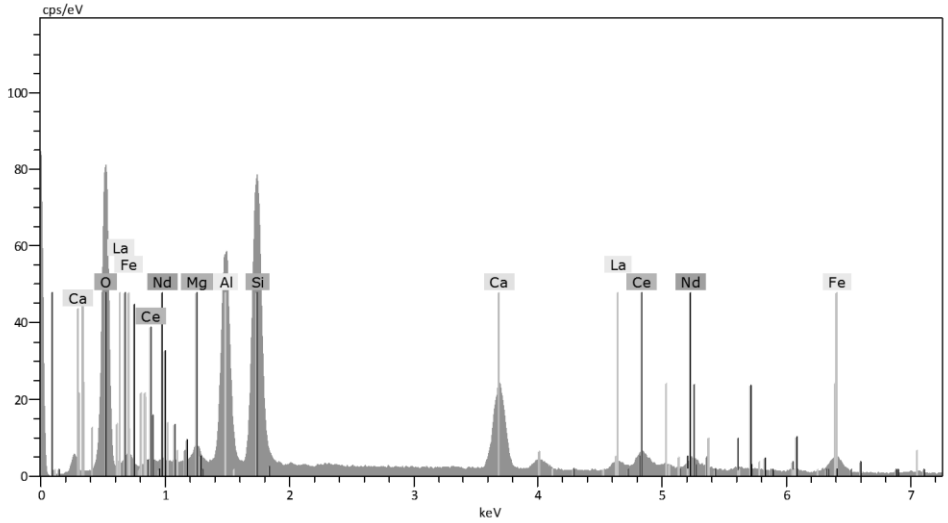
cps/eV
keV
Ca
O
La
Fe
Nd
Mg
Al
Si
Ce

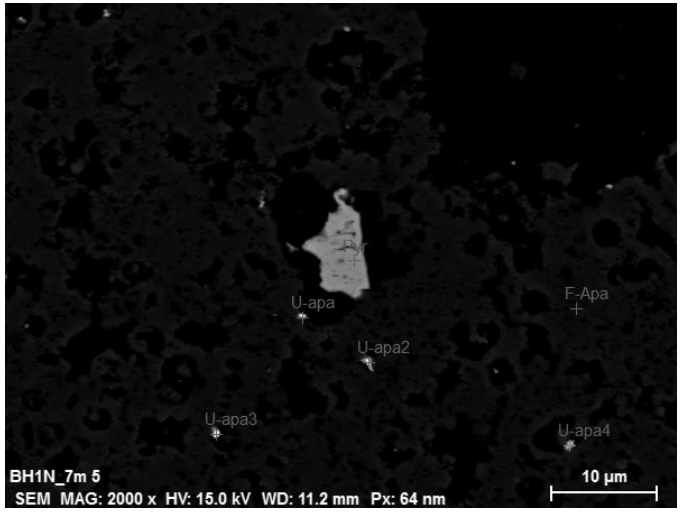
Pyr
U-apa
U-apa2
U-apa3
F-Apa
U-apa4
BH1N_7m 5
SEM MAG: 2000 x HV: 15.0 kV WD: 11.2 mm Px: 64 nm
10 µm

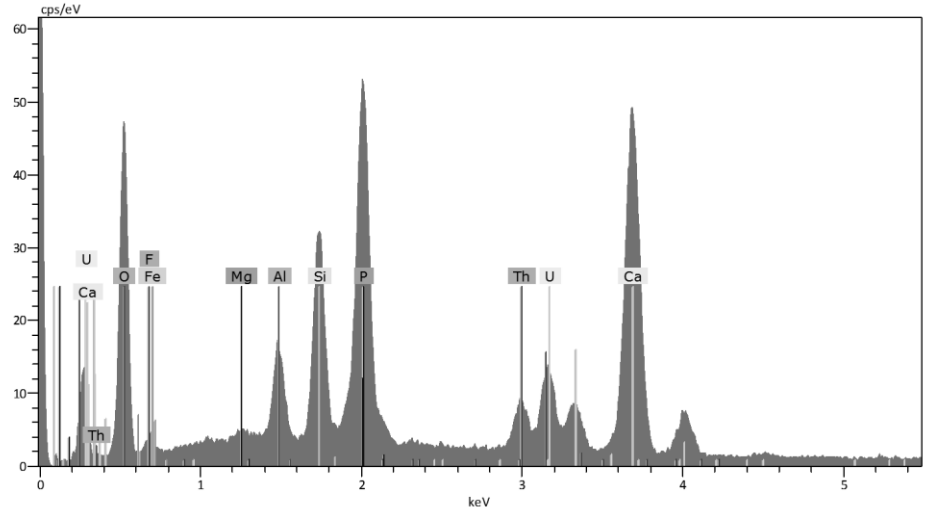
cps/eV
keV
U
Ca
Th
F
O
Fe
Mg
Al
Si
P
Th
U
Ca

Quantification of element content in different minerals sorted after thick section and scan, BH1N.

Sample	Scan/Figure	O	F	Na	Al	Si	P	S	Ca	Mg	Fe	Ti	La	Ce	Nd	Th	Y	U	Pb	Mineral
BH1N-7m	BH1N-7m 5	59,82	3,05		2,75	4,83	7,87		14,69	1,06						1,56		4,37		U-Apatite
BH1N-7m	BH1N-7m 5	52,64	3,12		3,19	6,77	12,16		19,73							0,94		1,46		U-Apatite
BH1N-7m	Figure 18	64,50			3,34	14,68	6,48	1,04	3,20									6,76		U-Apatite
BH1N-7m	Figure 18	69,31			0,81	5,99					2,44							19,65	1,79	U-Si
BH1N-7m	BH1N-7m 5	55,04	5,11			0,26	13,50		26,10											F-Apatite
BH1N-7m	Figure 18	67,96			1,38	6,73	2,10					1,07						17,26	1,20	U-Si
BH1N-7m	Figure 18	53,67		0,98	5,12	11,80		6,28			6,17	8,04						1,54	5,45	Rutile
BH1N-7m	Figure 20	57,01		0,76	10,44	15,35		1,82	6,81	0,69	4,22		0,81	1,59	0,51					Allanite
BH1N-7m	BH1N-7m 12	65,38	1,35		0,98	11,41	5,86		4,32								3,35	6,94	0,41	U-Apatite
BH1N-7m	BH1N-7m 4	7,26		K: 0,21	1,27	2,66		43,07		0,51	45,02									Pyrrhotite

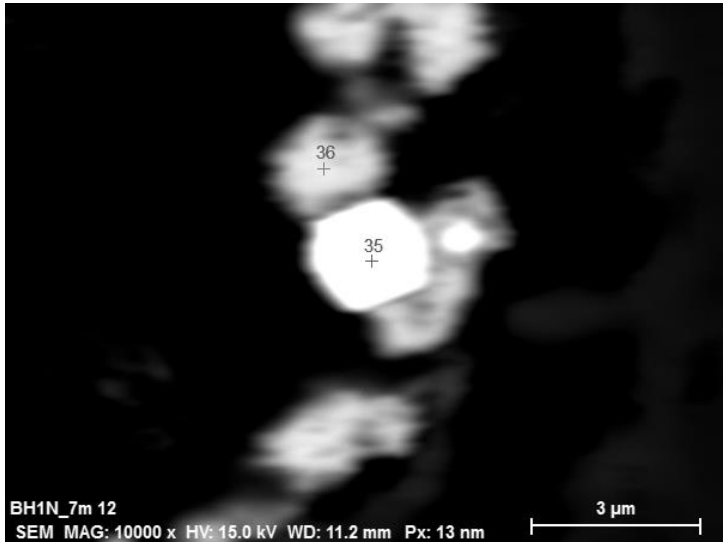
36
35
BH1N_7m 12
SEM MAG: 10000 x HV: 15.0 kV WD: 11.2 mm Px: 13 nm
3 µm

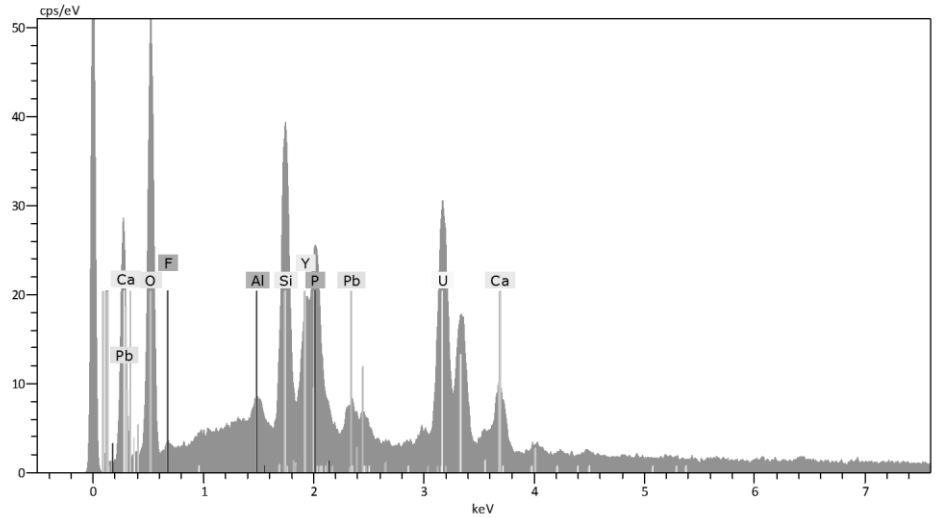
cps/eV
Ca
O
F
Pb
Al
Si
Y
P
Pb
U
Ca
keV

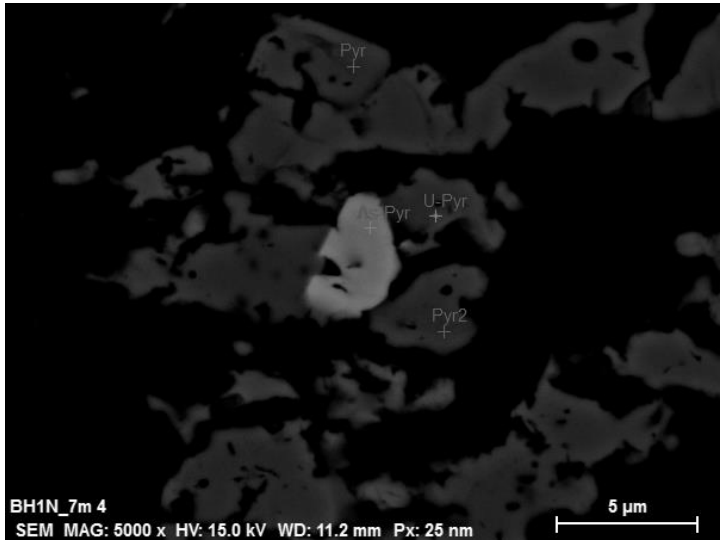
Pyr
As-Pyr
U-Pyr
Pyr2
BH1N_7m 4
SEM MAG: 5000 x HV: 15.0 kV WD: 11.2 mm Px: 25 nm
5 µm

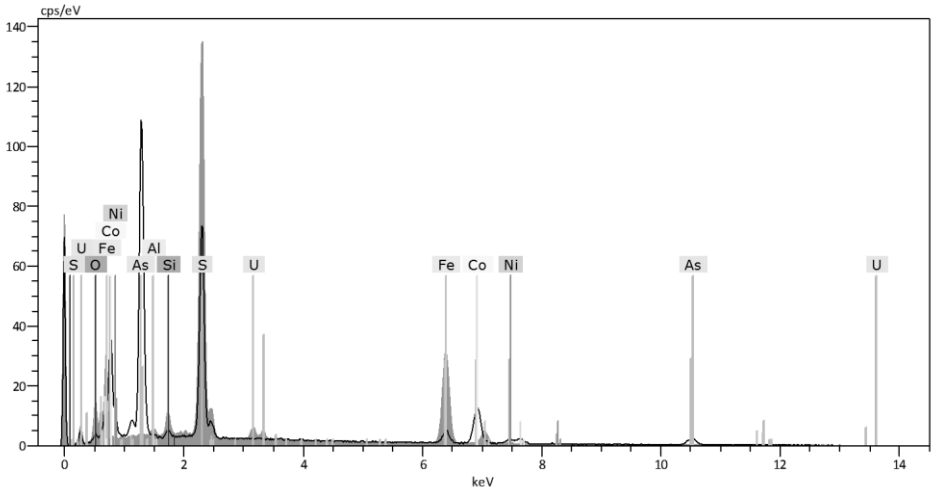
cps/eV
Ni
Co
U
Fe
Al
S
O
As
Si
S
U
Fe
Co
Ni
As
U
keV

Quantification of element content in different minerals sorted after thick section and figure.

Sample	Scan/Figure	O	Na	K	Al	Si	Se	S	Fe	Co	Ni	As	U	Pb	Mineral
BH1N-7m	BH1N-7m 2	4,08				0,65		48,01	47,26						Pyrrhotite
BH1N-7m	Figure 20	8,13	0,99		0,88	2,18		44,47	43,35						Pyrrhotite
BH1N-7m	Figure 18	4,20				0,52		47,86	47,42						Pyrrhotite
BH1N-7m	BH1N-7m 4	4,66				0,79		48,02	46,53						Pyrrhotite
BH1N-7m	BH1N-7m 4	3,01				1,60		33,47	6,90	27,24	4,52	23,27			Cobaltite
BH1N-7m	BH1N-7m 2	4,33				1,26		29,89	3,47	26,60	3,82	30,63			Cobaltite
BH1N-7m	Figure 18	58,41		1,88	6,34	10,96		7,91	3,76					9,67	Galena (Surroundings)
BH1N-7m	BH1N-7m 8	10,67					2,23	36,57						50,53	Galena
BH1N-7m	BH1N-7m 12	32,60				4,33	2,07	24,82					1,98	34,19	Galena
BH1N-7m	BH1N-7m 4	18,38			0,96	2,53		38,91	38,28				0,94		Pyrrhotite (U-Si)

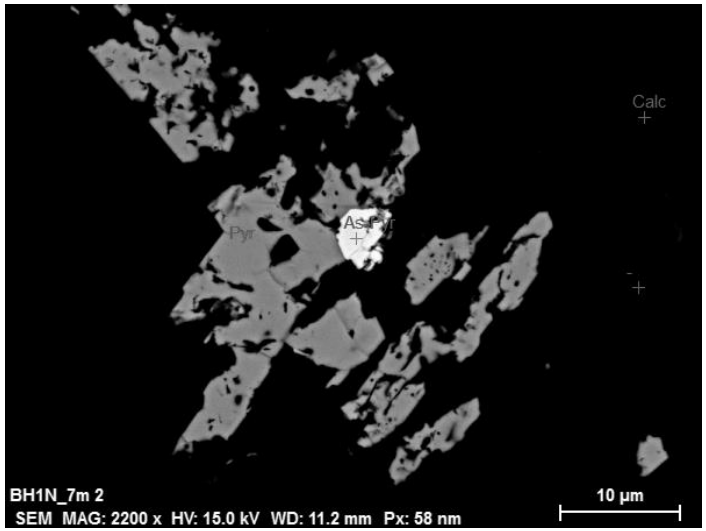
Calc
Pyr
As-Pyr
BH1N_7m 2
SEM MAG: 2200 x HV: 15.0 kV WD: 11.2 mm Px: 58 nm
10 µm

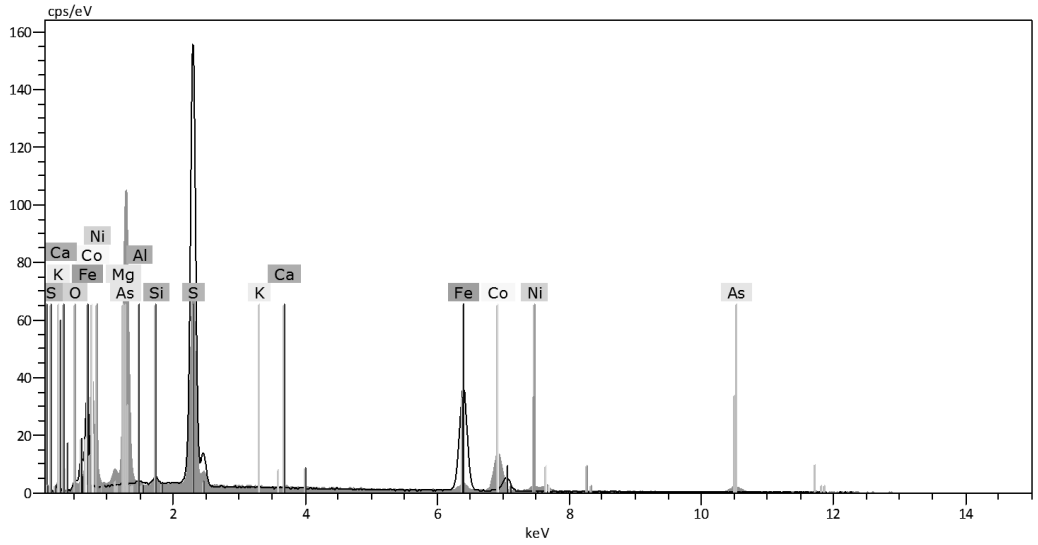
cps/eV
160
140
120
100
80
60
40
20
0
Ca
Ni
Co
Al
K
Fe
Mg
S
O
As
Si
S
K
Ca
Fe
Co
Ni
As
2
4
6
8
10
12
14
keV

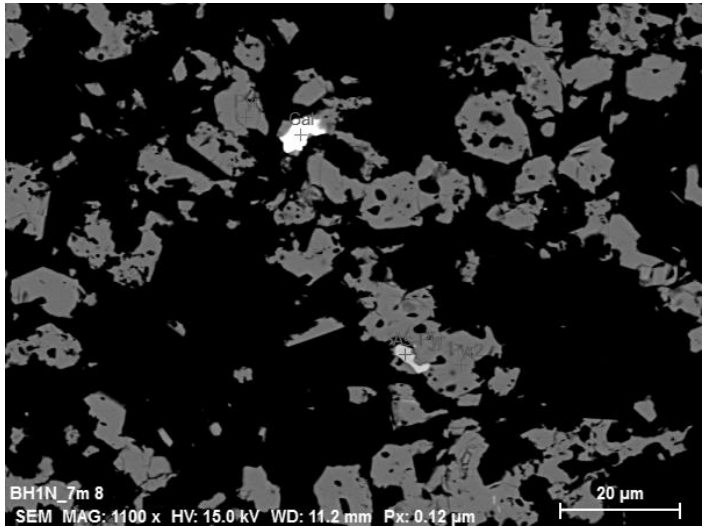
Cal
BH1N_7m 8
SEM MAG: 1100 x HV: 15.0 kV WD: 11.2 mm Px: 0.12 µm
20 µm

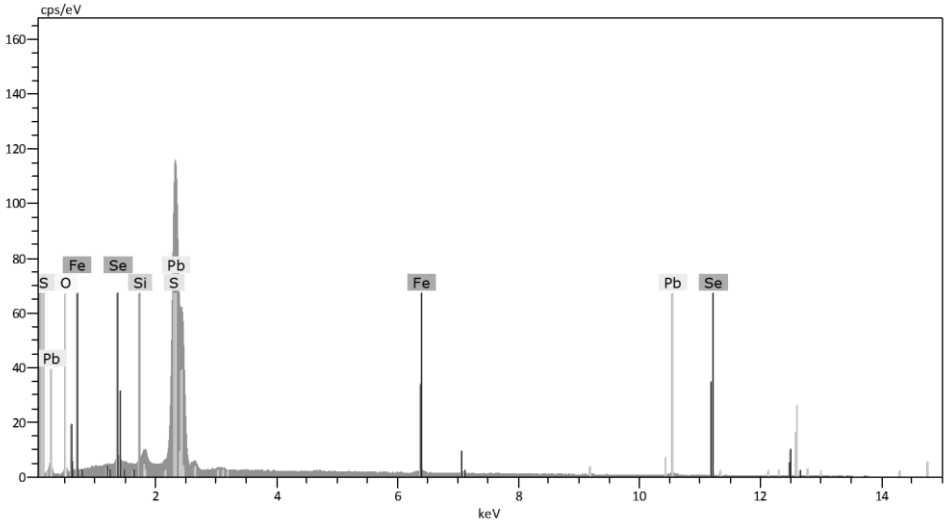
cps/eV
160
140
120
100
80
60
40
20
0
Fe
Se
Pb
S
O
Si
S
Pb
Fe
Pb
Se
2
4
6
8
10
12
14
keV

Quantification of element content in different minerals sorted after thick section and figure, BH2S.

Sample	Scan/Figure	O	Al	Si	P	S	Ca	Fe	Co	Zn	Cu	As	La	Ce	Nd	Mineral
BH2S-0-1m	BH2S_0-1m 7	3,10		0,83		31,27		31,72	4,93			28,15				Arsenopyrite
BH2S-0-1m	BH2S_0-1m 7	4,03		0,82		47,48		47,67								Pyrrhotite
BH2S-0-1m	Figure 22	4,64		0,65		42,33		26,54			25,84					Chalcopyrite
BH2S-0-1m	Figure 22	3,72		0,63		60,29		35,36								Pyrite
BH2S-0-1m	Figure 22	16,11	1,95	2,11		33,11		7,13		39,59						Sphalerite
BH2S-0-1m	Figure 22	6,74		0,69		45,68		46,88								Pyrrhotite
BH2S-0-1m	Figure 22	62,14		0,47		8,24	0,19	28,95								Fe-Oxide
BH2S-0-1m	Figure 22	59,32	0,14	5,58	15,03	0,49		3,54					4,39	8,82	2,69	Monazite
BH2S_9-10m	Figure 23	2,05				18,14		28,25	4,88			44,85				Arsenopyrite
BH2S_9-10m	Figure 23	1,53				32,44		58,11								Pyrrhotite?
BH2S_9-10m	Figure 23	1,81				18,19		25,16	7,66			44,81				Arsenopyrite

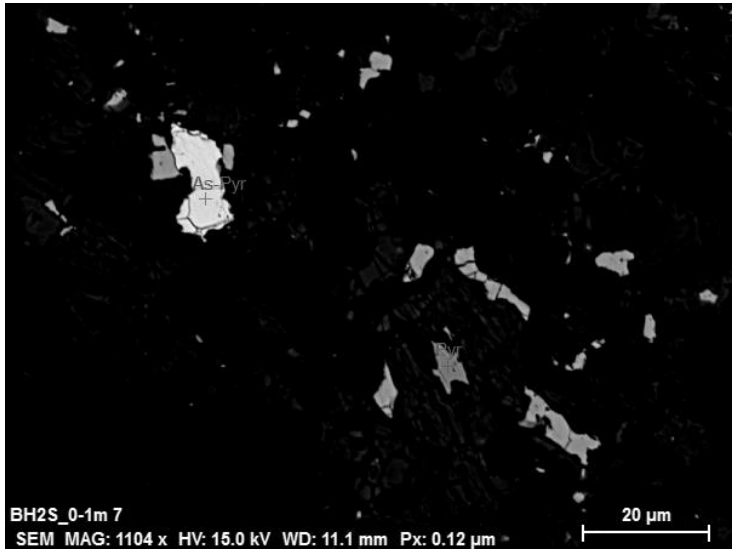

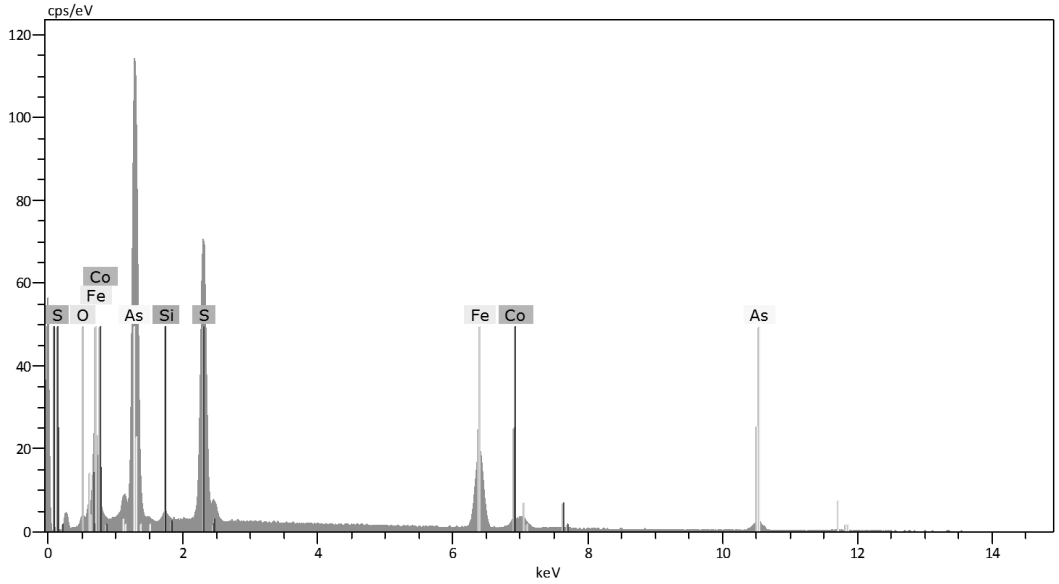

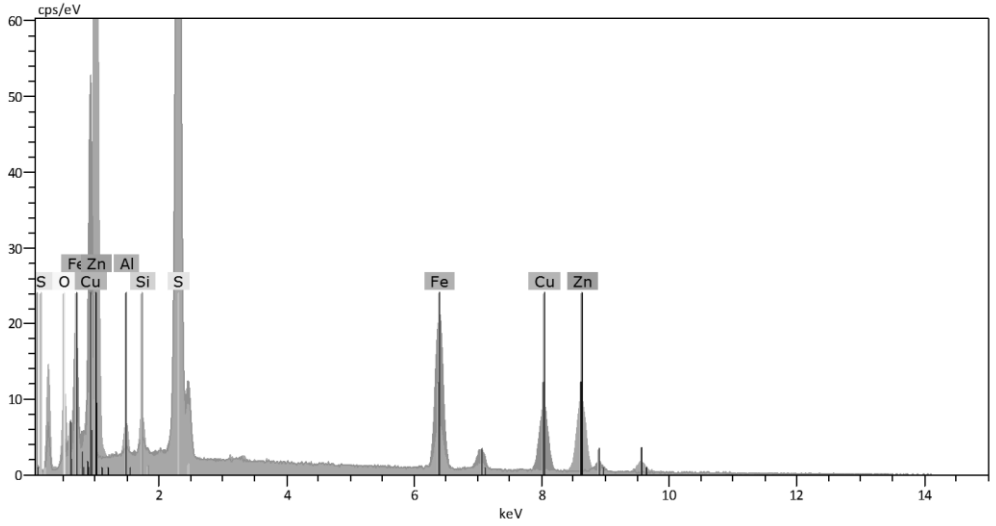

Corresponding to Figure 22

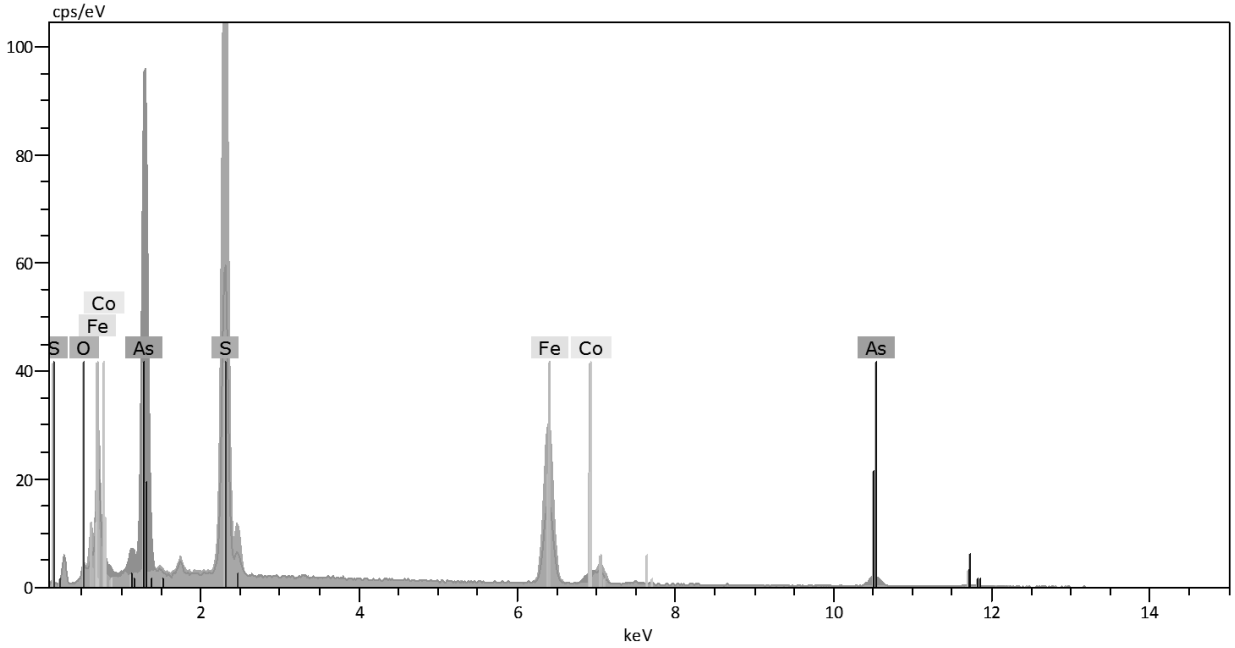

Corresponding to Figure 23

Quantification of element content in different minerals sorted after thick section and figure, G.

Sample	Scan/Figure	O	F	Al	Si	P	S	Na	K	Ca	Mg	Fe	Ti	Zn	Sr	Ba	La	Ce	Nd	Mineral
G2	G2 2	7,46		0,76	1,50		52,58					21,01		16,69						Sphalerite
G2	G2 2	4,62			0,87		47,70					46,81								Pyrrhotite
G3K	X (G3K_bar)	60,41	0,09	3,75	6,81	9,85			1,03	11,88	0,53	0,78					1,32	2,42	1,11	Monazite
G3K	X (G3K_bar)	64,00		0,54	0,94		14,85	0,53	0,55	0,75					2,44	15,25				Barite
G3K	X (G3K_bar)	61,17		0,45	1,11		16,54	0,45		0,81		1,20			2,03	16,23				Barite
G3K	X (G3K_bar)	58,28		4,16	10,37		0,19		0,39	0,33	3,94	22,34								Fe-oxide
G3K	X (G3K_bar)	61,04		2,89	9,35		0,20		0,06	0,22	3,88	22,36								Fe-oxide
G3K	X (G3K_bar)	60,62		12,91	18,68				4,94		1,29	1,55								Muscovite
G3K	X (G3K_bar)	66,05		1,64	2,43				0,40			0,37	29,12							Rutile
G3K	X (G3K_bar)	68,25			0,54								31,21							Rutile
G3K	X (G3K_bar)	21,90		1,04	1,49		35,73					39,84								Pyrrhotite?
G3K	X (G3K_weathered)	57,07		0,83	1,56		8,95					31,59								Fe-Sulphate

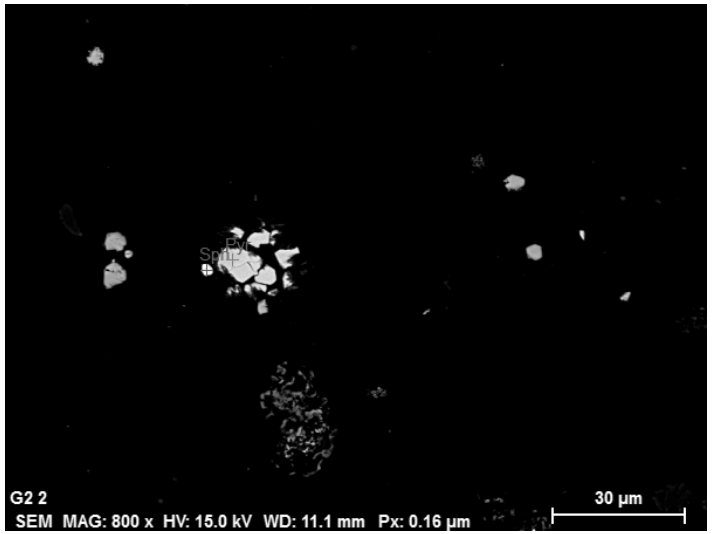
Pyr
Sph1
G2 2
SEM MAG: 800 x HV: 15.0 kV WD: 11.1 mm Px: 0.16 µm
30 µm

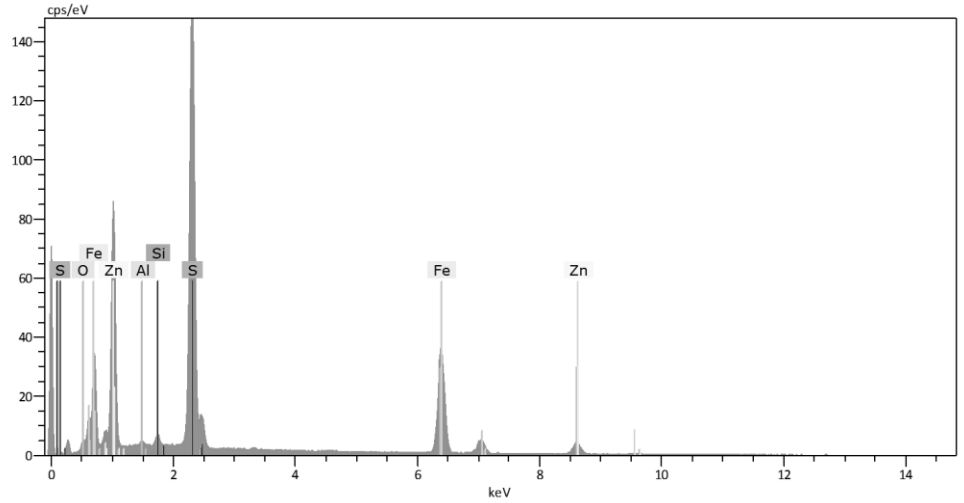
cps/eV
S
O
Fe
Zn
Al
Si
S
Fe
Zn
keV

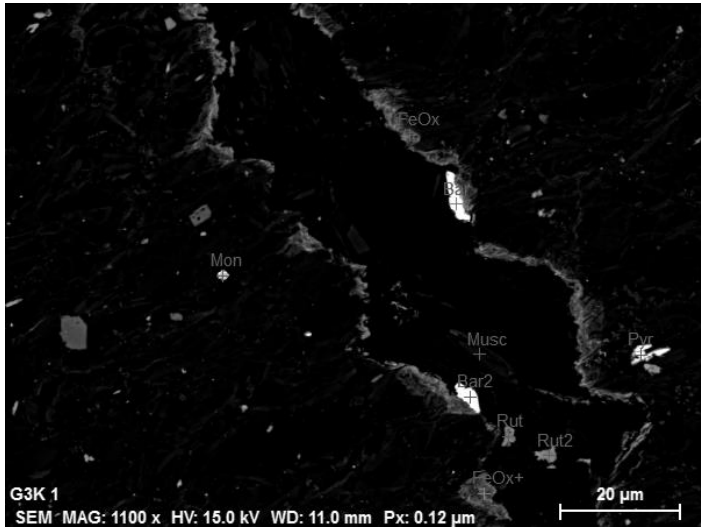
FeOx
Mon
Musc
Pyr
Bar2
Rut
Rut2
FeOx+
G3K 1
SEM MAG: 1100 x HV: 15.0 kV WD: 11.0 mm Px: 0.12 µm
20 µm

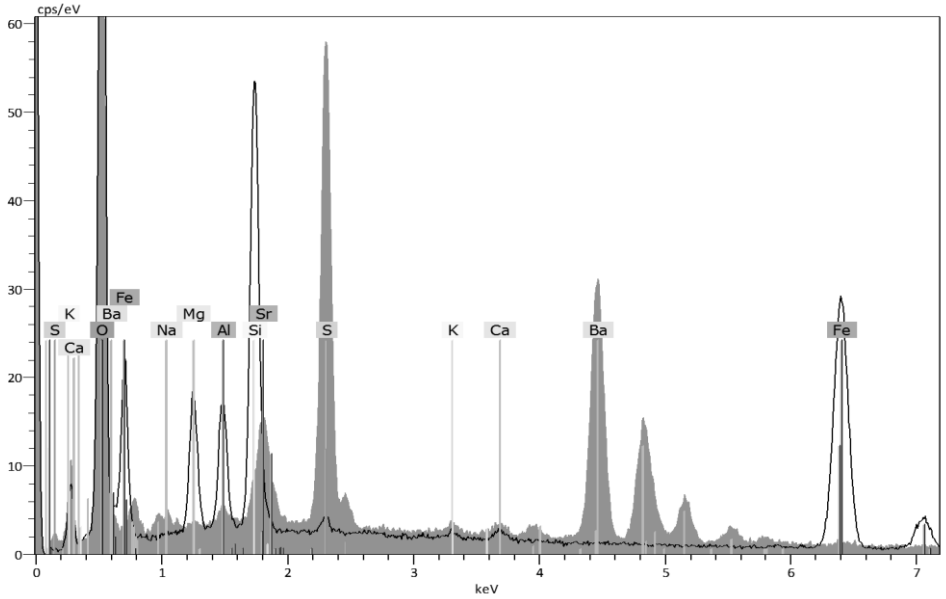
cps/eV
S
Ca
K
Ba
Fe
O
Na
Mg
Al
Si
Sr
S
K
Ca
Ba
Fe
keV

Appendix 4 – Pallet Experiment Water Samples

mg/l	Na	K	Mg	Ca	F	Cl	SO_4	NO_3	Br	PO_4	pH (felt)	EC (µS/cm)	Prec. (mm)	pe	%err
A1 5/10	1,03	12,05	8,04	260,96	0,15	12,14	623,27	0,99	n.a.	n.a.	7,73	834,00	24,80	n.a	3,20
A1 19/10	1,75	4,97	6,64	170,35	1,55	3,72	510,71	10,00	6,20	n.a.	8,02	622,00	5,20	3,85	-12,59
A1 1/11	1,93	5,97	14,17	379,13	0,09	3,18	1060,31	0,00	n.a.	n.a.	7,67	1061,00	19,00	3,34	-5,25
A1 16/11	1,45	2,95	5,14	175,25	0,65	3,03	4085,02	3,78	n.a.	n.a.	7,92	490,00	25,20	3,79	-87,82
A3 5/10	4,62	14,08	78,23	605,52	0,19	0,45	1552,87	0,60	n.a	n.a.	7,45	1853	24,80	n.a	9,79
A3 19/10	2,95	8,94	35,97	308,04	0,00	4,73	854,19	6,52	6,51	n.a.	8,05	1040	5,20	3,46	1,48
A3 1/11	4,13	12,04	122,42	475,72	0,59	3,77	1595,98	2,38	n.a.	n.a.	7,7	1550	19,00	3,12	1,96
A3 16/11	2,89	7,75	43,22	466,62	0,51	2,56	1414,43	0	n.a.	n.a.	7,68	1238	25,20	3,46	-5,17
A2K 1/11	3,96	9,19	68,19	538,12	0,09	3,19	1451,87	2,38	n.a.	n.a.	8,05	1630,00	19,00	3,06	5,73
A2K 16/11	3,17	8,69	111,61	419,00	0,00	2,57	1542,06	0,00	n.a.	n.a.	7,73	1381,00	25,20	3,46	-3,42

µg/l	Al	V	Cr	Fe	Co	Ni	Cu	Zn	Sr	Mo	Cd	Pb	U-norm
A1 5/10	44,19	0,51	105,94	312,37	3,67	362,15	6,59	594,38	2919,81	427,55	0,89	0,42	554,67
A1 19/10	25,38	0,10	19,19	73,86	2,33	210,47	4,04	201,94	1709,69	211,40	1,51	0,09	358,23
A1 1/11	23,20	0,07	25,18	136,21	2,61	385,86	13,76	56,64	3688,50	423,70	0,84	0,09	1202,71
A1 16/11	30,92	0,01	0,23	33,65	12,34	289,12	2,62	45,91	1656,04	351,90	0,92	0,45	585,37
A3 5/10	24,43	0,20	53,90	273,35	29,24	1492,13	5,15	186,25	9121,04	47,73	3,04	0,67	633,62
A3 19/10	25,97	0,47	137,22	399,38	5,54	749,46	9,19	174,75	4547,88	38,55	1,41	0,29	275,75
A3 1/11	27,89	0,13	56,89	233,57	30,76	1429,08	3,95	177,72	7262,06	32,15	2,80	0,14	591,47
A3 16/11	29,58	0,08	22,84	143,31	46,03	911,27	4,46	86,83	4939,64	40,44	1,70	0,12	622,39
A2K 1/11	27,24	0,06	13,05	197,12	4,42	765,35	4,60	70,92	6680,31	140,55	0,91	0,56	1281,89
A2K 16/11	30,42	0,14	31,87	208,92	30,92	711,28	3,56	91,48	4526,27	92,89	1,18	0,14	1024,75

mg/l	Na	K	Mg	Ca	F	Cl	SO4	NO3	Br	PO_4	pH (felt)	EC	Precip (mm)	pe	%error
AT1 5/10	24,40	55,13	766,01	492,92	0,32	10,95	3931,14	1,60	n.a.	n.a.	7,19	552,00	24,80		8,59
AT1 19/10	20,67	113,33	683,48	416,76	1,97	132,62	7422,99	6,48	n.a.	n.a.	7,26	2171,00	5,20	4,36	-46,96
AT1 1/11	19,71	45,71	736,91	415,01	0,16	10,47	3697,68	1,63	n.a.	n.a.	7,02	2988,00	19,00	4,14	6,84
AT1 16/11	10,01	24,09	321,75	391,26	0,57	3,96	2306,80	3,45	n.a.	n.a.	7,72	1868,00	25,20	4,12	-0,99
AT2 5/10	28,08	74,80	902,40	506,24	0,28	0,54	4576,61	0,62	n.a.	n.a.	6,66	4055,00	24,80	0,00	7,74
AT2 19/10	13,13	61,15	484,73	316,62	1,86	46,29	5241,63	0,00	n.a.	n.a.	6,77	2668,00	5,20	4,84	-43,98
AT2 1/11	12,72	33,06	473,08	280,96	0,06	3,43	2533,78	0,00	n.a.	n.a.	7,30	2250,00	19,00	3,41	3,43
AT3K 5/10	12,00	36,03	377,63	494,12	0,22	0,42	2631,47	0,61	n.a.	n.a.	6,74	2390,00	24,80	0,00	4,05
AT3K 19/10	11,98	35,54	381,92	430,80	1,72	3,42	4973,57	0,00	n.a.	n.a.	7,24	2481,00	5,20	4,09	-43,86
AT3K 1/11	14,02	32,84	506,57	427,00	0,11	3,13	2952,24	0,00	n.a.	n.a.	7,34	2566,00	19,00	3,37	4,62
AT3K 16/11	2,73	7,34	79,25	342,51	0,52	2,46	1306,72	0,00	n.a.	n.a.	7,50	1528,00	25,20	3,52	-7,48
AT4K 5/10	31,48	52,60	578,54	486,30	0,23	0,42	3137,16	0,69	n.a.	n.a.	7,05	2940,00	24,80	0,00	10,42
AT4K 19/10	28,59	49,23	572,65	403,81	1,72	3,77	6324,92	0,00	n.a.	n.a.	7,16	3023,00	5,20	4,36	-44,94
AT4K 1/11	24,92	37,53	545,45	405,58	0,17	3,21	3031,05	4,55	n.a.	n.a.	7,44	2724,00	19,00	3,52	4,77
AT4K 16/11	10,21	24,07	226,03	397,94	0,71	2,69	1928,53	0,00	n.a.	n.a.	7,59	1650,00	25,20	3,50	-0,73

µg/l	Al	V	Cr	Fe	Co	Ni	Cu	Zn	Sr	Mo	Cd	Pb	U
AT1 5/10	26,39	0,51	64,15	330,81	774,26	22441,09	17,03	22175,96	16331,72	61,06	409,41	0,23	1734,57
AT1 19/10	46,33	0,34	4,89	81,68	620,43	18086,81	14,36	17619,91	12626,83	47,95	291,77	0,77	1417,22
AT1 1/11	36,30	0,25	21,02	129,13	260,72	14279,99	22,33	13774,19	12664,12	26,15	263,06	0,19	1121,46
AT1 16/11	52,90	0,12	27,38	161,62	155,32	7902,71	8,89	8264,89	8016,95	18,21	199,11	0,34	569,85
AT2 5/10	36,66	2,10	199,11	551,40	514,16	26684,69	112,17	34719,41	20804,31	29,44	737,33	0,53	1057,44
AT2 19/10	28,64	2,23	85,29	247,67	233,39	12319,66	43,46	15923,26	9972,54	16,71	352,24	0,46	476,72
AT2 1/11	31,09	2,13	39,24	133,15	218,16	11416,54	38,17	14262,45	8915,16	18,40	325,95	0,31	478,60
AT3K 5/10	30,94	1,03	284,38	967,89	110,82	8353,07	16,29	7429,09	11790,49	35,51	205,65	0,17	474,35
AT3K 19/10	31,64	0,07	2,18	83,24	103,99	7661,86	8,14	6963,02	10592,25	16,91	198,89	1,19	456,98
AT3K 1/11	55,48	0,24	50,07	311,53	89,46	11678,11	17,97	12968,77	10968,56	15,22	276,71	0,24	529,04
AT3K 16/11	38,57	0,12	26,42	165,57	56,65	4610,26	8,15	4822,94	5845,41	12,83	130,54	0,51	414,68
AT4K 5/10	31,56	0,44	66,96	263,52	47,90	4456,57	8,75	3673,80	12710,74	66,75	105,66	0,15	830,61
AT4K 19/10	29,24	0,27	31,21	152,11	47,22	4116,83	9,64	3380,85	10060,34	59,72	96,10	0,14	821,09
AT4K 1/11	31,75	0,56	120,75	396,55	19,28	5125,71	8,82	3659,12	11689,97	54,71	76,46	0,10	900,01
AT4K 16/11	29,32	0,15	20,44	134,08	19,70	2987,81	4,90	2357,64	7118,40	29,35	59,39	0,23	646,42

mg/l	Na	K	Mg	Ca	F	Cl	SO_4	NO_3	Br	PO_4	pH	pe	Prec. (mm)	%Error
G1 1/11	20,34	51,30	1016,88	418,47	0,21	3,17	4753,57	n.a.	n.a.	n.a.	7,60	3,17	19,00	6,03
G1 16/11	10,67	27,52	515,78	339,05	0,50	2,55	2848,58	3,50	n.a.	n.a.	7,62	3,57	25,20	1,41
G2 5/10	15,98	65,33	659,94	462,50	0,14	7,75	3641,84	1,21	n.a.	n.a.	7,24		24,80	3,66
G2 19/10	13,95	53,45	571,38	320,03	1,28	3,85	5854,11	5,79	n.a.	n.a.	7,84	3,87	5,20	-44,87
G2 1/11	20,41	52,39	902,71	422,20	0,09	3,18	4370,93	n.a.	n.a.	n.a.	7,46	3,37	19,00	5,46
G2 16/11	15,41	39,03	618,83	346,54	0,48	2,54	3244,04	3,47	n.a.	n.a.	7,51	3,77	25,20	2,48
G3K 5/10	15,08	54,55	568,42	512,22	0,16	10,03	3312,05	1,72	n.a.	n.a.	7,35		24,80	5,41
G3K 19/10	5,55	17,49	187,82	201,12	1,20	3,32	2624,55	5,63	n.a.	n.a.	7,89	3,68	5,20	-46,77
G3K 1/11	19,83	41,32	807,48	451,27	0,06	3,71	4048,00	1,55	n.a.	n.a.	7,67	3,17	19,00	5,82
G3K 16/11	14,59	27,80	532,22	335,39	0,52	2,70	2891,10	3,66	n.a.	n.a.	7,51	3,63	25,20	1,93

µg/l	Al	V	Cr	Fe	Co	Ni	Cu	Zn	Sr	Mo	Cd	Pb	U-norm
G1 1/11	30,58	0,23	68,81	299,55	54,30	1227,09	6,27	1239,17	9626,82	103,90	7,01	0,38	34,96
G1 16/11	30,01	0,09	18,92	127,71	42,06	853,87	3,56	790,89	6089,78	55,75	4,44	0,10	18,88
G2 5/10	31,93	0,07	4,78	104,74	34,03	946,93	2,66	795,70	9885,98	99,99	5,28	1,26	15,21
G2 19/10	26,20	0,16	41,59	180,71	28,73	798,28	5,86	681,37	7323,84	88,25	4,38	0,11	16,19
G2 1/11	30,59	0,08	18,12	166,80	27,47	1027,25	4,09	839,19	9452,17	92,70	4,37	0,19	21,06
G2 16/11	31,36	0,00	0,23	86,74	23,66	746,25	3,53	542,05	5989,96	62,55	3,00	0,51	15,71
G3K 5/10	25,36	0,17	6,69	118,12	34,03	679,91	2,43	644,07	9216,76	166,50	6,32	0,07	37,23
G3K 19/10	25,90	0,30	67,18	183,65	13,33	321,98	6,13	267,18	3409,67	64,62	3,13	0,09	18,27
G3K 1/11	32,71	0,34	73,86	392,55	27,90	727,24	7,18	493,94	8615,81	171,55	3,03	0,26	39,40
G3K 16/11	30,51	0,02	0,23	74,48	19,20	421,48	3,32	335,98	4792,41	118,70	2,12	0,37	26,96

Appendix 5 – Column Experiment

	Date	Al (ppb)	V (ppb)	Cr (ppb)	Fe (ppn)	Co (ppb)	Ni (ppb)	Cu (ppb)	Zn (ppb)	Sr (ppb)	Mo (ppb)	Cd (ppb)	Pb (ppb)	U (ppb)	Na (ppm)	K (ppm)	Mg (ppm)	Ca (ppm)
1	07.12	35,03	3,30	0,06	3,39	0,22	7,86	0,93	13,56	66,89	381,39	0,707	0,051	**70**	1,37	7,43	1,26	14,05
1	08.12	21,79	4,66	0,23	1,64	0,01	**4,00**	0,34	3,32	16,59	19,06	0,033	0,031	**6,6**	0,49	0,92	0,41	7,45
1	09.12	25,77	2,02	0,22	1,30	0,04	**4,00**	0,35	3,65	16,01	12,09	0,01	0,106	**1,9**	0,43	0,36	0,65	7,18
1	12.12	32,44	0,51	0,16	1,50	0,04	**4,00**	1,93	27,13	14,06	7,36	0,029	0,031	**2,8**	0,50	0,24	0,44	6,81
1	13.12	32,64	0,43	0,20	1,82	0,09	**4,00**	2,12	121,0	13,88	7,33	0,05	0,074	**3,5**	0,59	0,73	0,39	6,87
1	14.12	23,41	0,30	0,18	2,13	0,04	**4,00**	1,28	36,13	13,81	7,57	0,027	0,088	**3,2**	0,58	0,40	0,39	6,97
1	15.12	21,31	0,24	0,15	1,59	0,02	**4,00**	0,45	3,17	14,39	8,15	0,023	0,035	**2,9**	0,45	0,20	0,41	7,20
1	16.12	21,02	0,10	0,08	3,95	0,07	**4,00**	1,94	3,80	44,05	70,88	0,111	0,026	**25**	0,78	0,28	0,88	20,40
1	16.01	9,72	0,08	0,14	31,13	3,19	69,98	3,39	105,0	498,3	14,43	0,128	0,106	**288**	2,27	1,60	11,85	n.a
2	07.12	65,08	2,74	0,09	4,63	0,16	14,62	0,86	5,85	111,5	299,26	0,428	0,017	**100**	3,34	9,98	1,49	23,20
2	08.12	125,60	4,61	0,33	1,81	0,02	**4,00**	0,33	3,43	25,16	9,15	0,032	0,012	**13**	0,51	0,74	0,48	7,37
2	09.12	96,26	2,36	0,29	2,51	0,01	**4,00**	0,49	2,70	19,84	5,40	0,013	0,017	**8,0**	0,51	0,37	0,37	7,67
2	12.12	43,13	0,82	0,21	1,59	0,03	**4,00**	1,30	16,97	16,84	3,40	0,056	0,031	**7,1**	0,53	0,28	0,46	6,88
2	13.12	37,71	0,72	0,20	1,48	0,04	**4,00**	0,83	49,88	15,48	3,05	0,013	0,029	**6,3**	0,48	0,27	0,32	6,85
2	14.12	25,59	0,59	0,18	1,41	0,03	**4,00**	0,64	27,34	15,18	2,66	0,012	0,029	**5,4**	0,53	0,43	0,32	7,07
2	15.12	23,70	0,46	0,18	1,35	0,01	**4,00**	0,40	2,76	14,68	2,74	0,01	0,028	**5,0**	0,43	0,23	n.a	6,77
2	16.12	20,92	0,19	0,15	3,32	0,03	**4,00**	0,36	2,54	42,10	26,66	0,044	0,064	**31**	0,70	0,35	0,50	16,56
2	19.12	23,64	0,23	0,18	2,51	0,04	**4,00**	0,48	2,69	29,85	11,75	0,024	0,029	**33**	0,50	0,54	0,54	11,99
2	21.12	21,53	0,26	0,26	1,92	0,03	**4,00**	0,49	5,06	20,80	6,75	0,026	0,049	**14**	0,48	0,36	0,45	8,56
2	16.01	9,13	0,06	0,10	20,22	2,33	46,62	2,15	52,82	290,8	22,87	0,089	0,113	**256**	1,78	1,06	3,49	
3	07.12	116,98	5,18	0,08	3,24	0,09	10,47	0,55	4,39	95,71	216,30	0,31	0,024	**46**	2,44	3,21	1,31	17,24
3	08.12	104,20	2,52	0,18	1,53	0,01	**4,00**	0,39	2,22	23,16	11,70	0,021	0,007	**10**	0,46	0,26	n.a	7,17
3	09.12	30,65	1,89	0,24	3,95	0,10	**4,00**	2,04	4,73	19,57	9,91	0,031	0,183	**6,8**	0,57	0,45	0,35	6,83
3	12.12	23,18	0,55	0,09	1,45	0,13	**4,00**	1,24	21,62	21,81	3,98	0,191	0,022	**3,9**	0,54	0,29	0,76	7,04
3	13.12	21,52	0,48	0,10	1,38	0,03	**4,00**	0,59	31,17	14,03	3,78	0,010	0,018	**3,2**	0,41	0,24	0,32	6,53
3	14.12	18,02	1,01	0,10	1,43	0,02	**4,00**	0,36	2,50	14,63	2,39	0,009	0,03	**5,3**	0,62	0,25	0,31	6,58
3	15.12	14,78	0,36	0,09	1,21	0,01	**4,00**	0,46	2,93	12,98	3,24	0,012	0,038	**2,3**	0,47	0,20	0,31	6,37
3	16.12	13,40	0,19	0,18	2,54	0,04	**4,00**	0,37	3,06	32,23	41,33	0,064	0,019	**12**	0,50	0,24	0,38	13,44
3	19.12	22,39	0,30	0,17	1,59	0,03	**4,00**	0,48	2,80	20,42	12,28	0,021	0,03	**9,0**	0,42	0,19	0,36	8,24
3	21.12	16,09	0,31	0,13	1,50	0,04	**4,00**	0,66	3,20	17,83	7,83	0,017	0,027	**7,0**	0,20	n.a	n.a	2,10
3	16.01	6,82	0,10	0,06	23,01	4,60	49,56	1,14	38,30	370,8	48,10	0,095	0,051	**256**	1,80	0,77	3,98	n.a

	Date	Al (ppb)	V (ppb)	Cr (ppb)	Fe (ppn)	Co (ppb)	Ni (ppb)	Cu (ppb)	Zn (ppb)	Sr (ppb)	Mo (ppb)	Cd (ppb)	Pb (ppb)	**U (ppb)**	Na (ppm)	K (ppm)	Mg (ppm)	Ca (ppm)
4	07.12	58,82	5,76	0,10	5,21	0,17	19,91	0,95	7,16	127,4	127,16	0,329	0,069	**86**	1,88	4,39	1,41	25,87
4	08.12	111,46	6,83	0,28	2,23	0,03	**4,00**	0,41	2,63	28,53	7,10	0,0969	0,022	**13**	0,43	0,55	0,55	7,82
4	09.12	41,85	2,98	0,16	1,33	0,02	**4,00**	0,36	2,81	18,89	4,00	0,014	0,017	**8,2**	0,45	0,29	0,40	7,16
4	12.12	21,80	1,30	0,12	1,61	0,02	**4,00**	1,10	16,19	15,10	2,79	0,013	0,042	**6,3**	0,55	0,28	0,35	6,72
4	13.12	20,25	1,17	0,12	1,41	0,03	**4,00**	0,90	32,68	14,96	2,59	0,013	0,037	**5,6**	0,47	0,28	0,38	6,53
4	14.12	19,03	0,41	0,09	1,44	0,03	**4,00**	0,77	22,73	13,81	3,27	0,017	0,053	**2,7**	0,55	0,24	n.a	6,69
4	15.12	14,17	0,83	0,10	1,43	0,01	**4,00**	0,36	2,59	14,10	2,45	0,007	0,008	**4,6**	0,39	0,28	0,33	6,58
4	16.12	15,41	0,33	0,09	3,00	0,04	**4,00**	0,63	3,38	37,70	22,06	0,040	0,022	**21**	0,56	0,25	0,58	15,25
4	19.12	20,24	0,49	0,20	2,07	0,03	**4,00**	0,60	3,19	22,46	8,51	0,02	0,016	**23**	0,50	0,29	0,46	9,10
4	21.12	21,94	0,58	0,20	1,64	0,03	**4,00**	1,74	11,96	19,15	7,32	0,032	0,076	**12**	0,71	4,02	0,43	8,04
4	16.01	7,58	0,08	0,06	19,54	3,19	80,53	1,04	39,94	267,3	28,63	0,136	0,061	**226**	1,37	0,80	3,78	n.a
K	07.12	7,29	0,45	0,08	2,98	0,03	4,00	1,39	17,64	14,24	0,36	0,289	0,095	**0,0585**	2,11	0,90	0,87	2,18
K	08.12	4,40	0,11	0,04	0,65	0,00	4,00	1,10	13,57	4,06	0,10	0,453	0,016	0,0100	0,51	0,15	0,33	1,76
K	09.12	4,53	0,09	0,03	0,56	0,04	4,00	5,20	42,81	4,57	0,10	0,326	0,076	**0,0293**	0,50	0,24	0,41	1,91
K	12.12	4,19	0,06	0,06	0,78	0,02	4,00	2,64	30,85	2,85	0,10	0,094	0,047	0,0100	0,52	0,15	n.a.	1,61
K	13.12	4,59	0,06	0,06	0,44	0,02	4,00	2,45	23,51	2,57	0,10	0,105	0,075	**0,0293**	0,74	0,36	n.a.	1,41
K	14.12	4,13	0,05	0,02	0,64	0,01	4,00	1,26	5,26	2,29	0,10	0,106	0,022	0,0100	0,44	0,32	n.a.	1,44
K	15.12	4,29	0,05	0,03	0,40	0,01	4,00	1,30	4,98	2,08	0,10	0,075	0,044	0,0100	0,46	0,15	n.a.	1,43
K	16.12	5,60	0,08	0,04	0,96	0,02	4,00	4,24	8,08	7,94	0,10	0,281	0,043	**0,0293**	0,45	0,15	n.a.	4,57
K	19.12	4,67	0,11	0,02	0,56	0,01	4,00	0,96	4,16	4,19	0,10	0,135	0,02	**0,0195**	0,46	0,16	n.a.	2,83
K	21.12	5,03	0,09	0,03	0,60	0,01	4,00	0,91	4,09	3,50	0,10	0,102	0,023	**0,0098**	0,48	0,24	n.a.	2,33
K	16.01	11,29	0,26	0,11	4,64	0,05	4,00	16,85	10,75	36,37	0,22	0,536	0,043	**0,6243**	n.a.	0,32	n.a.	n.a.

Appendix 6 – Correlation analysis

A	*Al*	*V*	*Cr*	*Fe*	*Co*	*Ni*	*Cu*	*Zn*	*Sr*	*Sr*	*Mo*	*Mo*	*Cd*	*Pb*	*U*	*Na*	*K*	*Mg*	*Ca*	*F*	*Cl*	*SO4*	*NO3*	*pH*	*EC*
Al	1,00																								
V	0,51	1,00																							
Cr	0,32	0,96	1,00																						
Fe	0,21	0,85	0,91	1,00																					
Co	-0,06	-0,28	-0,18	-0,02	1,00																				
Ni	-0,29	-0,01	0,17	0,43	0,66	1,00																			
Cu	-0,23	0,30	0,35	0,29	-0,44	-0,20	1,00																		
Zn	0,78	*0,78*	0,63	0,49	-0,26	-0,12	0,04	1,00																	
Sr	-0,33	-0,02	0,12	0,46	0,48	0,94	-0,07	-0,13	1,00																
Sr	-0,33	-0,02	0,12	0,46	0,49	0,94	-0,06	-0,14	1,00	1,00															
Mo	0,42	0,05	-0,13	-0,34	-0,64	-0,76	0,37	0,33	-0,66	-0,66	1,00														
Mo	0,41	0,03	-0,14	-0,35	-0,63	-0,75	0,38	0,31	-0,66	-0,66	1,00	1,00													
Cd	-0,33	-0,03	0,13	0,25	0,58	0,87	-0,27	-0,01	0,73	0,72	-0,66	-0,66	1,00												
Pb	0,15	0,18	0,10	0,26	-0,14	0,26	-0,21	0,18	0,42	0,40	0,01	0,00	0,14	1,00											
U	-0,16	-0,47	-0,50	-0,22	-0,05	-0,02	0,23	-0,40	0,22	0,24	0,19	0,21	-0,35	0,06	1,00										
Na	-0,50	-0,18	0,00	0,34	0,51	0,90	-0,21	-0,36	0,94	0,94	-0,82	-0,82	0,70	0,29	0,21	1,00									
K	0,21	0,50	0,54	0,75	0,31	0,75	-0,02	0,50	0,78	0,78	-0,40	-0,41	0,62	0,40	-0,04	0,60	1,00								
Mg	-0,20	-0,15	-0,01	0,30	0,61	0,79	-0,34	-0,23	0,74	0,75	-0,71	-0,71	0,58	0,00	0,26	0,83	0,57	1,00							
Ca	-0,32	-0,17	-0,06	0,32	0,54	0,83	-0,01	-0,25	0,94	0,94	-0,58	-0,58	0,54	0,30	0,47	0,88	0,67	0,72	1,00						
F	-0,15	-0,37	-0,39	-0,62	-0,06	-0,27	-0,41	-0,03	-0,41	-0,42	0,05	0,04	0,16	-0,33	-0,47	-0,29	-0,44	-0,30	-0,49	1,00					
Cl	0,85	0,71	0,56	0,36	-0,44	-0,42	0,16	0,88	-0,42	-0,42	0,54	0,52	-0,41	0,01	-0,24	-0,60	0,18	-0,39	-0,46	-0,10	1,00				
SO4	-0,01	-0,50	-0,48	-0,49	0,20	-0,02	-0,43	-0,46	-0,11	-0,12	0,11	0,12	-0,06	0,30	0,07	-0,04	-0,40	0,00	-0,12	0,03	-0,34	1,00			
NO3	-0,20	0,14	0,17	-0,11	-0,42	-0,36	-0,11	0,07	-0,47	-0,49	-0,03	-0,04	0,01	-0,23	-0,70	-0,32	-0,40	-0,39	-0,68	0,70	0,05	-0,14	1,00		
pH	-0,05	0,04	0,02	-0,11	-0,60	-0,54	-0,10	-0,13	-0,49	-0,49	0,06	0,05	-0,54	-0,07	-0,14	-0,29	-0,53	-0,34	-0,53	0,27	0,16	0,01	0,61	1,00	
EC	-0,31	-0,08	0,03	0,42	0,49	0,86	-0,05	-0,18	0,96	0,97	-0,64	-0,64	0,60	0,31	0,41	0,93	0,74	0,81	0,98	-0,48	-0,42	-0,18	-0,58	-0,48	1,00

AT	*Al*	*V*	*Cr*	*Fe*	*Co*	*Ni*	*Cu*	*Zn*	*Sr*	*Mo*	*Mo*	*Cd*	*Pb*	*U*	*Na*	*K*	*Mg*	*Ca*	*F*	*Cl*	*SO4*	*NO3*	*pH*
Al	1,00																						
V	-0,31	1,00																					
Cr	-0,22	0,48	1,00																				
Fe	-0,15	0,33	0,97	1,00																			
Co	0,00	0,25	0,04	0,03	1,00																		
Ni	0,10	0,45	0,23	0,19	0,90	1,00																	
Cu	-0,04	0,77	0,46	0,31	0,42	*0,71*	1,00																
Zn	0,10	0,58	0,27	0,20	0,81	0,98	*0,84*	1,00															
Sr	-0,12	0,35	0,47	0,42	0,67	0,81	0,68	0,78	1,00														
Mo	-0,40	-0,12	0,23	0,24	0,25	0,08	-0,08	-0,01	0,49	1,00													
Mo	-0,36	-0,26	0,01	0,04	0,19	-0,05	-0,31	-0,17	0,29	0,96	1,00												
Cd	0,07	0,65	0,35	0,26	0,72	0,93	*0,90*	0,98	0,76	-0,08	-0,27	1,00											
Pb	0,12	-0,02	-0,28	-0,31	0,22	0,21	0,12	0,21	0,02	-0,38	-0,40	0,24	1,00										
U	-0,10	-0,11	-0,06	-0,05	0,81	0,64	0,12	0,50	0,66	0,64	0,63	0,35	-0,10	1,00									
Na	-0,26	0,09	0,17	0,12	0,31	0,32	0,27	0,27	0,71	*0,84*	*0,77*	0,23	-0,29	0,63	1,00								
K	0,02	0,27	0,07	0,00	0,69	0,63	0,38	0,58	0,62	0,44	0,39	0,49	0,25	0,65	0,57	1,00							
Mg	-0,08	0,32	0,20	0,14	0,67	0,77	0,55	0,72	*0,89*	0,51	0,41	0,65	-0,08	0,75	0,81	0,73	1,00						
Ca	-0,02	-0,23	0,48	0,54	0,31	0,34	0,15	0,26	0,71	0,59	0,42	0,25	-0,06	0,48	0,54	0,30	0,48	1,00					
F	-0,09	-0,06	-0,36	-0,41	0,10	-0,06	-0,13	-0,07	-0,18	-0,03	0,05	-0,10	0,59	0,00	-0,03	0,45	-0,06	-0,22	1,00				
Cl	0,24	0,03	-0,24	-0,26	0,51	0,33	-0,03	0,25	0,07	0,09	0,16	0,13	0,38	0,40	0,06	0,78	0,24	-0,12	0,61	1,00			
SO4	-0,06	0,11	-0,14	-0,20	0,46	0,39	0,19	0,34	0,40	0,33	0,33	0,28	0,41	0,45	0,49	0,83	0,57	0,14	0,76	0,67	1,00		
NO3	0,36	-0,24	-0,10	-0,10	0,37	0,20	-0,17	0,08	0,15	0,31	0,37	-0,04	0,07	0,53	0,23	0,52	0,27	0,10	0,14	0,65	0,33	1,00	
pH	0,38	-0,62	-0,64	-0,57	-0,30	-0,49	-0,62	-0,52	-0,65	-0,22	-0,04	-0,57	-0,02	-0,14	-0,40	-0,47	-0,56	-0,38	-0,06	-0,06	-0,39	0,26	1,00

G	*Al*	*V*	*Cr*	*Fe*	*Co*	*Ni*	*Cu*	*Zn*	*Sr*	*Mo*	*Cd*	*Pb*	*U*	*pH*	*EC*	*Na*	*K*	*Mg*	*Ca*	*F*	*Cl*	*SO4*
AL	1,00																					
V	-0,24	1,00																				
Cr	-0,08	0,92	1,00																			
Fe	0,23	0,84	0,88	1,00																		
Co	0,21	0,06	0,14	0,29	1,00																	
Ni	0,40	-0,09	0,06	0,28	0,83	1,00																
Cu	0,01	0,80	0,95	0,86	0,01	0,03	1,00															
Zn	0,23	-0,05	0,10	0,23	0,92	0,96	0,01	1,00														
Sr	0,29	0,06	-0,01	0,32	0,64	0,80	-0,08	0,73	1,00													
Mo	0,04	0,39	0,13	0,42	0,08	-0,03	0,08	-0,06	0,49	1,00												
Cd	-0,20	0,14	0,09	0,14	0,82	0,70	-0,11	0,82	0,71	0,17	1,00											
Pb	0,56	-0,37	-0,33	-0,22	0,12	0,28	-0,35	0,19	0,34	-0,05	0,10	1,00										
U	0,06	0,53	0,37	0,60	0,32	0,08	0,28	0,14	0,38	0,85	0,28	-0,29	1,00									
pH	-0,38	0,56	0,70	0,41	-0,26	-0,34	0,78	-0,29	-0,58	-0,30	-0,34	-0,62	-0,10	1,00								
EC	0,44	0,04	0,10	0,45	0,61	0,84	0,13	0,74	0,91	0,42	0,54	0,25	0,38	-0,39	1,00							
Na	0,59	-0,05	0,01	0,41	0,45	0,70	0,08	0,57	0,80	0,50	0,32	0,24	0,48	-0,46	0,94	1,00						
K	0,13	-0,13	-0,19	0,06	0,47	0,69	-0,22	0,61	0,90	0,36	0,65	0,47	0,10	-0,58	0,81	0,66	1,00					
Mg	0,58	0,00	0,12	0,47	0,64	0,84	0,16	0,75	0,80	0,33	0,45	0,20	0,43	-0,37	0,95	0,96	0,62	1,00				
Ca	0,32	-0,04	-0,23	0,17	0,51	0,55	-0,32	0,48	0,89	0,70	0,56	0,31	0,55	-0,76	0,75	0,75	0,77	0,67	1,00			
F	-0,63	0,12	0,21	-0,19	-0,44	-0,51	0,30	-0,42	-0,70	-0,52	-0,33	-0,35	-0,52	0,77	-0,63	-0,74	-0,45	-0,70	-0,85	1,00		
Cl	-0,34	0,05	-0,29	-0,19	0,14	0,03	-0,47	0,08	0,51	0,54	0,54	0,27	0,26	-0,59	0,16	0,06	0,59	-0,05	0,64	-0,31	1,00	
SO4	-0,04	0,20	0,33	0,43	0,36	0,58	0,44	0,53	0,54	0,13	0,37	-0,05	0,06	0,20	0,71	0,54	0,63	0,57	0,23	0,09	-0,04	1,00

Appendix 7 – PHREEQC Code

```
SOLUTION_SPREAD
-units    ppm
Al          Fe           Cu         Zn          Na       K       Mg      Ca     S(6)          pH      pe    Temperature
ppb        ppb          ppb        ppb                                      charge
28.92   201.17   5.79     168.68        2.79    8.66    49.36  379.87  1469.07        7.80    3.44             2
35.79   274.00  22.61   11466.35       17.64   45.50   509.09  413.86  3733.09        7.20     4.2             2
29.52   173.51   4.50     662.95       15.18   43.02   638.15  380.88  3758.88        7.57    3.53             2
0        0       0       0       0      0        0       0     0         7       4                4

INVERSE_MODELING
-solutions    4 3
-uncertainty  0.05
-multiple_precision true
-mp_tolerance 1e-7
-mineral_water false
-phases
Pyriteforce dis
Illiteforce dis
Muscovite     force dis
Maximum_Microcline   force dis
Albiteforce dis
Chalcopyrite  force dis
Sphalerite    force dis
Calcite       force dis
CO2(g)force dis
O2(g)  force dis
Gypsumforce pre
Jarosite      force pre
Fe(OH)3       force pre
Goethite      force pre
Gibbsite      force pre
Kaolinite     force pre
Montmor-Ca    force pre
C      force pre
```

Appendix 8 – Tunnel Geological Cross-Section

Modified from Multiconsult (2013). 10200 – Southbound tunnel, 10300 - Northbound tunnel. Alum shale is brown, while Galgeberg is pink.